Impact Mitigation Properties and Mechanical Material Characterization of Women's Lacrosse Headgears at Ambient and Cold Temperatures

by

Grant Baker

A thesis submitted in partial fulfillment
of the requirements for the degree of
Master of Science in Engineering
(Bioengineering)
in the University of Michigan-Dearborn
2021

Master's Thesis Committee:

Associate Professor Amanda Esquivel, Chair
Professor Alan Argento
Associate Professor Joe Fujiou Lo
Associate Research Scientist Wonsuk Kim

Acknowledgements

I would like to thank my advisor, Dr. Amanda Esquivel, for providing me with the opportunity to work on this research. Her guidance, advice, and teaching throughout this thesis work and since I first had her as a professor have helped mold me into the researcher and engineer that I am today. I would also like to thank the rest of my committee members, Dr. Alan Argento, Dr. Joe Lo, and Dr. Wonsuk Kim, for taking an interest in my research and asking thought-provoking questions that could push the future directions that this research takes. Dr. Argento and Dr. Kim also allowed me to use their equipment for material testing and gave me invaluable advice on how to approach that area of my research.

Addtionally, I would like to thank my lab members Mirel Ajdaroski, Madison Rowe, Zoie Mink, Ryan Exell, and Lorraine Nichols for their help in acquiring data. Mirel also helped me write some of my first MATLAB scripts years ago, and without his early help I would not have been able to write the scripts that I did in this thesis. I would also like to thank Matthew Brown for coming up and carrying out an innovative way to cut uniform samples of the materials from the headgears.

I am grateful for my colleagues and friends, Eric Anttila and David Gross, for giving me the encouragement that I needed throughout the end stages of my thesis work. The ear that Eric lended for me to bounce ideas off of or just to unload information on helped me get through the tough times of balancing work and my research.

Lastly, I would like to thank Anja. This thesis would double in length if I took the time to thank her for everything. Her willingness to take on extra responsibilities allowed me to devote the time that I needed towards this research and her undying encouragement and support helped keep me afloat. I am glad that we are spending the rest of our lives together because any less time would not be long enough to thank her as many times as she deserves.

Table of Contents

List of Tables

List of Figures

List of Appendices

Abstract

The rate of concussion in women's lacrosse is alarmingly high despite the sport being non-contact. Conflicting opinions on the potential effectiveness of helmet use in the sport led to the development of an ASTM standard in 2015 for optional headgear. These headgears are unique to most other head protection in that they do not have a hard outer shell because it could endanger players that choose not to wear the optional headgear. Because these headgears are so new and have unique design constraints, there is still much to learn about their ability to protect the players wearing them. The purpose of this research was to determine the impact mitigation properties of two commercially available women's lacrosse headgears (the Cascade LX and the Hummingbird v2) across a variety of impact types and severities and to incorporate rotational velocity kinematic concussion metrics in impact analysis because of their correlation to brain strains. Because polymers that are commonly used in sports headgears have been shown to exhibit cold temperature hardening, the influence of cold temperatures on the ability of the headgears to mitigate impacts was also studied.

Linear impactor and ball impact testing was performed on ambient and cold conditioned headgears. The kinematic concussion metrics peak linear acceleration (PLA), peak rotational acceleration (PRA), peak rotational velocity (PRV), head injury criterion (HIC_{15}), and brain injury criterion (BrIC) were calculated for each impact. Results showed that both headgears were able to significantly reduce all five metrics, but that this reduction was much more subtle for the two rotational velocity metrics (PRV and BrIC). Cold conditioning did not have significant

effects on the headgears' ability to mitigate impacts. Materials that were used in the headgears were then tested in compression at various strain rates and at ambient and cold temperatures to acquire their mechanical characterizations. These characterizations can be used in future finite element analysis studies to more accurately investigate how the headgears are able to protect against concussions through brain strain analysis and to study how much they may endanger other players that are not wearing headgear.

Chapter 1: Introduction

1.1 Concussion/Mild Traumatic Brain Injury

1.1.1 Definition of Concussion/Mild Traumatic Brain Injury

The terms concussion and mild traumatic brain injury (mTBI) are often used synonymously and interchangeably in literature [1],[2]. Therefore, going forward, the term concussion will primarily be used, but will mean the same thing as mTBI. Concussions, along with other severity-levels of traumatic brain injury, are often defined using the Glasgow Coma Scale (GCS). Developed in 1974, the GCS assesses individuals on their eye-opening, motor, and verbal responsiveness and gives them an accompanying score [3]. Scores in the range of 13-15 categorizes a brain injury as a concussion [3]. The US Department of Veterans Affairs and the US Department of Defense classifies a concussion as having the following characteristics for each category: a normal image in structural brain imaging; 0-30 minutes of loss of consciousness; fewer than 24 hours of altered mental state; fewer than one day of post-trauma amnesia; a GCS score of 13-15 [1]. Although scales and guidelines have been developed to diagnose concussions more accurately, they are still imperfect and erroneous and there is still ambiguity in our understanding of concussions. This is because of the inherently complex nature of brain tissue and because of the difficulty in obtaining accurate concussion thresholds, both of which are addressed in the following sections.

1.1.2 Material Properties of Brain Tissue

Understanding the material and mechanical properties of the brain has been a goal of biomechanical research because of the role that brain tissue characteristics play in brain injury and the determination of brain injury criteria [4], [5]. However, this is not an easily achieved goal due to the complexity of the human brain. Research agrees that the brain exhibits nonlinear and viscoelastic behavior [4]–[7], but its mechanical and material properties are not as straightforward. One of the aspects of brain tissue that makes it difficult to characterize is that it exhibits different properties when subject to tensile [4], [5], [8]–[11], compressive [4]–[6], [12]–[15], and shear [4], [5], [13], [16]–[19] loads. Additionally, the neuroarchitecture and the heterogeneous nature of different areas (corpus callosum, corona radiata, thalamus) and different tissue types (white and gray matter) of the brain create a high level of anisotropy [4], [5], [20]–[22]. This anisotropic nature of the brain causes the same mechanical load to have different effects depending on the area and the type of tissue [22].

The delicate and fragile nature and the use of different types (human, porcine, bovine, rodent) of brain tissue, along with differences in experimental methodology, have resulted in discrepancies about the material properties of brain tissue [4], [5], [22], [23]. However, even with this discrepancy, comparative results between loading modes consistently highlight that brain tissue most easily deforms when subject to shear stress [4], [5], [22], [23]. This is highlighted by Figure 1, which shows the tensile, compressive, and shear stresses at 50% strain of brain tissue at low, medium, and high strain rates all using the same methodology [5]. Although brain tissue deforms most easily from shear stresses, compressive and tensile stress behavior is still of interest for understanding brain injuries because injurious events are virtually always a combination of compression/tension and shear loads [24], [25].

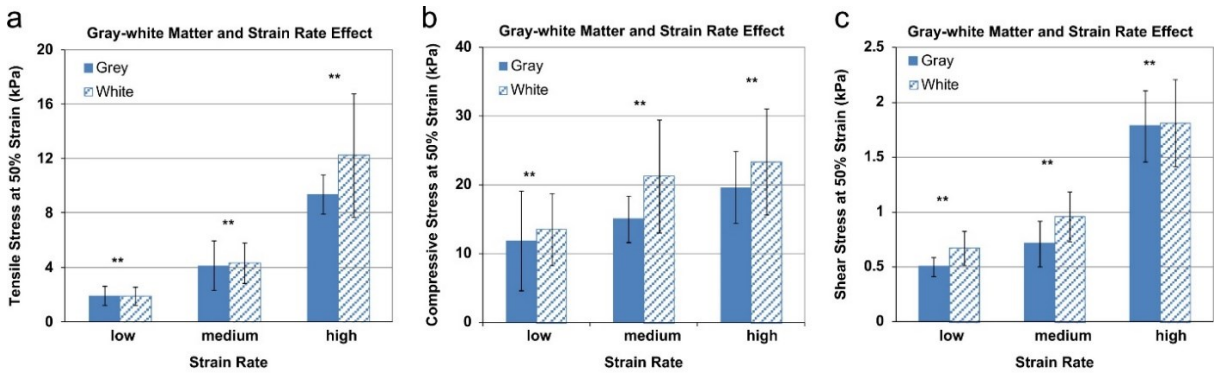

Figure 1 | (a) Tensile, (b) compressive, and (c) shear stresses at 50% strain of gray and white matter brain tissue at low, medium, and high strain rates [5].

1.1.3 Mechanisms of Concussion

The two main types of brain damage are focal brain damage (contusions, hematomas, and lacerations) and diffuse brain damage (diffuse axonal injury, cerebral swelling, and cerebral ischemia) [24]. Forces that cause these types of brain damage (and ultimately concussions) can be classified as either contact or inertial (acceleration) forces. Both forces occur during the loading phase of an impact (head being struck or striking a surface), but only inertial forces occur during impulsive head motions that do not result from direct impact to the head [2].

Severe contact forces are linked to focal brain damage because they can cause local skull deformation and skull depression [2], [26]. This depression causes the skull to impact the brain at the impact site (Figure 2) [24], [26]. This impact can result in coup contusions and tissue deformation that create brain tissue strains large enough to elicit concussion [26]. Additionally, epidural hematomas can develop as the skull goes back to its starting position after undergoing elastic deformation [27]. Although severe contact forces can lead to devastating brain damage, these types of focal brain damage often occur during life-threatening head impacts rather than concussions [2]. Lower-severity contact forces, however, can lead to linear and rotational

acceleration of the head. These contact and inertial forces together can cause brain damage that is common in concussions [2].

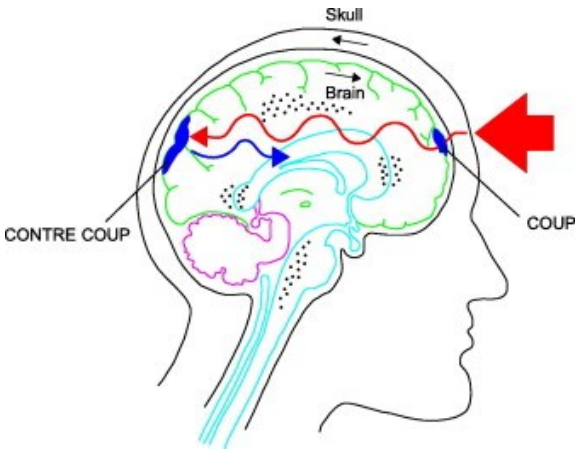

Figure 2 | Coup (impact site) and contrecoup (opposite of impact site) contusion locations of a head impact (arrow) [24].

To better understand concussions and what types of impacts can lead to them, early research focused on its relationship with linear acceleration of the head. Research found a strong correlation between peak intracranial pressure and peak linear acceleration of the head [28]–[30]. Since higher levels of intracranial pressure were proven to correlate with higher levels of brain deformation [28]–[30], it was established that linear acceleration of the brain contributed to brain injury and concussions because a pressure gradient is created. During a head impact, the skull moves faster than the brain does, causing the brain to lag behind. As a result, the brain pushes up against the skull at the site of impact, creating an area of high pressure, and translates away from the skull at the distal site, creating an area of negative pressure [27], [31], [32]. This creates an intracranial pressure gradient, which in turn creates shear stresses that lead to focal brain tissue damage [26], [33], [34]. Further research on the intracranial pressure gradient that leads to brain damage found that both compressive and tensile waves were found at the impact and distal sites,

respectively [34], which confirmed the presence of the gradient since the compressive/tensile loads are what create the gradient.

Recent research has focused on the link between rotational acceleration of the head and concussion because of its promising cause and effect relationship with brain strain. When the head rotates, the brain's inability to rotate in unison with the skull can lead to high levels of shear stresses and strains from the brain sliding against the skull [35], [36]. Rotational acceleration can also cause diffuse shearing of brain tissue (Figure 3) [37], [38], often causing diffuse axonal (DAI), which occurs when axons in different brain regions (white and gray matter) undergo severe shearing and break because of the difference in densities of the regions [24], [39]. These brain injury mechanisms occur because rotational acceleration creates such high levels of shear stress in the brain [2], [25]. In fact, by applying non-impact rotational accelerations to monkeys, it was determined that rotational acceleration alone could cause concussion and even severe level brain injury [40]. Further studies concluded that lower magnitude, longer duration rotational acceleration pulses lead to DAI while higher magnitude, shorter duration rotational acceleration pulses lead to acute subdural hematomas [41].

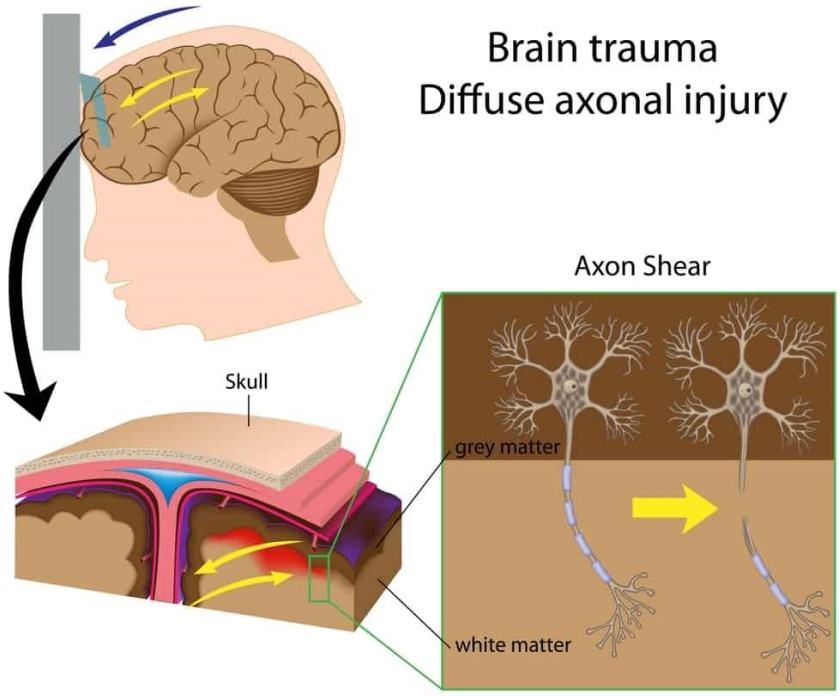

Figure 3 | Diffuse axonal injury [42]

In summary, linear acceleration of the brain creates a pressure gradient that induces compressive/tensile stresses and strains within the brain and low levels of shear stresses and strains at the coup and contrecoup. Animal studies have shown that linear accelerations caused by inertial forces may not be able to cause brain strains large enough to cause concussion on their own in the absence of angular motion [2], [25], [43], [44]. Recalling the previous section, this finding makes sense since brain tissue deforms most easily from shear stresses, which linear acceleration and the pressure gradient that it induces create little of, and is more resistant to compressive stresses that are associated with translation [45]. The brain strains that result from the high levels of shear stress that accompany rotational acceleration of the brain have been proven to be able to cause concussive brain injuries on their own [40], [41], [43], [44]. However, this does not mean that linear acceleration induced brain damage should be completely ignored.

Real world impacts virtually always consist of both linear and rotational acceleration components, highlighting the need to consider both for a full understanding of the mechanisms of concussion [46]. Post et al. (2017) found that although increasing the magnitude of rotational acceleration has a greater influence on the maximum principal strain in the brain, an increase in concussion-level-strains become more likely at higher levels of both linear and rotational acceleration [47]. Some studies even suggest that the linear acceleration from an impact is correlated with the rotational acceleration of the impact [25]. The same magnitudes of linear and rotational accelerations can have different brain damage effects depending on impact location and direction [2], [25], [48], [49], which is consistent with the anisotropic nature of brain tissue described in the previous section and highlights the need for multiple impact locations in head impact studies, which is addressed in future sections.

1.2 Concussion Prediction

Brain damage, and ultimately concussion, is most accurately measured from tissue-based metrics including maximum principal strains (MPS), von Mises stresses, and cumulative strain damage measure (CSDM) because these measurements can account for all aspects and complexities of an impact to the head, including spatial and temporal responses of the brain [50]–[53]. Of these measurements, the strain-based measures, especially MPS, are seen as the most accurate predictors because they directly measure the primary mechanism of brain tissue damage, which is deformation of the tissue [52]–[54]. Although tissue-based metrics for measuring concussions are ideal, directly measuring brain strain during head impacts is difficult because of the delicate/fragile nature of brain tissue and because of a lack of access to equipment that is capable of accurately measuring brain strains during dynamic impacts, such as high-speed biplanar x-ray [55]. Furthermore, anthropomorphic test devices (ATDs) that are currently used in

head impact research are not capable of directly measuring brain strains [53]. Kinematic metrics, on the other hand, only measure head motion and are related to the inertial force mechanisms of concussion and brain injury described in the previous section. Therefore, they are directly related to the intracranial pressure gradients and relative brain motion that lead to brain damage, but indirectly related to the resulting injurious strains themselves, making them a less desirable metric compared to tissue-based metrics in terms of accuracy. However, kinematic metrics are much easier to measure than tissue-based metrics, so the goal of concussion-related research has been to relate kinematic measurements of the head with the tissue-based metrics (strains, stresses) that they produce [53], [56]. In doing so, mathematical models have been developed to predict concussions solely based on kinematic measurements. Before explaining the kinematic-based concussion predictors, a brief overview on the methods of how kinematics are experimentally measured and related to tissue-based concussion metrics is given, with an emphasis on measurements for sports-related impacts.

1.2.1 Methods of Studying Concussions in Sports

1.2.1.1 Anthropomorphic Test Devices

Anthropomorphic test devices (ATDs) in head injury and concussion research are designed to mimic the human head while also having the capability of recording kinematic data. Although multiple ATDs have been developed and used for head impact research (NOCSAE, DOT, ISO), the most widely used headform is the Hybrid III, shown in Figure 4. The Hybrid III headform was designed to accurately mimic the human head's mechanical response to rigid surface impacts [57], [58]. Although it is made of a steel skull that is covered with vinyl "skin", the Hybrid III headform is highly biofidelic and is considered the gold standard for measuring head kinematics [58], [59]. Use of a Hybrid III neck with the Hybrid III headform (called a head-

neck assembly) allows for an even more biofidelic impact response than a fully constrained headform because the neck, which is made of rubber and metal disks, allows the head to rotate as it would in a real-world impact [59]. The Hybrid III headform measure head kinematics using tri-axial accelerometers and gyroscopes that are housed at the center of gravity of the headform and are capable of measuring linear acceleration and rotational velocity, respectively.

Figure 4 | Hybrid III head and neck assembly.

Laboratory head impact studies using ATDs are conducted to replicate real-world impacts. For sports, this means that specific sports related impacts can be reconstructed by altering the impact characteristics (mass, material, velocity) and location [47]. Consequently, ATDs have been used for head impact and concussion studies in a wide variety of sports such as football [60]–[62], hockey [63]–[65], lacrosse [66]–[70] and soccer [71], [72]. Although ATDs

and the Hybrid III headform specifically are seen as the gold standard for measuring head kinematics, its measurements are not perfect. ATD skulls are hollow and do not include a deformable brain like a real head does, which may influence the inertial measurements at the center of gravity of a headform [25], [73]. Nonetheless, the way that ATDs are constructed still allows for accurate kinematic measurements [25].

1.2.1.2 On-Field Analysis

The experimental setup of studies that use ATDs to measure head kinematics is highly dependent on using video analysis or direct observation of sports related impacts to reconstruct them in the laboratory [47]. Although the use of human subjects to recreate impacts can help combat this limitation, the impacts in a laboratory are not likely to exactly mimic what occurs in a real sporting event. To address this limitation in measuring sports-related head impact kinematics, on-field head impact measurement devices have been developed. These devices usually incorporate tri-axial accelerometers and angular rate sensors to measure head kinematics. On-field head impact measurement devices have been used in various helmeted and non-helmeted sports, but have proven to have questionable accuracy in measurements [70], [72], [74]–[96].

1.2.1.3 Finite Element Analysis

Finite element analysis (FEA) provides the link between kinematic metrics and the tissue-based brain injury metrics that they create since finite element models are capable of measuring brain strains and stresses through the use of anatomically accurate head-brain models. Finite element models for head impacts can be constructed using two methods. The first method is to entirely recreate the impact conditions in the model, which can either be done by applying a force over an area or by having something dynamically impact the head [97]. From this analysis,

head center of gravity kinematics and brain strain are simultaneously measured and can be related. However, this method is prone to the same reconstruction errors that ATD laboratory testing apparatuses are subject to [68] and these models require complex contact definitions for the parts impacting the head (and for the helmet contacting the head if a helmet is included in analysis) [98]. This method is only as accurate as its inputs and boundary conditions are. The second method for using FEA to relate kinematic and tissue-based kinematics is to use acceleration time history measurements from an ATD as an input to the center of gravity of the finite element brain [98]. Although the input parameters are subject to the error associated with using ATDs, the resulting tissue-based metrics are based on how the brain would realistically respond and is not subject to the contact errors that the first method is.

1.2.2 Purely Linear Kinematic Predictors

As described in Section 1.1.3, it has been confirmed that linear acceleration of the head is correlated with intracranial pressure [28], [29], which in turn is somewhat related to strains in the brain. This correlation has led to the widespread use of peak resultant linear acceleration (PLA) values as a brain injury metric [99]. In 1966, Gurdjian et al. developed an acceleration – time tolerance curve known as the Wayne State Tolerance Curve (WSTC) (Figure 5), by analyzing animal and cadaver impacts [100]. The incorporation of impact duration into the relationship between linear acceleration and brain injury significantly improved its predictive capabilities [47], [101]. However, the WSTC was developed using skull fracture as the curve boundary since skull fracture and more severe brain injury are highly correlated [47]. This raises questions about its validity in predicting less severe brain injuries like concussion. Nonetheless, the WSTC was instrumental for future linear acceleration-based brain injury metrics because it was the first to incorporate impact duration and found that lower magnitude accelerations could be tolerated for

longer durations while higher magnitude accelerations could only be tolerated for short durations of time.

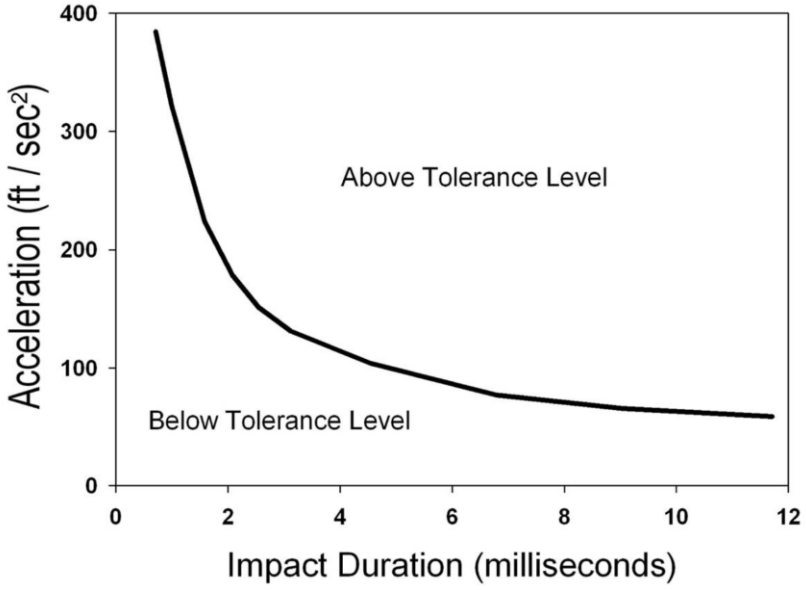

Figure 5 | The Wayne State Tolerance Curve [102].

To develop a predictive model that could be used in the automotive industry to guide the design of head protective devices, Gadd (1966) integrated the WSTC acceleration – time curve and incorporated a weighted coefficient to create the Gadd Severity Index (GSI), shown in Equation 1 below [101].

Equation 1 | Gadd Severity Index (GSI)

$$GSI = \int |\boldsymbol{a}(t)|^{2.5} dt,$$

In this equation, **a**(t) is the acceleration-time curve (with acceleration in units of g) and 2.5 is the weighting coefficient. Integrals are evaluated from the time that the acceleration first surpasses 4 g until it falls below 4 g [103]. Versace (1971) attempted to improve the GSI by incorporating a

time-averaging component [104]. The resulting metric, called Head Injury Criterion (HIC), is shown in Equation 2 below.

Equation 2 | Head injury criterion (HIC)

$$HIC = max\left\{(t - t_0)\left[\left(\frac{1}{t - t_0}\right)\int_{t_0}^{t} |\boldsymbol{a}(t)|dt\right]^{2.5}\right\},$$

For HIC, $t - t_0$ is the selected time domain for the impact and is usually selected as 15 ms or less in current standards for impacts. Linear acceleration itself, GSI, and HIC are the mostly widely and frequently used brain/head injury metrics used for head impact analysis. However, by failing to incorporate rotational kinematics that have been proven to be more shear strains and ultimately brain injury [26], they are often not accurate in predicting lower-severity brain injuries like concussions [47].

1.2.3 Mixed Linear and Rotational Kinematic Predictors

To incorporate the ability of rotational acceleration to more accurately predict shear strains within the brain while still accounting for the translational aspect of head impacts, kinematic brain injury metrics have been developed that incorporate both linear and rotational acceleration. Newman and his research team developed two kinematic brain injury metrics that utilize both linear and acceleration components, GAMBIT [105] and HIP [106], by recreating football impacts on ATDs. Greenwald et al. (2008) attempted to create a measurement for predicting concussions by correlating standardized linear acceleration, GSI, HIC, and rotational acceleration to HIT system recorded football impact data, called Principal Component Score (PCS) [102]. Kleiven (2007) used finite element simulations of football head impacts to correlate a combination of rotational velocity and HIC to brain tissue MPS [107]. These mixed linear and

rotational kinematic brain injury metrics are infrequently used in studies and may be less accurate than other kinematic metrics in predicting tissue-based brain injury metrics, so the specific mathematical models for them will not be described in this section.

1.2.4 Purely Rotational Kinematic Predictors

Kinematic-based brain injury metrics that only incorporate rotational kinematics have recently been developed because of the recent findings on the relationship between head rotational and resulting brain strains. Like with linear acceleration, the most basic brain injury metrics for rotational kinematics are peak resultant rotational acceleration (PRA) and peak resultant rotational velocity (PRV) [99]. Kimpara et al. (2012) used football head impact data correlated with FEA tissue-based metrics to develop the Rotational Injury Criterion (RIC), which uses the same equation as HIC but with rotational acceleration in the place of linear acceleration [108]. By relating the maximum magnitude of rotational velocity in each orthogonal head direction to finite element model strains from impacts, Takhounts et al. (2013) developed the Brain Injury Criterion (BrIC), shown in Equation 3 below:

Equation 3 | Brain injury criterion (BrIC)

$$BrIC = \sqrt{\left(\frac{\omega_x}{\omega_{xcr}}\right)^2 + \left(\frac{\omega_y}{\omega_{ycr}}\right)^2 + \left(\frac{\omega_z}{\omega_{zcr}}\right)^2},$$

where ω_i are the maximum magnitudes of angular acceleration and ω_{icr} are directionally dependent critical values (ω_{xcr} = 66.25 rad/s, ω_{ycr} = 56.45, and ω_{zcr} = 42.87) that were determined from FEA [52]. Yanaoka et al. (2015) also used finite element model brain strains that resulted from head impacts and developed the Rotational Velocity Change Index (RVCI), shown in Equation 4 below:

Equation 4 | Rotational velocity change index (RVCI)

$$RVCI = max\sqrt{R_x\left(\int_{t_0}^{t}\alpha_x dt\right)^2 + R_y\left(\int_{t_0}^{t}\alpha_y dt\right)^2 + R_z\left(\int_{t_0}^{t}\alpha_z dt\right)^2},$$

where α_i are angular accelerations about each orthogonal axis and R_i are weighting factors corresponding to each orthogonal axis that were determined from finite element modeling [109]. Recently, other promising brain injury metrics have been developed that use rotational velocity [110], [111], but strain-based risk functions have not been created and validated for them yet (only correlations to strain).

1.2.5 Accuracy of Kinematic-Based Concussion Predictors

As a disclaimer, more kinematic-based brain injury metrics that were not mentioned in the previous sections exist but were not mentioned because they are not used as often in head impact studies and/or have been shown to have lower correlations with brain strain. Several reviews on kinematic-based brain injury metrics have been conducted that further explain and compare the aforementioned concussion metrics [46], [99], [102], [112]. In 2016, Gabler et al. (2016) assessed the accuracy of fifteen kinematic-based brain injury metrics by using ATD kinematic data from 660 head impacts of various types [99]. The kinematic data was applied to two commonly used finite element head models, the Simulated Injury Monitor (SIMon) and the Global Human Body Models Consortium-owned (GHBMC) head models, to measure the maximum principal strain (MPS) and the cumulative strain damage measure (CSDM) in the brain from the head impacts. The same kinematic data was applied to each of the kinematic-based brain injury metrics and their abilities to predict the finite element tissue-based brain injury metrics was compared as shown in Table 1 [99].

Table 1 | Kinematics-based concussion prediction metrics ranked from highest (1) to lowest (15) correlation with maximum principal brain strain [99].

	MPS		CSDM	
Rank	GHBMC	SIMon	GHBMC	SIMon
1	BrIC	RVCI	RVCI	BrIC
2	RVCI	BrIC	BrIC	RVCI
3	BRIC	ω_m	BRIC	ω_m
4	RIC	RIC	RIC	RIC
5	ω_m	α_m	α_m	BRIC
6	α_m	BRIC	ω_m	α_m
7	KLC	KLC	KLC	KLC
8	PRHIC	PRHIC	PRHIC	PRHIC
9	HIP	HIP	HIP	HIP
10	GSI	GSI	GSI	GSI
11	PCS	PCS	PCS	PCS
12	CP	CP	CP	CP
13	HIC	HIC	HIC	HIC
14	GAMBIT	GAMBIT	GAMBIT	GAMBIT
15	a_m	a_m	a_m	a_m

Analysis of Table 1 clearly indicates the superior accuracy of rotational kinematic-based brain injury metrics since the top six highest correlations for both measurements (MPS and CSDM) and both finite element models (GHBMC and SIMon) are from purely rotational kinematic metrics. These results from suggest that BrIC and RVCI may be the most accurate kinematic-based brain injury metrics for predicting the highly accurate tissue-based brain injury metrics [99].

1.2.6 Concussion Thresholds

In the literature, kinematic- and tissue-based concussion and brain injury thresholds differ and there is no single agreed upon threshold for any metric since it is so difficult to accurately determine these thresholds. A review by Post and Hoshizaki (2012) brings together some of the reported concussion and brain injury thresholds for PLA, PRA, and tissue-based metrics [26].

Later in this research, impact severities will be compared to 50% probability of concussion thresholds for PLA, HIC_{15}, PRA, PRV, and BrIC. Therefore, it is worth noting here that the values for these thresholds are PLA = 82 g [60], HIC_{15} = 240 [60], PRA = 5900 rad/s^2 [60], PRV = 28.3 rad/s [113], and BrIC = 0.50 [52].

1.3 Concussion in Sports

Sports related concussion (SRC) rates are high in the US, with roughly 300,000 occurring annually [114]. Concussion rates and mechanisms vary by sport and have been reported in several epidemiological studies [83], [114]–[118]. One consensus of these studies is that football players suffer the most and highest rate of concussions. In gender-comparable sports, female athletes had higher (1.7 times) the concussion rate of their male counterparts [114]. Injury mechanisms can be broadly categorized as player-to-player, player-to-ground, or player-equipment contacts. Player-to-player contacts were the most common mechanism of SRCs in football, boy's soccer, boy's lacrosse, boy's basketball, girl's basketball, and boy's wrestling while player-equipment contacts were the most common mechanism of SRCs in boy's baseball, girl's softball, girl's volleyball, girl's lacrosse, and girl's field hockey [83].

1.3.1 Women's Lacrosse

Women's lacrosse is a unique case for SRCs. Although men's and women's lacrosse have similar game objectives and utilize the same type of sticks and balls, women's lacrosse is governed by a completely different set of rules than men's lacrosse is. In men's lacrosse, players are allowed to collide with each other, stick-check each other, and block shots all without penalty. Conversely, the rules of women's lacrosse prohibit any player-to-layer contact, stick-to-player contact, and shot blocking [119]. Consequently, men's lacrosse players are required to

wear helmets and protective gear while women's lacrosse players are only required to wear protective eye goggles (Figure 6). Even though rules do not allow any intentional contacts, unintentional impacts occur and can result in concussion [119], [120].

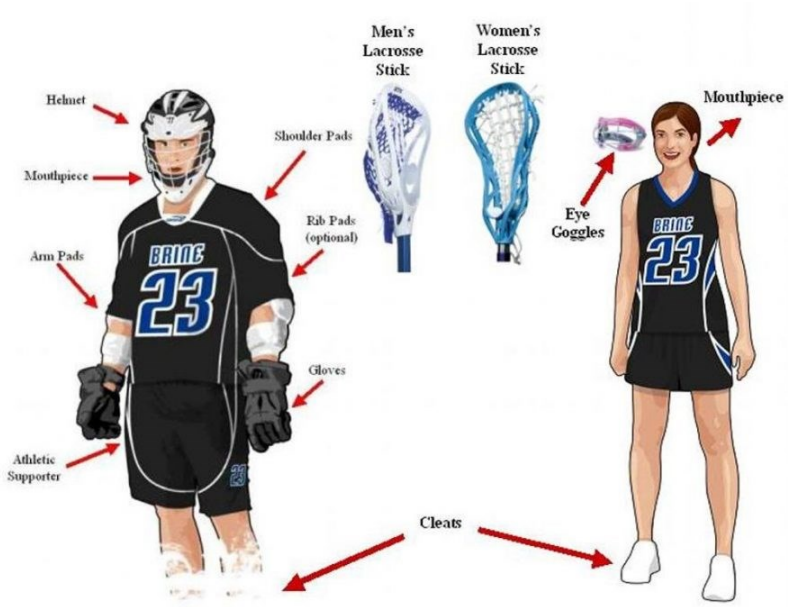

Figure 6 | Comparison of men's (left) and women's (right) lacrosse required equipment [121].

Epidemiological studies on concussions in women's lacrosse highlight the alarming rate of head injury and concussion in the sport. In a comparison of concussions in multiple sports, Marar et al. (2012) found that of all the female sports analyzed, women's lacrosse had the highest rate (21.1%) of injuries being concussions [114]. Similarly, a 10-year analysis of injuries in men's and women's collegiate lacrosse found that although injury rates were lower in women's lacrosse than they were in men's, a higher percentage of their injuries (30.1%) were to the head and face, which can pose a high risk for concussion [122]. Lincoln et al. (2007) also found that the rate of head and face injuries was significantly higher in women's lacrosse when compared to men's lacrosse [120]. Their study also determined that over their four years of

competition, 40% of high school and 41% of collegiate female lacrosse players sustained concussions [120].

Multiple studies have identified player-equipment contacts, especially stick-to-head contacts, as the most common mechanism of head impacts and concussions in women's lacrosse [83], [91], [114], [123], [124]. Considering that the rules prohibit any intentional player-to-player collisions, it makes sense that accidental stick impacts from shot/pass follow-throughs and attempts to steal the ball would result in the highest amount of head injuries. When including other equipment-related contacts and player-to-ground contacts, 65.8% of head impacts are accounted for [91]. Additionally, an FEA study on women's lacrosse related head impacts concluded that player-to-ground impacts from falls and ball-to-head impacts resulted in the highest levels of MPS in the brain, which were well within concussion range [98]. This suggests that the addition of protective headgear to the sport, rather than a change in rules, may have a greater impact on player safety.

Laboratory studies [69], [125] and FEA studies [97], [98] that perform women's lacrosse related impacts to helmeted and non-helmeted headforms and head models have confirmed that the use of helmets in women's lacrosse could significantly decrease head impact severity and potentially concussions. Although these findings would make it seemingly obvious that women's lacrosse players should wear helmets while they play, there is still debate over the use of helmets because some people believe that they will end up resulting in higher rates of concussion and head injury due to the ensuing increase in aggressive play that accompanies helmet usage [126].

To address the potential benefits of protective headwear in women's lacrosse while also listening to the concerns of those again its usage, US Lacrosse and the American Society for Testing and Materials (ASTM) created a standard for optional women's lacrosse headgear in

2015 [127]. This standard is unique because of the optional nature of the headgear. Since the headgear is optional, the headgears must be designed so that players that choose not to wear headgear are not an increased risk of injury when impacted by the headgear of a player who is wearing one. Consequently, headgear that have flexible/"soft" outer shells have been developed, which is different than the hard outer shell of most sports helmets [66]. Since the creation of this standard in 2015, two headgears have become commercially available for players to use. These are the Hummingbird (v1 and v2) (Hummingbird Sports; Holmdel, NJ) and the Cascade LX (Cascade; Liverpool, NY), shown in

Figure 7 | The (a) Hummingbird v2 and (b) Cascade LX women's lacrosse headgears.

1.4 Purpose of Research

The purpose of this research was to investigate the impact mitigation capabilities of women's headgears. Because these headgears are so new, few laboratory studies have tested their abilities to mitigate impacts and consequently the headgears have not been tested for all impact types that players are likely to experience during competition. In this study, a variety of impact types and severities were used to test the headgears and rotational velocity kinematic

concussion metrics were included in impact mitigation characterization because of their higher accuracy of correlation to brain strains than other kinematic concussion metrics. Impact mitigation capabilities were characterized for the headgears at ambient and cold temperatures to determine the effect of cold temperatures on the safety of the headgears. Materials from the women's lacrosse headgears were then tested in compression to acquire their mechanical characterizations at various strain rates and at ambient and cold temperatures with the goal of providing information needed for future research to more accurately study the impact mitigation properties of the headgears and the affect that the headgears have on the safety of players not wearing them.

Chapter 2: Headgear Impact Testing

2.1 Introduction

Current helmet safety standards created by ASTM and the National Committee on Standards for Athletic Equipment (NOCSAE) only consider linear acceleration-based impact metrics (peak linear acceleration and HIC). Since these metrics were developed through the correlation of linear acceleration with skull fracture and not with concussion, ASTM and NOCSAE standards assess a helmet's ability to reduce skull fracture more than they do their ability to reduce concussion [47], [128]. Consequently, sports helmets have effectively reduced the occurrence of traumatic brain injury in sports but have not had such success at reducing concussion [128]. Furthermore, helmet safety standards often only require the helmets to be tested at ambient and warm temperatures, even though the materials commonly used in sports helmets have been shown to act harder at colder temperatures [129]–[132].

To more accurately characterize the safety of headgear used in sports, researchers conduct impact tests on ATDs with and without protective headgear to establish the impact mitigation effectiveness of protective headgear through their ability to decrease concussion metrics. Many helmet safety testing standards only incorporate single axis drop tests that do not realistically simulate the impacts that frequently happen within sports. Laboratory impact test tests usually produce more insightful and informative results than the aforementioned tests used in helmet standards because (1) they utilize more relevant and sport-specific impact instead of using

consistent test methods and acceptance criteria across all sports and (2) they usually include concussion metrics other than peak linear acceleration and HIC in their analysis.

Even though women's lacrosse headgears have only been commercially available since 2016, impact studies involving ATDs have already been conducted to characterize their ability to mitigate impacts [66], [67]. Although these studies have provided an important initial insight on a more realistic understanding of the safety that the headgears provide to players, they only considered peak linear and rotational accelerations in their analysis. Since studies have shown that rotational velocity-based concussion metrics are the kinematics-based concussion metrics that are most closely correlated with brain strain [99], their inclusion in the analysis of helmet safety would provide a more comprehensive understanding of how well the headgears can reduce concussion. Furthermore, the impact studies previously done on the women's lacrosse headgears only tested impacts that may not be representative of those that cause the highest brain strains and have not studied the effects of cold temperature on the impact mitigation properties of the headgears. The purpose of this study was to examine the effectiveness of the women's lacrosse soft headgear to minimize various concussion metric in various impacts that are representative of lower- and higher-severity impacts in the sport at ambient and cold temperatures and to include rotational velocity-based concussion metrics in the analysis.

2.2 Methodology

2.2.1 Test System Overview

Impact testing was conducted on a Hybrid III 50th Percentile Male Headform mounted on a Hybrid III 50th Percentile Neck (Humanetics, Farmington Hills, MI) (Figure 8). As described in Chapter 1, the Hybrid III is highly biofidelic and is considered to be the gold standard for

measuring experimental head kinematics. The incorporation of the neck component elicits even more accurate head impact physics because it allows the headform to rotate like a real head would during impacts instead of being constricted to a specific axis of movement.

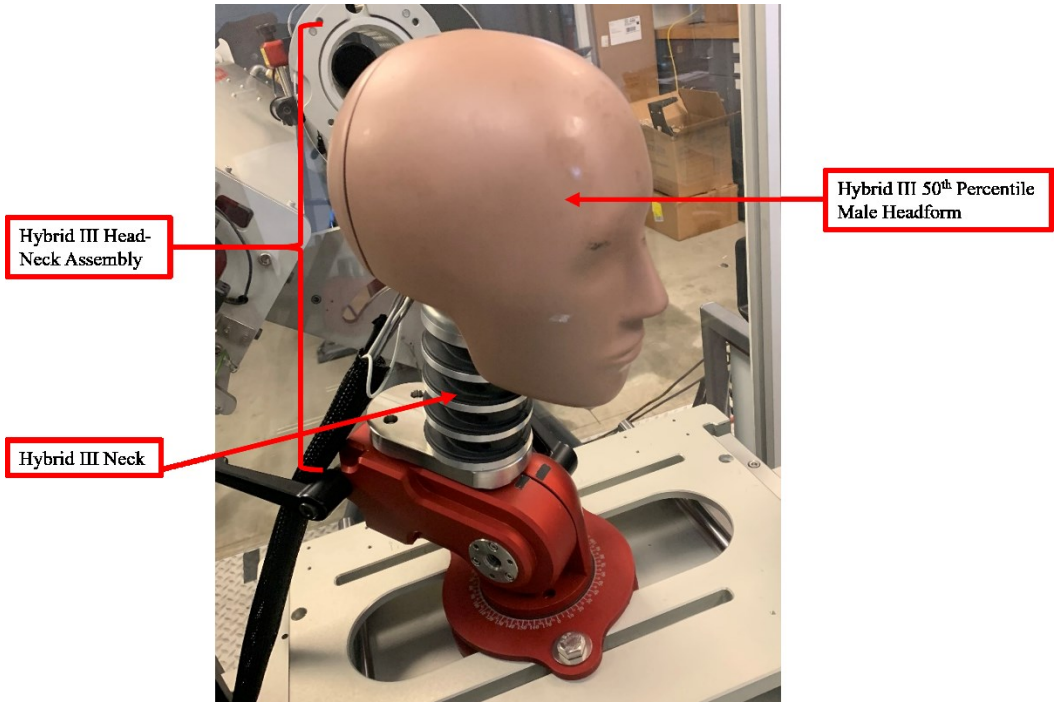

Figure 8 | Hybrid III head-neck assembly used for impact testing.

All impacts were administered using a Linear Impacting and Projectile Shooting Machine (Cadex, St-Jean-sur-Richelieu, Quebec, Canada) with Linear Bearing Table. This machine, shown in Figure 9, is a pneumatic impacting machine that uses compressed, pressurized air to propel a striker piston into the impactor rod, which then impacts the headform. A linear relationship between air pressure and its accompanying impactor velocity was established to determine what pressure is needed for the machine to achieve a desired impact velocity. The machine can produce the velocities desired for this impact testing within the acceptable tolerance ranges for both the linear impactor (+/- 2%) and projectile shooting (+/- 3%) components. The

testing velocities and the origin of their tolerances are described in a later section of this Chapter. The mount within the impacting cage of the machine can rotate 360° and tilt forward and backward, which allowed for the headform to be configured in desired impact locations.

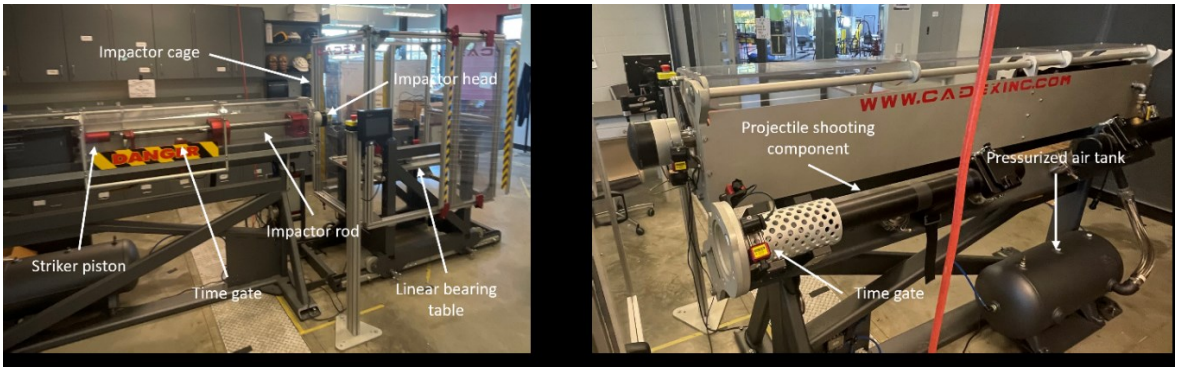

Figure 9 | The Cadex Linear Impacting and Projectile Shooting Machine.

The headform was instrumented with tri-axial A64C piezo-resistive accelerometers (Diversified Technical Systems, Inc., Seal Beach, CA) and tri-axial ARS PRO-8K angular rate sensors (Diversified Technical Systems, Inc., Seal Beach, CA) that collected linear acceleration and angular velocity data, respectively. The sensors were fixed at the center of gravity (CG) of the headform and connected to a SLICE MICRO data acquisition system (Diversified Technical Systems, Inc., Seal Beach, CA), which was integrated with SLICEWare software (Diversified Technical Systems, Inc., Seal Beach, CA). Interfacing the accelerometers and angular rate sensors with the SLICE MICRO data acquisition system and SLICEWare software allowed for all kinematic data to be collected simultaneously under one universal time interval at a rate of 20 kHz.

2.2.2 Experimental Procedure

2.2.2.1 Linear Impactor Testing

Linear impactor testing was conducted in accordance with the NOCSAE Standard Pneumatic Ram Test Method ND081 [133]. The NOCSAE standard describes the standard test method and equipment used to evaluate the performance characteristics of protective headgear through the use of linear impact testing. Although NOCSAE developed this standard test method, it does not utilize the test method for evaluation of all headgear type (drop testing is used instead). The ASTM standard specification for women's lacrosse headgear (ASTM F3137-15) also only incorporates drop testing. Nonetheless, this test method provides baseline instructions for researchers to follow when conducting linear impact testing on sports headgear. By adhering to the basic procedural elements and equipment specifications outlined in ND081, but slightly altering some procedural components to better represent impacts of the sport being studied, researchers can gain more realistic insight on headgear impact mitigation while still using a methodology that can be easily replicated. All equipment described in the previous section is compliant with the equipment specifications in ND081.

Impacts were conducted at the six different impact locations described in ND081. These impact locations are shown in Figure 10 and described in Table 2. The impact locations correspond to those for a medium size NOCSAE headform since it is comparable in dimensions to the 50th Percentile Male Hybrid III headform used in this methodology. Prior to collecting any data, it was verified that the linear impactor was impacting the correct impact location (indicated by the laser crosshairs) by sliding the impactor rod/head assembly out to where it would impact the headform at.

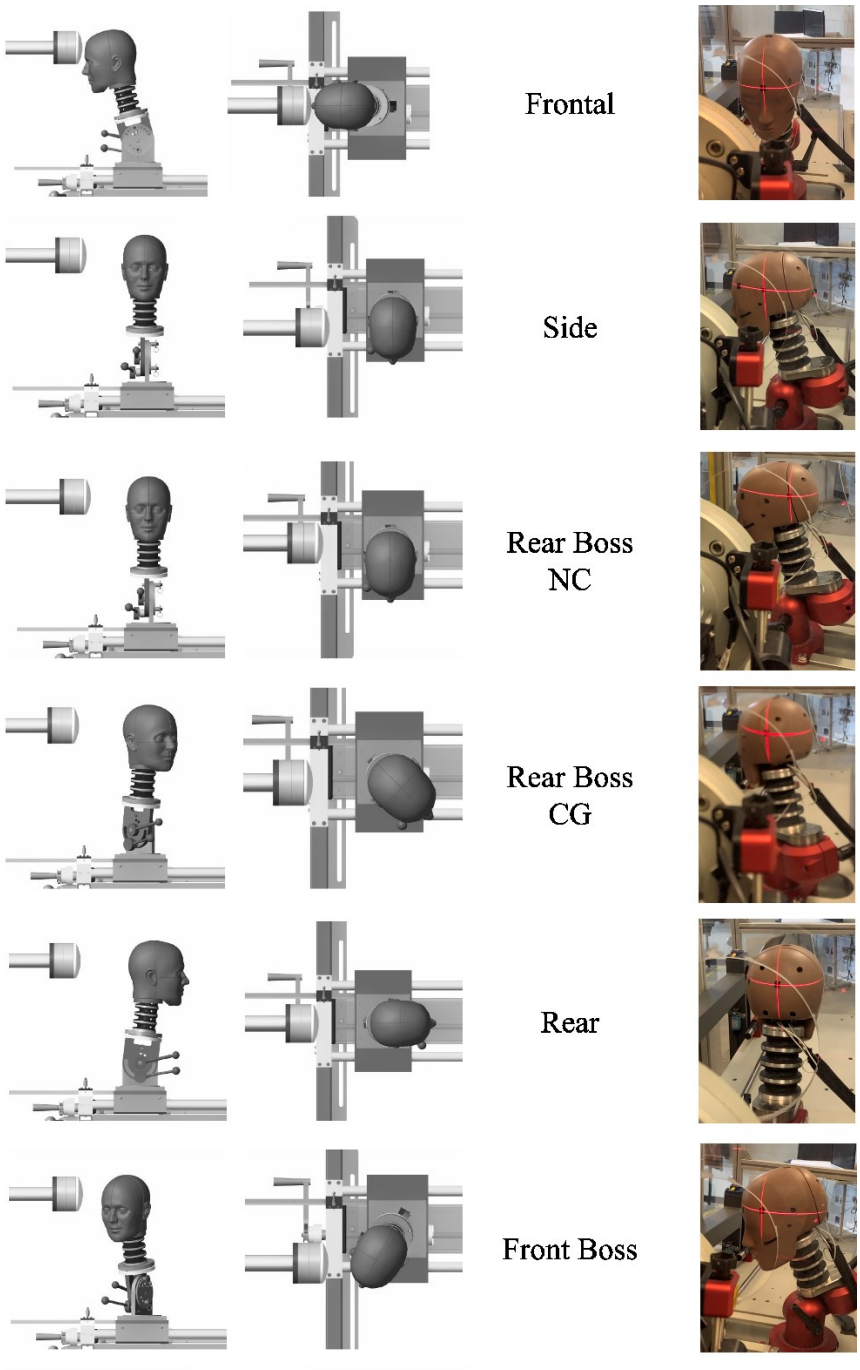

Figure 10 | Impact locations. The left side shows the impact location depictions in the ND081 standard [133]. The right side shows a laser crosshair aiming of where the linear impactor impacted the Hybrid III headform for each impact location in this methodology.

Table 2 | Description of impact locations based on a medium size NOCSAE headform [133]. α and β refer to the forward tilt angle and the rotation angle of the headform, respectively. β can be positive or negative, as either results in the same impact location on opposite sides of the headform.

Impact Location	α	β	Z-Axis Relative to Basic Plane	Y-Axis
Frontal	15 °	0 °	+78 mm	on the midsagittal plane
Side	7 °	90 °	+60 mm	on the coronal plane
Rear Boss NC	7 °	90 °	+60 mm	64 mm posterior to coronal plane
Rear Boss CG	7 °	135 °	+60 mm	81 mm posterior to coronal plane
Rear	7 °	180 °	+60 mm	on the midsagittal plane
Front Boss	15 °	60 °	+73 mm	56 mm anterior to coronal plane

The impact speeds used for the linear impactor testing were 2.2 m/s, 2.9 m/s, and 5.0 m/s. The 2.2 m/s impact speed was tested because it is the impact speed used in the shock absorption test of the ASTM specification for women's lacrosse headgear [134]. The 2.9 m/s impact speed was tested because it replicates lower severity, frequently occurring women's lacrosse related impacts and was used in a previous impact study on women's lacrosse headgear [67]. The 5.0 m/s was chosen because it corresponds to the high-speed running of a female in competitive sports [135], [136] and was used in a previous study to determine the ability of men's lacrosse helmets to mitigate women's lacrosse replicated impacts [68]. The velocity of the impactor was measured using the time gate component of the Cadex Linear Impacting and Projectile Shooting Machine. The velocity-measuring time gate was placed so that the impactor rod travelled no more than one inch after passing through the time gate before initial contact of the impactor head with the Hybrid III headform. Measured impactor velocities were within +/- 2% of the desired velocities, per the NOCSAE ND081 standard.

All three impact speeds were tested at all six impact locations on the bare headform with no headgear and on the headform with each of the two commercially available women's lacrosse headgears, the Cascade LX (called "Cascade" hereafter) and the Hummingbird v2 (called

"Hummingbird" hereafter). Each combination of impact speed with impact location was tested for three trials, totaling in 54 impacts for each headgear condition at ambient temperature. At each impact location for each condition (no headgear, Cascade headgear, or Hummingbird headgear), the distance that the headform had to be moved down the linear bearing table so that the impactor head made initial contact with the headform or headgear roughly 2 inches from where it bottoms out was established. This allowed for repeatability across trials and ensured that each impact was equivalent for all impact locations and all headgear conditions.

The same linear impactor testing methodology was used for testing the headgear at cold temperature for a total of 54 additional impacts for both headgear conditions, but with a cold-conditioning step added in before any impacting occurred. Since the headform itself could not be cold conditioned, there were only ambient linear impactor impacts for the no headgear condition. Cold conditioning was done by placing both headgears in a freezer at ~5 °C for a minimum of one hour before any impacts were conducted on a given testing day. The minimum one hour of cold conditioning replicated how long women's lacrosse players would be outside in cold temperatures during practices and games.

All linear impactor testing trials followed the same procedure. First the headform was oriented in the desired impact location configuration. Next, if applicable, a headgear was fit onto the headform according to each brand's suggested fitting instructions. Then, the headform (with or without headgear) was placed at the appropriate distance along the linear bearing table to allow the impactor to travel roughly 2 inches after making initial contact. Once the headform was in the correct position, the impact speed was set on the digital control panel of the linear impacting machine. Next, data acquisition was set up using the SLICEWare software. All sensors in the headform went through diagnostics to ensure that no data was collected with a

faulty sensor. All three accelerometers were assigned a 2g (where g = the acceleration of gravity) trigger since 2g was above the noise signal level for the accelerometers. This trigger allowed the SLICEWare software to constantly collect data before an impact occurred, but to only download data that was in an assigned region of interest (+/- 0.5 seconds) around the trigger. After the sensors were armed and waiting for a trigger, the linear impactor was fired using the digital control panel and the impact occurred. Data from the accelerometers and angular rate sensors within the region of interest of the impact were automatically downloaded by SLICEWare. Immediately following the impact, the impactor velocity was displayed on the digital control panel and it was determined whether or not it was within +/- 2% of the desired impact velocity. If the impact velocity was not within the velocity tolerance, the trial was discarded and redone.

Impact testing of cold-conditioned headgears followed the same procedure, with the addition of a temperature measurement step after the sensors were triggered and before the linear impactor was fired. In this step, the exterior temperature of the headgear was constantly monitored until its temperature rose to -0.5 °C. Once this temperature was reached, the button to fire the impactor was pressed. Pressing the button to fire the impactor when the temperature of the headgear was -0.5 °C instead of 0 °C was done because there is a safety-driven delay before the impactor is actually fired after pressing the button. It was assumed that the helmet would only heat up to ~0 °C during the delay time, which was the desired cold-conditioned temperature. The headgears were placed back into the cold-conditioning freezer for a minimum of five minutes in between cold-conditioned trials. A schematic of the linear impactor testing for both ambient- and cold-conditioned testing is shown in Figure 11.

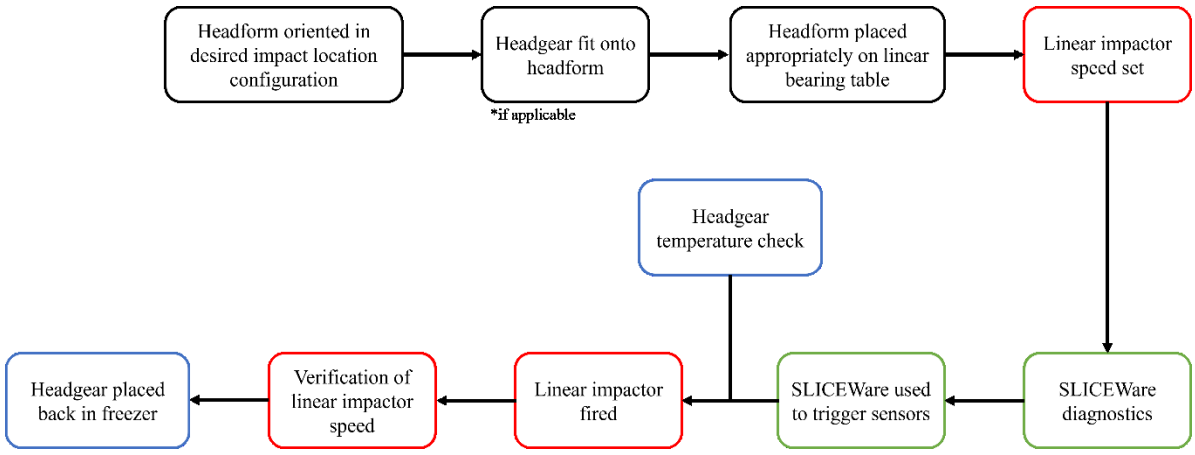

Figure 11 | Linear impactor testing procedural schematic. Black boxes indicate steps involving setup of the headform and headgear, red boxes indicate steps involving the linear impactor, green steps indicate steps involving SLICEWare data acquisition, and blue boxes indicate additional cold-conditioned testing steps.

2.2.2.2 Ball Impact Testing

Ball impact testing utilized the same methodology as the linear impactor testing. However, NOCSAE certified lacrosse balls (used in competition) were used instead of the linear impactor to impact the headform. To administer the lacrosse ball impacts, the Linear Impacting and Projectile Shooting Machine was swiveled into the projectile shooting configuration. Lacrosse ball impact speeds of 13.4 m/s and 27.0 m/s were chosen because they correspond to women's lacrosse passing and shooting speeds, respectively [137]. Also, 27.0 m/s is the impact speed used for the ball impact absorption test in the ASTM F3137-15 standard specification for women's lacrosse headgear [134]. Ball impact speed was measured using a velocity time gate and the impact speeds were considered within tolerance if they were within +/- 3% of the desired impact speed. Since only two impact speeds were tested, each headgear condition had a total of 36 ambient-conditioned impacts instead of the 54 ambient-conditioned impacts for the linear impactor testing. Cold-conditioned lacrosse balls were also used during the cold-conditioned

testing of both headgears. For ball impact testing, an additional step at the end of the experimental procedure was added. A high-speed camera (Apple, Cupertino, CA) was used to record all ball impacts at 120 frames per second. After all impacts, the high-speed recording was used to confirm that the lacrosse ball successfully impacted the impact location. If it was determined that the lacrosse ball did not accurately hit the desired location, the trial was redone.

2.2.3 Data Analysis

All linear impactor and ball impact data processing was conducted using DIAdem (NI, Austin, TX). The first step in data processing was to invert the necessary data channels to align the orientation of the Hybrid III sensor data with that of the Society of Automotive Engineers (SAE) J211-1 axes convention [138], shown in Figure 12.

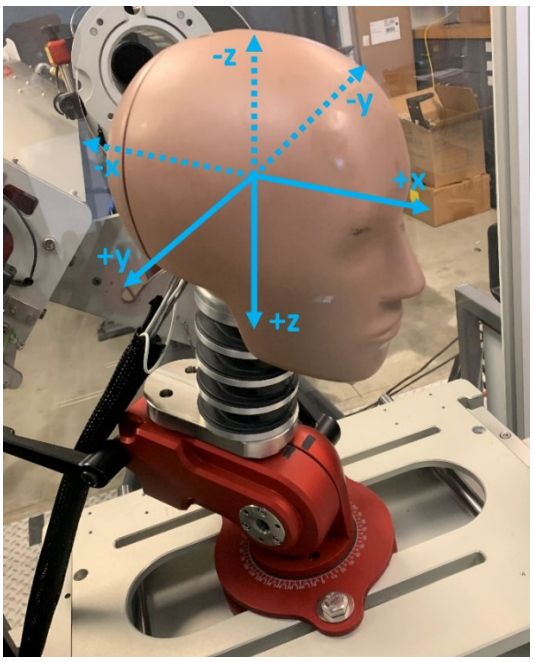

Figure 12 | SAE J211 axes orientation

Once all linear acceleration and rotational velocity data was in the SAE J211 orientation, the data was filtered using DIAdem Crash Analysis Toolkit built-in impact data filters. Linear acceleration data was filtered using the SAE J211 channel frequency class (CFC) 1000 filter, as it is the filter that SAE suggests for filtering linear acceleration impact data. SAE does not specify a filter that should be used for filtering rotational impact data. Therefore, the CFC 60 filter was used to filter rotational velocity data since it has been used to filter rotational impact data in a previous study [99]. After being filtered, rotational velocity data was used to calculate rotational acceleration in DIAdem.

Concussion metrics peak resultant linear acceleration (PLA), peak resultant rotational acceleration (PLA), peak resultant rotational velocity (PRV), head injury criterion (HIC_{15}), and brain injury criterion (BrIC) were calculated using the DIAdem Crash Analysis Toolkit. DIAdem calculates peak resultant metrics using Equation 5

Equation 5 | Peak resultant metric.

$$Peak\ resultant\ metric = maximum\left(\sqrt{x^2 + y^2 + z^2}\right),$$

where x, y, and z are the x-axis, y-axis, and z-axis components, respectively, of linear acceleration, rotational acceleration, or rotational velocity. HIC_{15} was calculated using Equation 2 with a 15 ms time interval. BrIC was calculated using Equation 3.

2.2.4 Statistical Analysis

Comparison of impact metric magnitude statistical analysis was conducted to determine the effects of the two headgears on each impact metric as well as the effect of temperature on each impact metric within headgear. For these analyses, data was either grouped all-together (all three impact speeds and all six impact speeds), grouped by impact speed, or grouped by impact

location to be able to draw specific conclusions from the results. Data was only grouped by impact location for the headgear comparison and not for the temperature comparison since it was not desired to determine the effect that impact location had on the results of temperature comparison.

For statistical analysis, data was first tested for normality to inform what type of statistical test should be done to compare impact metric magnitude between headgears and no headgear. Only data from the all data together grouping method could be tested for normality because of the sample size restriction of the other two grouping methods. The all-together datasets were tested for normality on a 95% confidence interval ($\alpha = 0.05$) using a Chi-square goodness of fit test in MATLAB (MATLAB R2020a; MathWorks, Natick, MA), with the null hypothesis being that the data is normally distributed. These tests all resulted in a p-value below 0.05, indicating that none of the all-together datasets were normally distributed.

Since all types of data grouping were either not normally distributed or did not have a large enough sample size to test the distribution of the data, Mann-Whitney U tests were used to compare the mean between two sets of data. The use of Mann-Whitney U tests was statistically relevant for all grouping types since this statistical test is used for nonparametric datasets, meaning that the distribution either cannot be characterized by common distribution types or is unknown. Statistical significance of the Mann-Whitney U tests was determined on a 95% confidence interval ($\alpha = 0.05$), with a separate test being done for each concussion metric as the dependent variable for every comparison. All Mann-Whitney U tests were conducted in MATLAB (Appendix A, Script 1).

2.3 Results

2.3.1 Headgear Comparison

2.3.1.1 Concussion Metrics at All Impact Speeds and Impact Locations

Impact testing results for the Hybrid III headform with no headgear, with the Cascade headgear, and with the Hummingbird headgear are depicted in Figure 13, Figure 14, and Figure 15 for linear impactor testing and in Figure 16 and Figure 17 for ball impact testing. These figures show the averaged results for each impact speed of linear impactor testing and ball impact testing at all six impact locations, along with an average across all impact locations. Each of these figures contains five subfigures, one for each of the concussion metrics analyzed for this research (PLA, PRV, PRA, HIC, and BrIC). A value for a 50% probability of concussion threshold for each of the concussion metrics is plotted on the figures to give some context about the severity of the impacts according to previous studies. These values correspond to 82 g for PLA [60], 28.3 rad/s for PRV [113], 5900 rad/s^2 for PRA [60], 240 for HIC [60], and 0.50 for BrIC [52]. Table format of the data in these figures can be found in Appendix B. This subsection simply compares mean values to concussion thresholds presented in literature and qualitatively compares these values between headgear types. Statistical significance is addressed in the following subsection.

For linear impactor impacts at 2.2 m/s (Figure 13), none of the averaged impact metrics were above the 50% probability of concussion threshold at any impact location across all three headgear conditions (Cascade, Hummingbird, and No Headgear). This was true for the 2.9 m/s impacts as well (Figure 14), besides all impact locations of the No Headgear condition being above the PLA 50% probability threshold. At 5.0 m/s (Figure 14), the No Headgear values were

above the 50% probability threshold for all concussion metrics at nearly every impact location. For all five metrics, the average across all impact locations for the No Headgear condition was above the threshold. The Cascade and Hummingbird averages across impact locations were only above the 50% probability of concussion threshold for PLA. However, the other metrics had average that were all close to the threshold and had certain impact locations with values above the threshold.

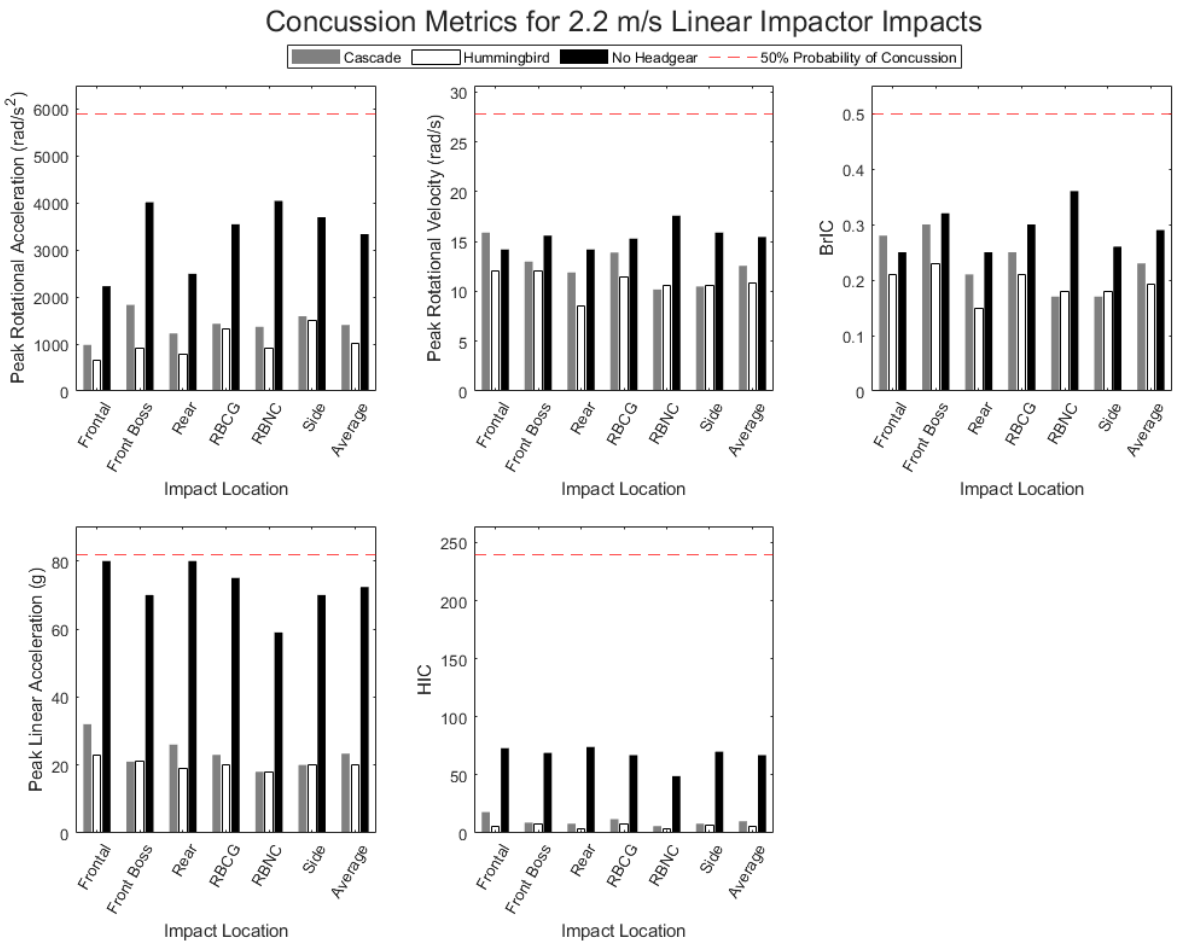

Figure 13 | Averaged concussion metrics at each impact location for 2.2 m/s linear impactor impacts.

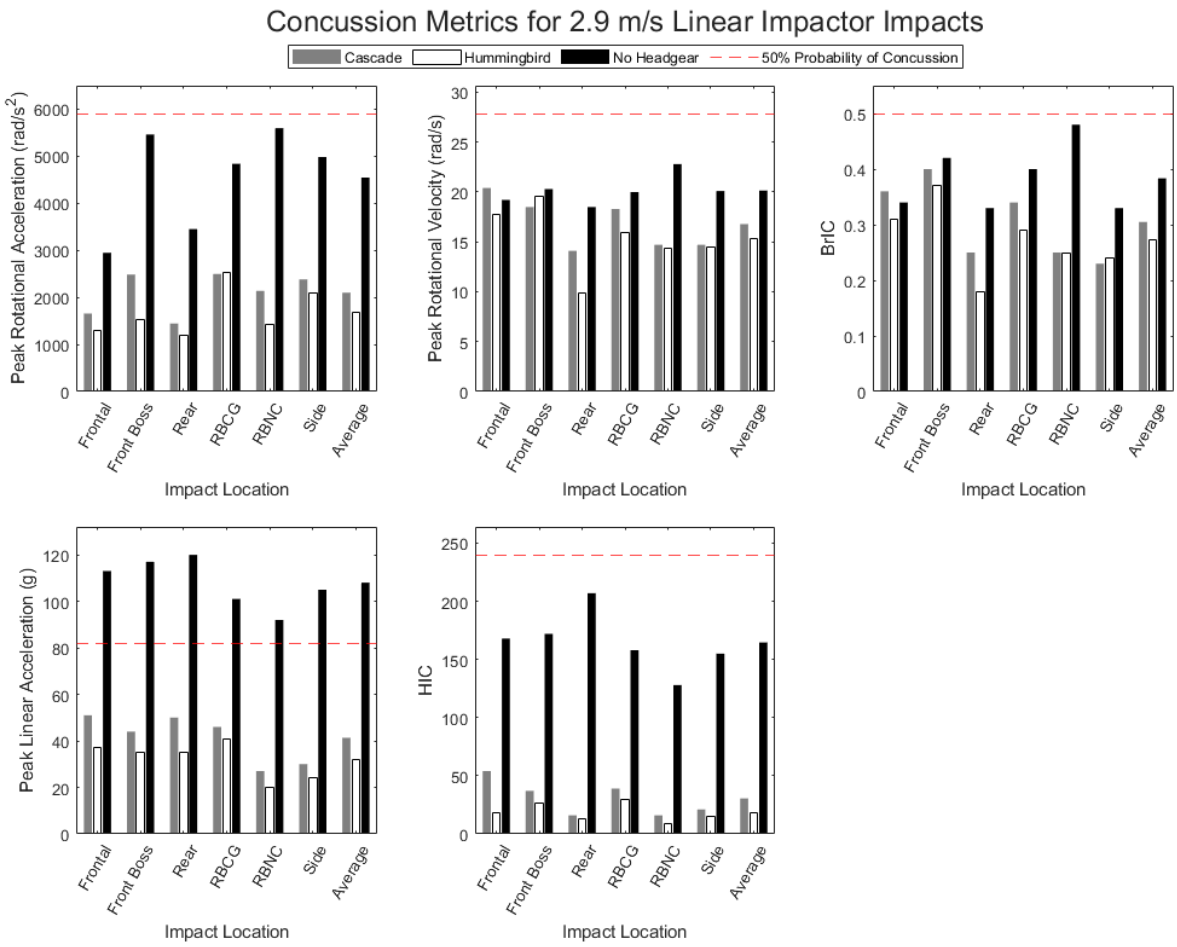

Figure 14 | Averaged concussion metrics at each impact location for 2.9 m/s linear impactor impacts.

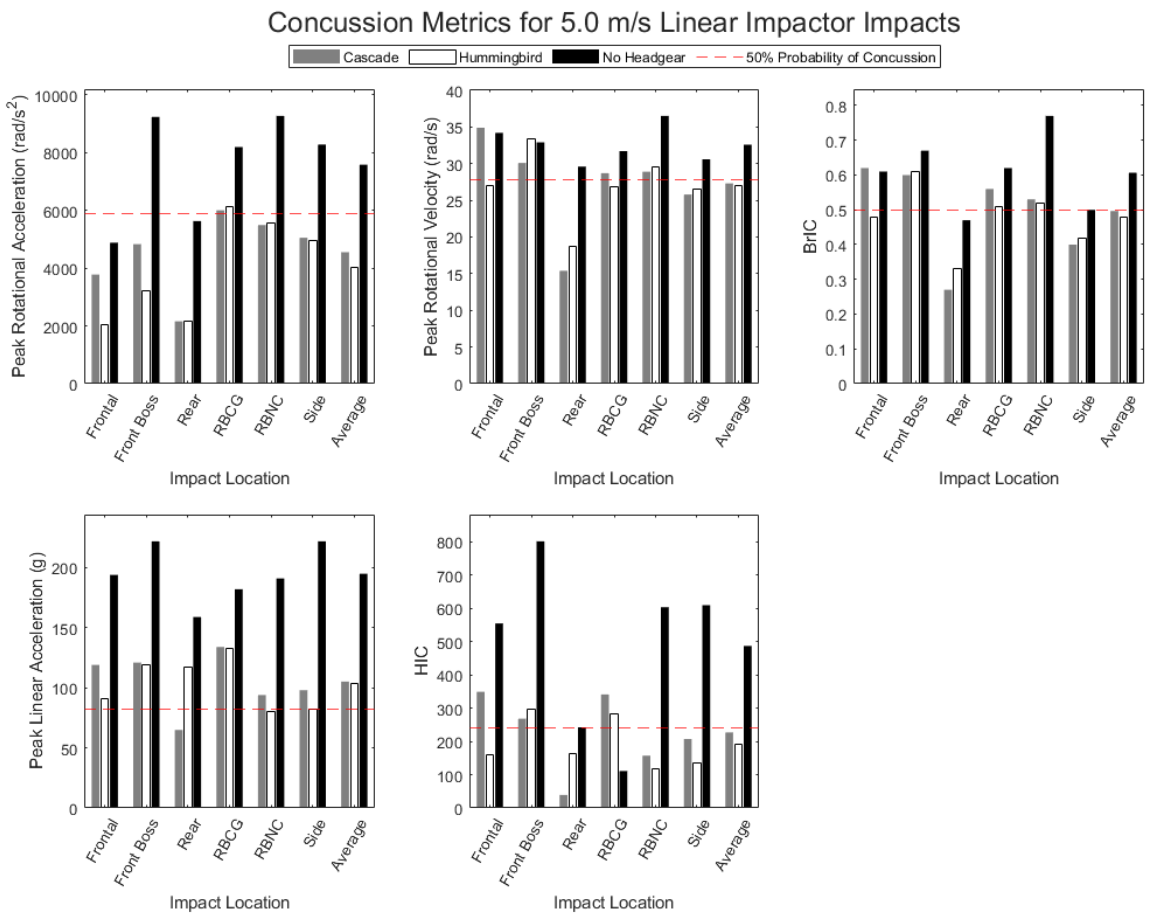

Figure 15 | Averaged concussion metrics at each impact location for 5.0 m/s linear impactor impacts.

For ball impacts at 13.4 m/s (Figure 16), the average value across all impact locations for all five of the metrics for all three headgear conditions was below the 50% probability of concussion threshold. Only the rear impact location for the No Headgear condition had a PLA value above the threshold. At 27.0 m/s (Figure 17), the average across all impact locations was above the PLA 50% probability of concussion threshold for the No Headgear, the Cascade, and the Hummingbird. All other impact locations were below the threshold of all other metrics besides PLA for each headgear condition.

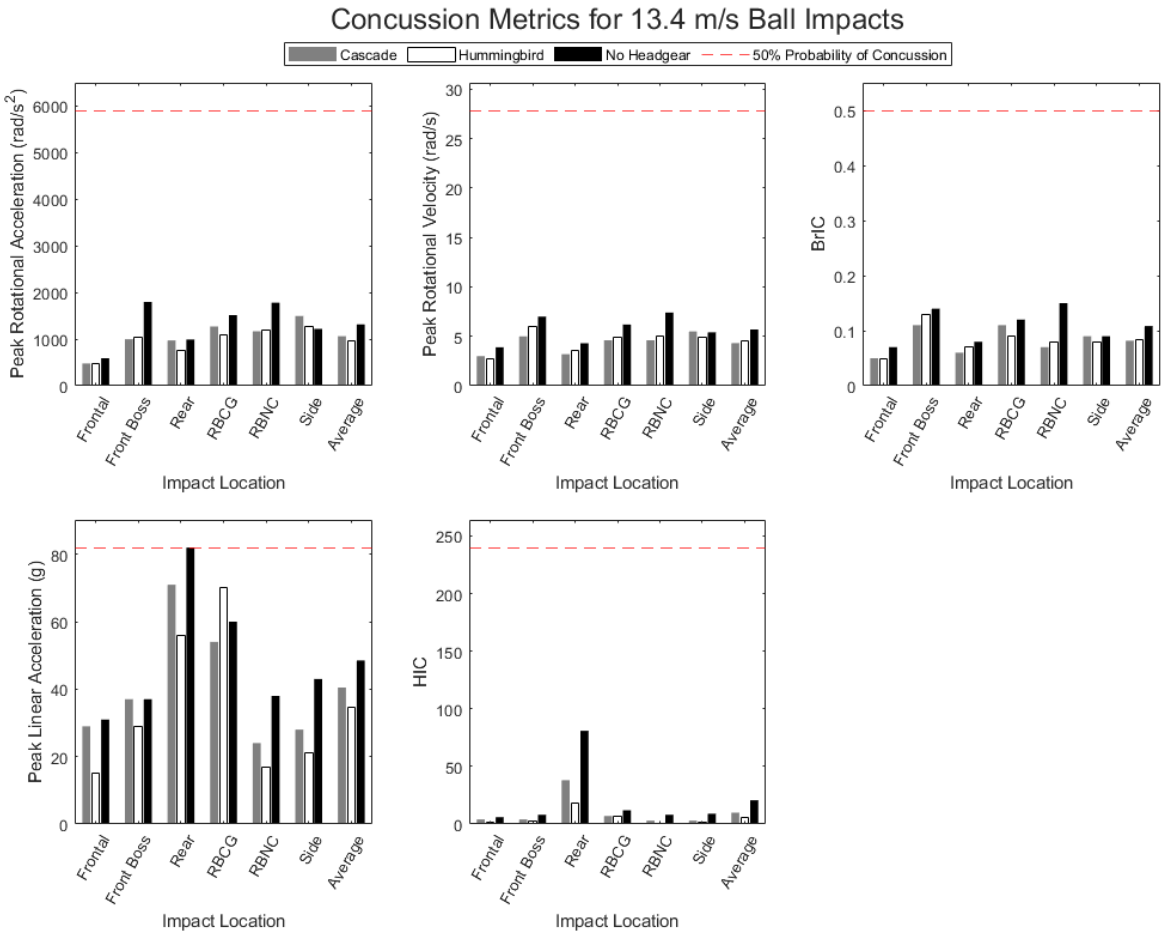

Figure 16 | Averaged concussion metrics at each impact location for 13.4 m/s ball impacts.

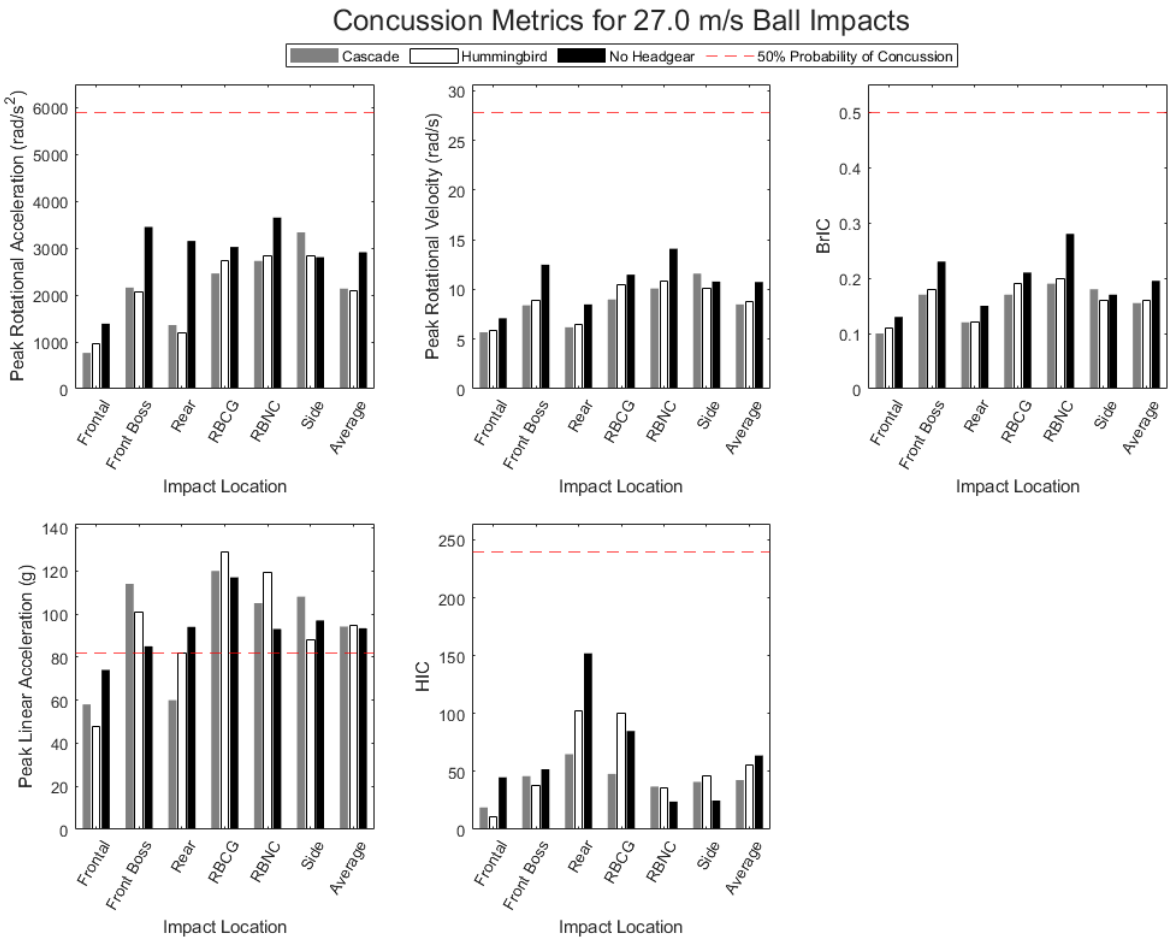

Figure 17 | Averaged concussion metrics at each impact location for 27.0 m/s ball impacts.

2.3.1.2 Statistical Analysis Results

Linear impactor testing Mann-Whitney U test results for comparison between headgear type are shown in Table 15, Table 16, and Table 17 of Appendix C.

Table 15 results come from the comparison of data that was grouped all together, including data from all impact speeds and all impact locations. For this comparison, both the Cascade and the Hummingbird headgears had significantly lower concussion metric values than No Headgear for all metrics. The comparison between both headgears displays that the only

significant difference between the two was for PRA, with the Cascade headgear having the higher mean value.

Table 16 results come from the comparison of data that was grouped by impact speed, with each impact speed group including data from all six impact locations. For this comparison, both the Cascade and the Hummingbird headgears had significantly lower concussion metric values than No Headgear for all metrics at all three impact speeds. Statistically significant differences in metric values occurred between the two headgears for PLA at 2.9 m/s, for PRA at 2.2 m/s and 2.9 m/s, and for HIC at 2.2 and 2.9 m/s. In all of these cases in which the difference was significant, the Cascade headgear had the greater mean value.

Table 17 results come from the comparison of data that was grouped by impact location, with each impact location group including data from all three impact speeds. For this comparison, both the Cascade and the Hummingbird headgears had significantly lower concussion metric values than No Headgear in 23/30 of the comparisons. Interestingly, the seven comparisons in which there was no significance between the headgear and No Headgear were the same for both the Cascade and Hummingbird comparison with No Headgear. There were no concussion metrics at any of the impact locations that had a statistically significant difference between the Cascade dataset and the Hummingbird dataset.

Ball impact testing Mann-Whitney U test results for comparison between headgear type are shown in Table 18, Table 19, and Table 20 of Appendix C.

Table 18 results show the comparison of data that was grouped all together, including data from all impact speeds and all impact locations. For this comparison, the Cascade data had significantly lower values than the No Headgear data for the PRV, PRA, and BrIC metrics. The

Hummingbird data had significantly lower values than the No Headgear data for PRV and PRA. There was no statistically significant difference between the values of any metrics between the Cascade and Hummingbird headgears.

Table 19 results show the comparison of data that was grouped by impact speed, with each impact speed group including data from all six impact locations. For comparison of this data grouping type, the Cascade data had significantly lower values than the No Headgear data at both ball impact speeds for PRV, at 13.4 m/s for HIC and BrIC, and at 27.0 m/s for PRA. The Hummingbird data had significantly lower values than the No Headgear data at both ball impact speeds for PRV and PRA, at 13.4 m/s for PLA and HIC, and at 27.0 m/s for BrIC. There was no statistically significant difference between the values of any metrics between the Cascade and Hummingbird headgears.

Table 20 results show the comparison of data that was grouped by impact location, with each impact location group including data from all three impact speeds. The Cascade headgear data only had significantly lower values than the No Headgear data at the rear impact location for PLA and HIC. There was no statistically significant difference between the values of any metrics at any of the impact locations between the Hummingbird headgear and No Headgear, as well as between the Cascade and Hummingbird headgears.

Interpretations and conclusions that can be drawn from each data grouping method used for the Mann-Whitney U tests are discussed in the following section, section 2.4.

2.3.2 Temperature Comparison

2.3.2.1 Concussion Metrics at All Impact Speeds and Impact Locations

The impact metrics at all impact speeds and impact locations for both headgears at both temperature conditions are shown in Figure 20, Figure 21, Figure 22, Figure 23, Figure 22, Figure 23 Figure 24, Figure 25, Figure 26, and Figure 27. Table format of the data in these figures can be found in Appendix B. Like with the headgear comparison figures, these figures all contain a line for the 50% probability of concussion threshold for each of the concussion metrics that they contain. This subsection simply compares mean values to concussion thresholds presented in literature and qualitatively compares these values between temperature conditions. Statistical significance is addressed in the following subsection.

For the Cascade headgear, the average value at each impact location for both temperature conditions was well below the 50% probability of concussion threshold for 2.2 m/s (Figure 18) and 2.9 m/s (Figure 19) impacts. At 5.0 m/s (Figure 20), both the ambient and cold conditions of the Cascade headgear had several impact locations with concussion metric values above the 50% probability of concussion threshold. For all three linear impactor speeds, the average values across all impact locations for each of the five metrics was greater for the cold temperature condition than it was for the ambient temperature condition.

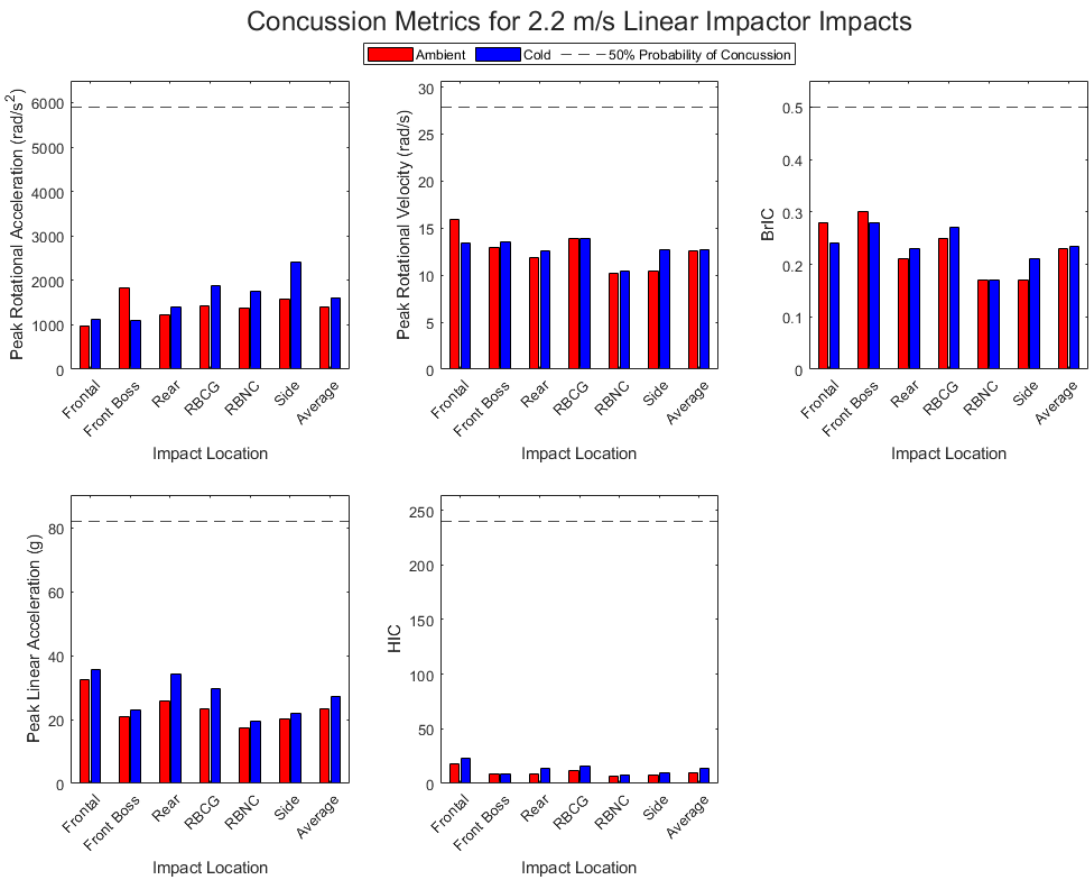

Figure 18 | Averaged concussion metrics at each impact location for 2.2 m/s linear impactor impacts on the Cascade headgear at ambient and cold temperatures.

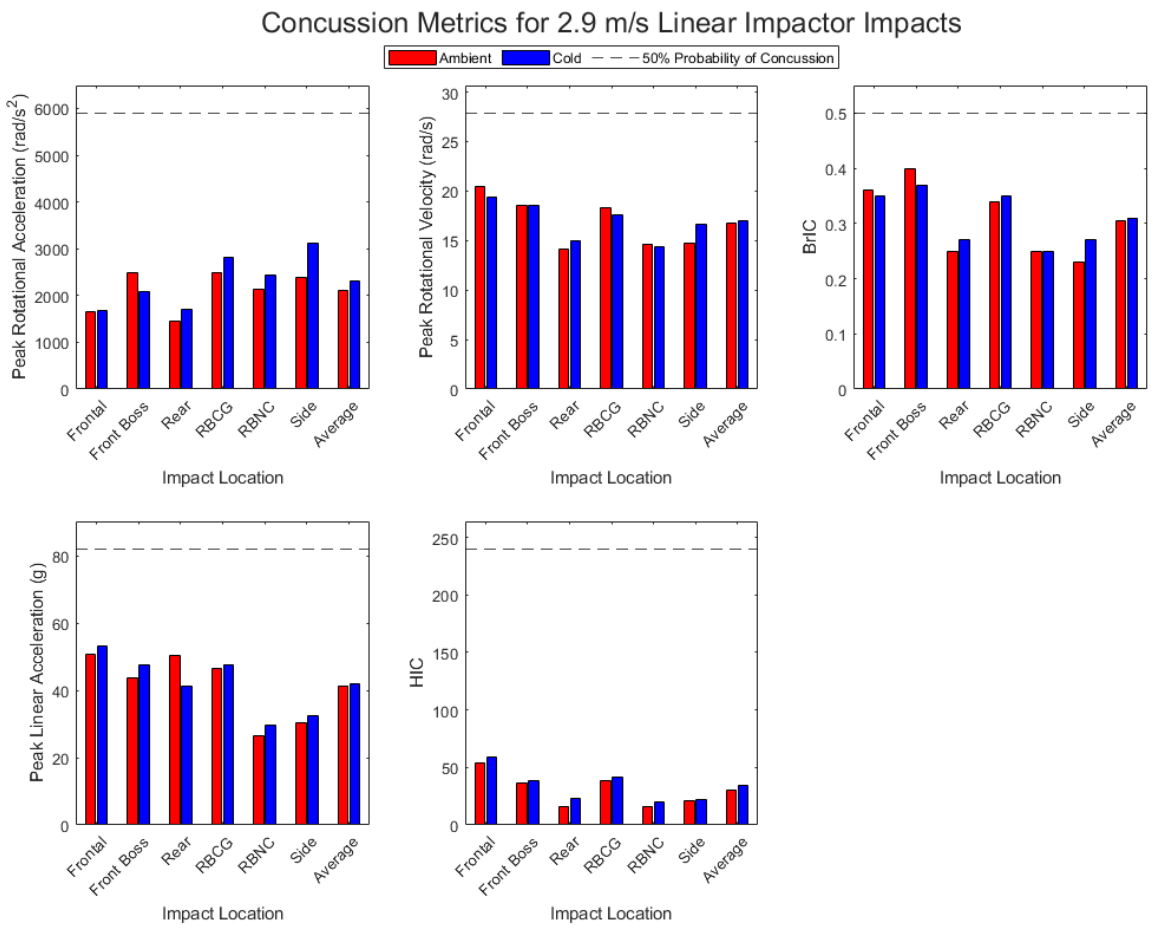

Figure 19 | Averaged concussion metrics at each impact location for 2.9 m/s linear impactor impacts on the Cascade headgear at ambient and cold temperatures.

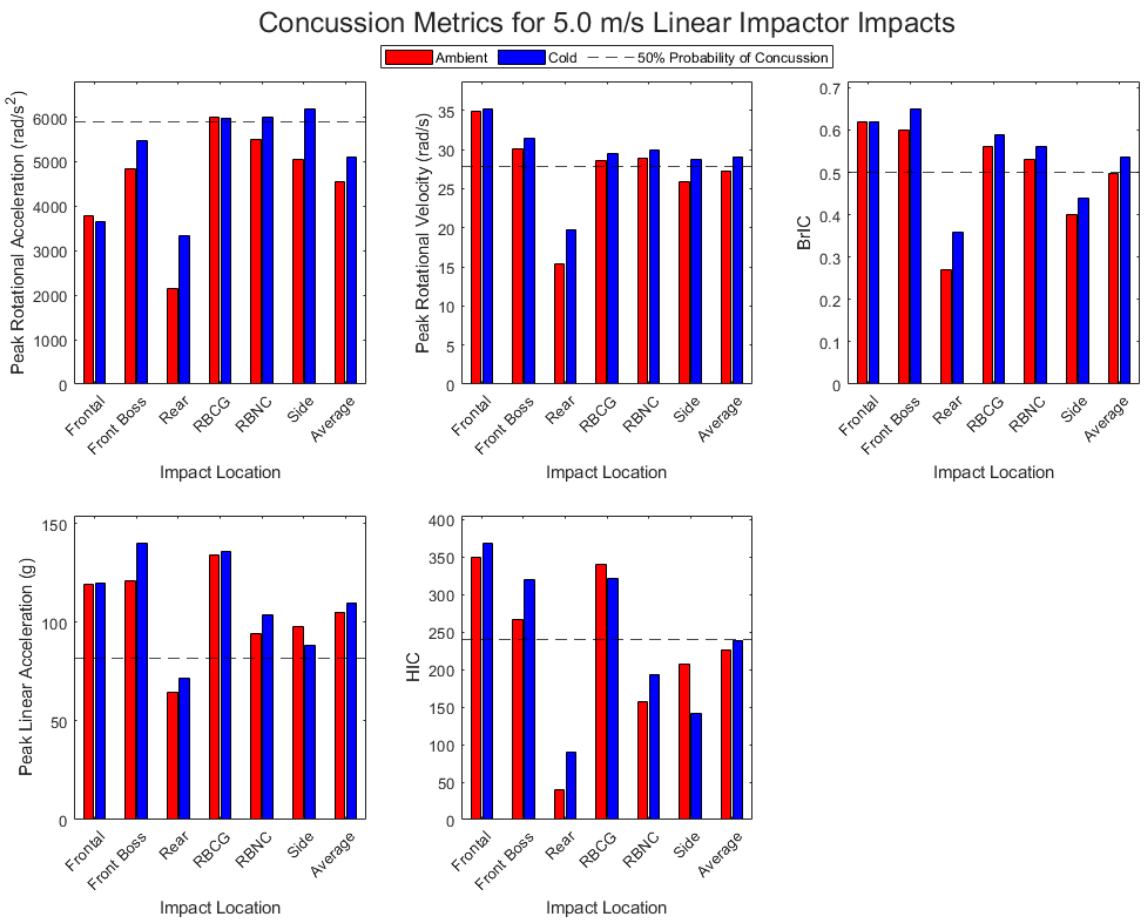

Figure 20 | Averaged concussion metrics at each impact location for 5.0 m/s linear impactor impacts on the Cascade headgear at ambient and cold temperatures.

For the Hummingbird headgear, like with the Cascade headgear, the average values at each impact location for both temperature conditions were well below the 50% probability of concussion threshold for 2.2 m/s (Figure 21) and 2.9 m/s (Figure 22) impacts. For 5.0 m/s impacts (Figure 23), both ambient and cold temperature values were above the threshold for at least one impact location for every metric. However, PLA was the only metric for both ambient and cold conditions in which the average value across all impact locations was above the threshold. The average value across all impact locations was greater for the cold temperature

condition when compared to ambient temperature condition for all five metrics at both 2.2 m/s and 2.9 m/s. For 5.0 m/s impacts, this was only true for PRA.

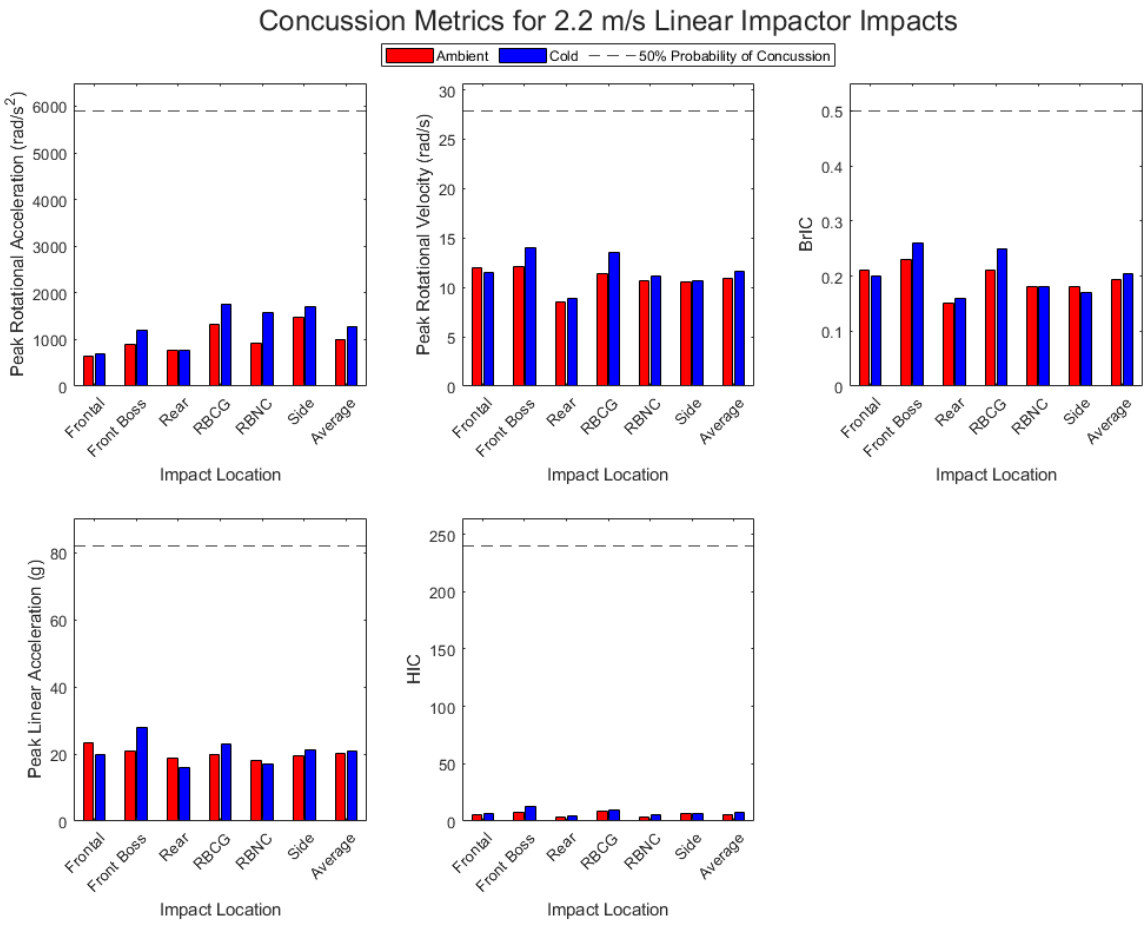

Figure 21 | Averaged concussion metrics at each impact location for 2.2 m/s linear impactor impacts on the Hummingbird headgear at ambient and cold temperatures.

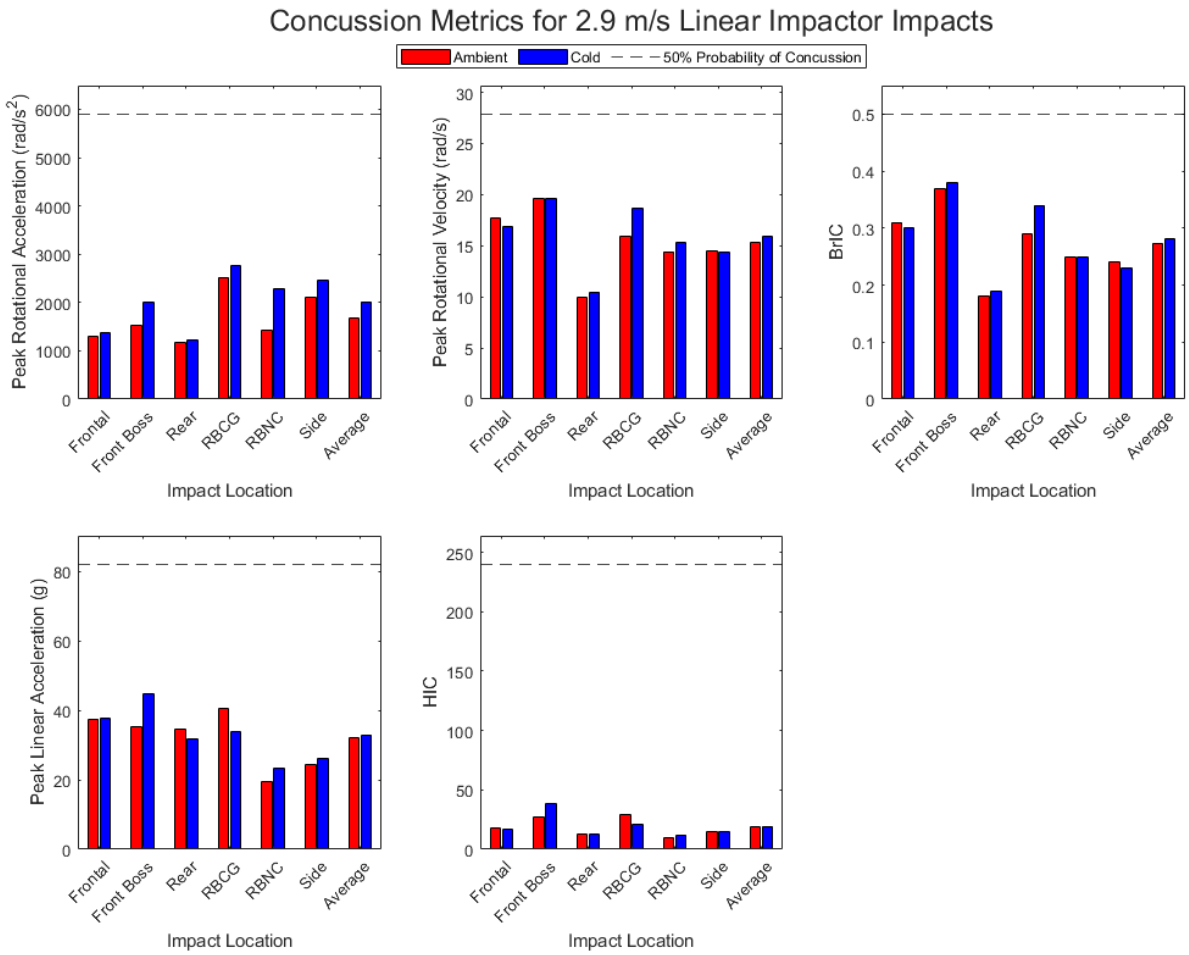

Figure 22 | Averaged concussion metrics at each impact location for 2.9 m/s linear impactor impacts on the Hummingbird headgear at ambient and cold temperatures.

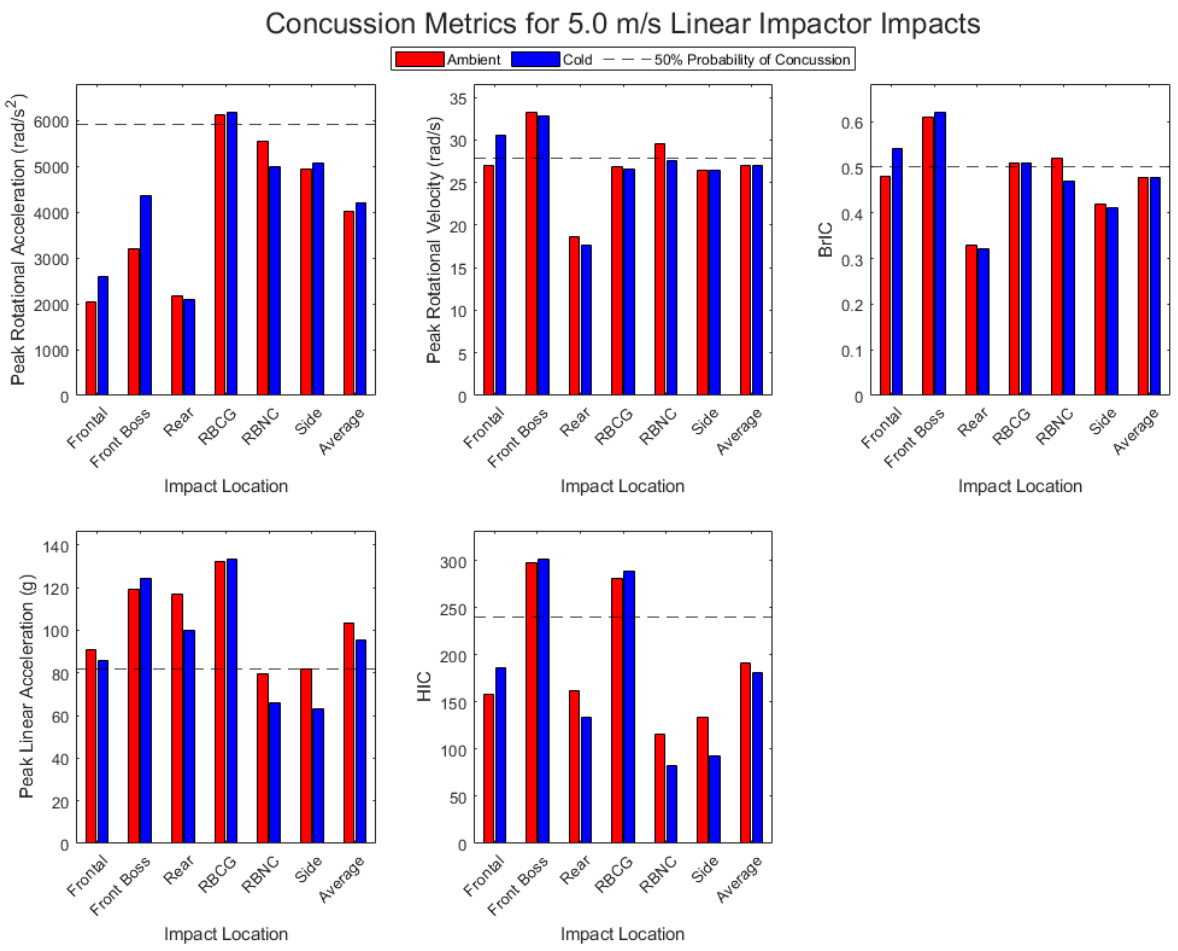

Figure 23 | Averaged concussion metrics at each impact location for 5.0 m/s linear impactor impacts on the Hummingbird headgear at ambient and cold temperatures.

Ball impacts at 13.4 m/s at both temperature conditions for the Cascade (Figure 24) and Hummingbird (Figure 26) headgears resulted in concussion metric values below the 50% probability of concussion threshold for all metrics at all impact locations. Both headgears also had some metrics in which the ambient condition had the greater average across all impact locations and some in which the cold condition had the greater average. For both headgears, PLA had much higher values relative to the threshold than any other metric. This head true for 27.0 m/s impacts as well (Figure 25 and Figure 27), where PLA was the only concussion metric that

had an average across all locations that was above the threshold (for both temperature conditions). Similar to the 13.4 m/s ball impacts, both headgears had some metrics in which the ambient condition had the greater average across all impact locations and some in which the cold condition had the greater average.

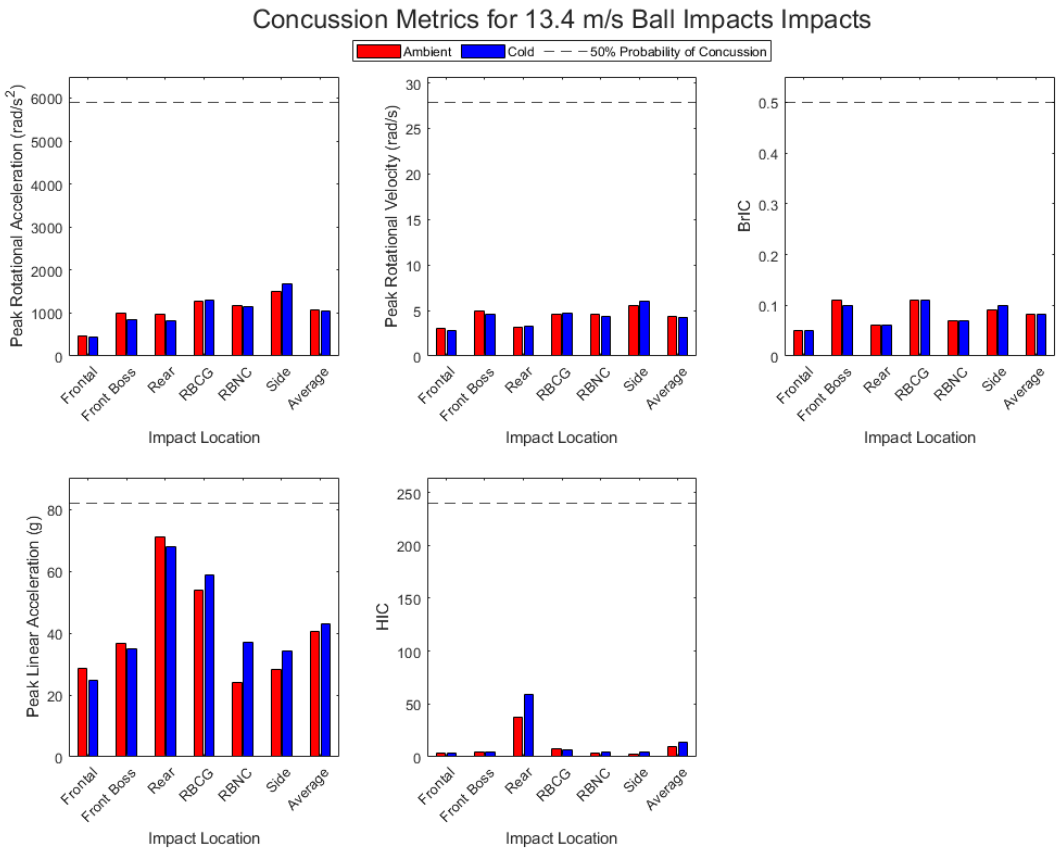

Figure 24 | Averaged concussion metrics at each impact location for 13.4 m/s ball impacts on the Cascade headgear at ambient and cold temperatures.

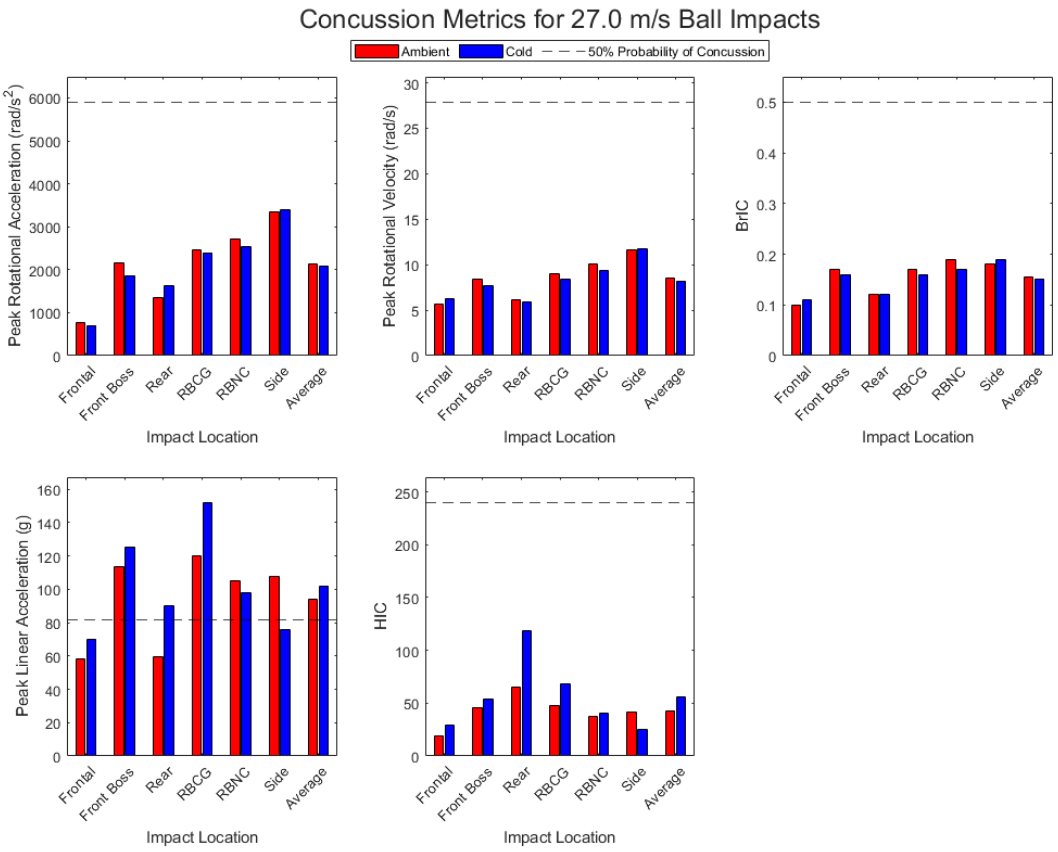

Figure 25 | Averaged concussion metrics at each impact location for 27.0 m/s ball impacts on the Cascade headgear at ambient and cold temperatures.

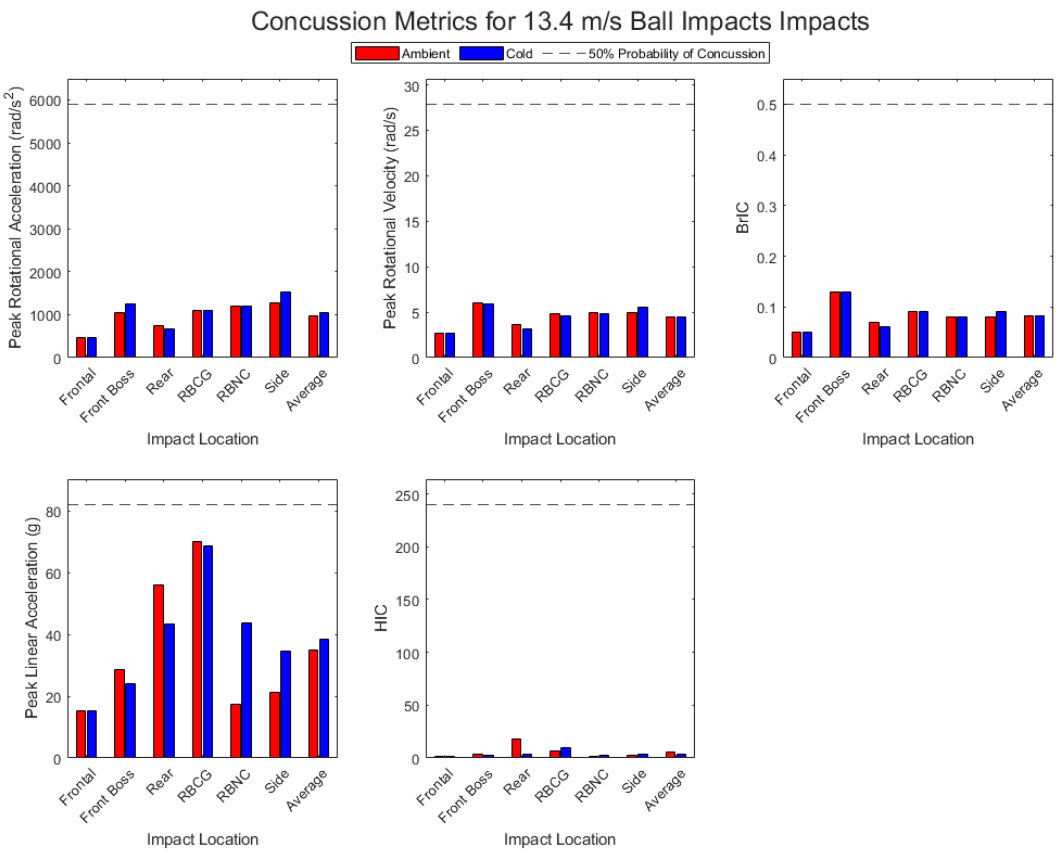

Figure 26 | Averaged concussion metrics at each impact location for 13.4 m/s ball impacts on the Hummingbird headgear at ambient and cold temperatures.

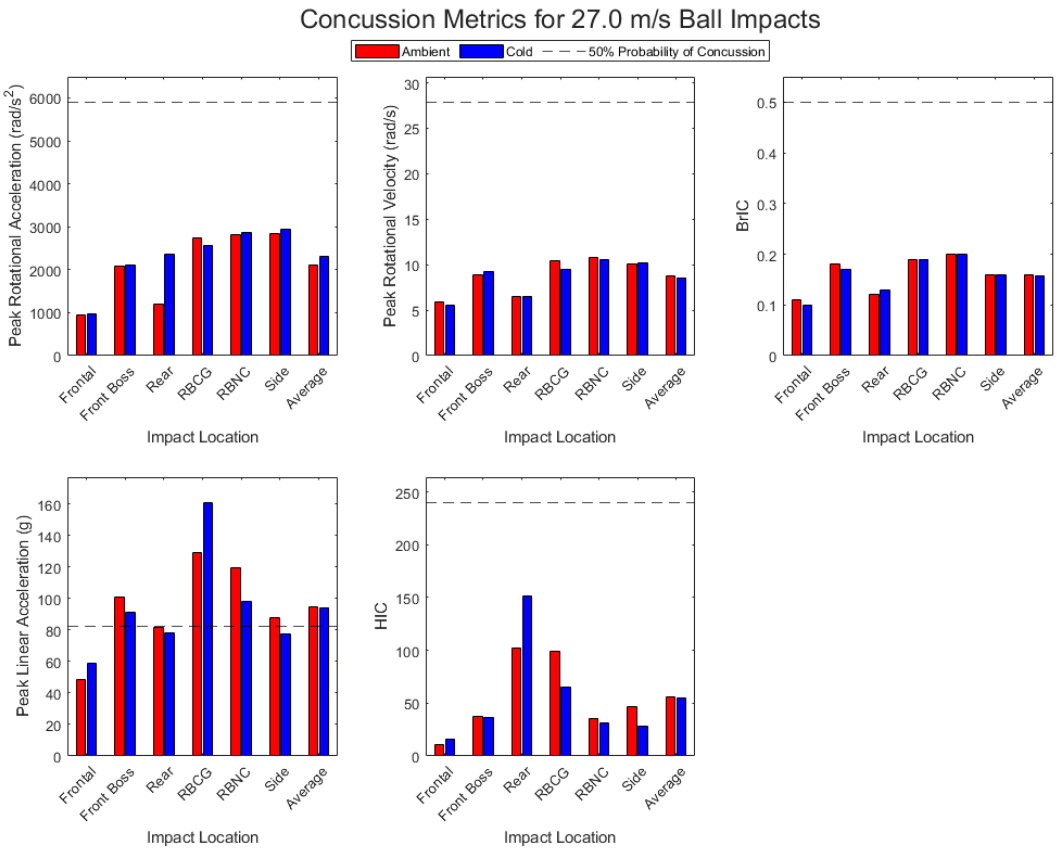

Figure 27 | Averaged concussion metrics at each impact location for 27.0 m/s ball impacts on the Hummingbird headgear at ambient and cold temperatures.

2.3.2.2 Statistical Analysis Results

Mann-Whitney U test results for the comparison of temperature condition of a headgear are shown in Table 21 and Table 22 of Appendix C for linear impactor testing and in Table 23 Table 24 of Appendix C for ball impact testing. When data was grouped all together, for both linear impactor (Table 21) and ball impact (Table 23) testing, there was no statistically significant difference in the values of the ambient and the cold data for both the Cascade and the Hummingbird headgears. This held true for when the data was grouped by impact speed (Table

22 and Table 24), besides the cold condition of the Cascade headgear having a significantly greater value for HIC at 2.2 m/s than the ambient condition.

As with the headgear comparison statistical analysis results, the interpretations and conclusions that can be drawn from each data grouping method used for the Mann-Whitney U tests are discussed in the following section (2.4).

2.4 Discussion

The purpose of this study was to gain insight on the impact mitigation properties of women's lacrosse headgears by addressing the current shortcomings in the impact research that has been conducted on them. To do so, impacts of low and high severity that occur in the sport were tested and rotational velocity-based metrics were included in analysis of the impacts. Furthermore, the effect that cold temperature has on the impact mitigation properties of the headgears was examined.

2.4.1 General Observations of Impacts

Data were grouped by impact speed and impact location for the PLA, PRA, PRV, HIC_{15}, and BrIC concussion metrics. Because the number of impacts for each group of impact speed and impact location was small (n = 3), there were no statistical differences between headgears or temperatures. Although there were no statistical differences, some overall general observations are discussed below.

The Chapter 2 results section compared the severity of concussion metrics at different impact locations and for different headgears, and these severities were compared to the values associated with a 50% probability of concussion threshold from literature in (Figure 14, Figure 15, Figure 16, Figure 17, and Figure 18). These comparisons were made using the grouping

method described above. For linear impactor and ball at each impact location, all five concussion metrics increased as impact speed increased. This is consistent with other studies that have tested multiple linear impactor speeds and/or multiple ball impact speeds relating to women's lacrosse [65], [66], [77]. Linear impactor impacts at 5.0 m/s resulted in the greatest values of all five concussion metrics with no headgear and with both of the headgears.

At all impact speeds, linear impactor concussion metric values for each headgear condition maintained relatively consistent across all impact locations for translational kinematic concussion metrics (PLA and HIC). Conversely, there was a greater variety for rotational kinematic concussion metrics (PRA, PRV, and BrIC) across impact locations. The location of an impact and the angle of the impact source relative to the impact location can greatly influence the resulting rotation of the head, which explains why rotational metrics saw more variation across different impact locations than translational metrics did. Impacts that occurred with the impactor or the ball not on a trajectory to go through the center of gravity of the head (Front Boss and RBNC), or with the head rotated so that one of its main axes was not parallel to the trajectory of the impactor or the ball (RBCG), resulted in the greatest rotational concussion metric values. These impact locations likely exhibited the highest rotational metric values because their orientation in reference to the impact source allowed for the most multi-axial rotation. This multi-axial rotation also explains why the rotational metric values at these impact locations stand out for being greater than the others even more for the BrIC metric, which incorporates rotational velocity values from each of the three orthogonal axes of the headform.

Ball impact concussion metrics followed similar trends as described above for rotational metrics. However, the translational metrics for ball impacts appeared to vary more across impact locations for both impact speeds than they did for linear impactor impacts because these impacts

are highly localized and only occur for a short time duration. Because the impact is so localized and brief, the tilt of the head at a given impact location has a greater effect on the translational metric values. Recall from Table 2 and Figure 10 that the Frontal and Front Boss impact locations both have a 15˚ forward tilt. The forward tilt of the headform allows the neck component to resist translation more effectively than it does in the other impact locations. This is likely why the Frontal and Front Boss impact locations had lower ball impact translation metric values and the Rear and RBCG locations had greater translational ball impact metrics values. It is hypothesized that the neck component's added resistance to translational movement became insignificant as the impact duration increased, which is why there was not as much variation in translational metrics for the longer-duration impacts that the linear impacts administered.

2.4.2 Headgear Impact Mitigation Characterization and Comparison

2.4.2.1 Data Grouped by Each Impact Speed and Impact Location Combination

For 2.2 m/s and 2.9 m/s linear impactor impacts, the mean PLA and HIC values at each impact location were greater for the Cascade headgear than they were for the Hummingbird headgear. This was true for 5.0 m/s linear impactor impacts as well, besides at the Rear impact location (and Front Boss location for HIC). In fact, HIC at the Rear impact location was over twice as high for the Hummingbird and PLA was nearly twice as high. A similar (but less pronounced) trend was seen for ball impacts, especially for 27.0 m/s impacts where it was prominent for the Rear, RBCG, and RBNC impact locations. The ability of the Cascade headgear to better reduce PLA at the Rear impact location at these higher severity impact speeds may be due to its rear component being better coupled with the head than the rear component of the Hummingbird headgear is. The Cascade headgear has a "floating" rear component that is only attached to the rest of the headgear by elastic bands. However, these bands are able to keep the

rear component of the headgear firmly pressed to and coupled with the rear portion of the head. Conversely, the Hummingbird headgear has two flaps at its rear that are buttoned together when the player puts on the headgear. This portion of the Hummingbird headgear is not firmly pressed against the rear portion of the head, allowing the headgear to easily move if impacted hard enough at the rear and sometimes even become unbuttoned. Consequently, the Hummingbird headgear was not able to reduce linear acceleration as effectively as the Cascade headgear at the rear location. Rotational concussion metrics did not exhibit as clear a trend. However, the average rotational metrics across all impact locations was greater for the Cascade headgear for all three linear impactor speeds. For the ball impacts, the Cascade headgear only had an average PRA higher than the Hummingbird whereas for PRV and BrIC it was the Hummingbird that had higher average values.

2.4.2.2 All Data Grouped Together

Impact data was grouped with all impact speeds and impact locations together to allow conclusion to be made about the overall impact mitigation capabilities of each headgear across a variety of impacts and impact locations that a player might be exposed to during competition. In this way, it provides the most comprehensive analysis of headgear impact mitigation properties. When linear impactor data were grouped this way, both headgears significantly reduced all five concussion metrics compared to the headform with no headgear. For the comparison between headgears, the only significant difference was that the Hummingbird had significantly reduced PRA compared to the Cascade. This is in line with previous studies on the impact mitigation properties of these headgears [66], [67]. For ball impacts, both headgears significantly reduced PRV and PRA compared to no headgear, and the Cascade was also able to significantly reduce BrIC. However, neither headgear was able to significantly reduce PLA or HIC. These results

suggest that the Cascade and the Hummingbird headgears may mitigate linear impactor impacts more effectively than ball impacts.

2.4.2.3 Data Grouped by Impact Speed

Comparing headgears in this way can be beneficial because players in women's lacrosse can be impacted at any location on the head at any given time. This data grouping method is visualized as the "Average" bars on Figure 13, Figure 14, Figure 15, Figure 16, and Figure 17.

For 2.2 m/s linear impacts, all five concussion metrics from the no headgear condition were significantly reduced by both the Cascade and the Hummingbird headgears. The ASTM F3137 standard requires that for a women's lacrosse headgear to satisfy the safety requirements, the PLA of a 2.2 m/s impact shock absorption test with the headgear on a headform cannot exceed 80 g. The ASTM shock absorption test consists of a headform being dropped from a certain height, falling uniaxially on a monorail until it impacts a hard surface at the bottom. The drop height is chosen to achieve a desired impact speed right before the headform impacts the bottom surface. The test headform is connected to the monorail via a rigid support arm that is not meant to bend at all like a real neck would during impact. Because the support arm of the shock absorption testing apparatus is rigid, it is thought that the shock absorption test would result in lower rotational metric values and equivalent or lower translational metric values than linear impact testing with the same impact speed. It is noteworthy that although both headgears reduced the PLA of the headform by a factor of three at 2.2 m/s, the headform itself still had a PLA value that was low enough (72.2 g) to pass the ASTM shock absorption test acceptance criterion. This highlights that the ASTM standard for women's lacrosse headgear should incorporate higher impact speeds for its shock absorption test that are more representative of impacts that players will experience while wearing the headgears. Furthermore, including linear impactor testing in

the standard and incorporating rotational concussion metrics could provide even better insight on the impact mitigation and concussion reduction capabilities of the headgears. PRA and HIC were significantly lower at 2.2 m/s impacts for the Hummingbird headgear when compared to the Cascade headgear. The scope of this study was not to identify design components of each headgear that may cause one to mitigate certain concussion metrics more effectively than the other. However, possible reasons for differences in impact mitigation are discussed later in this section.

The Cascade and the Hummingbird headgears were also able to significantly reduce all concussion metrics compared to the no headgear condition at 2.9 m/s linear impactor impacts. The Hummingbird headgear also had significantly lower PRA, PLA, and HIC values than the Cascade headgear. An impacting speed of 2.9 m/s was used in this study to be able to compare with impacts conducted by Bowman et al. Bowman et al. (2020) studied the impact mitigation properties of the Cascade and Hummingbird headgears by conducting impact testing using a pendulum impacting ram on a headform with each of the headgears [67]. They chose impact locations of front, front boss, side, and RBNC because they were deemed to be the most frequently impacted locations on the head for women's lacrosse players by a previous on-field head impact study [139]. A slow (1.5 m/s) and fast (2.9 m/s) impact speed were chosen to result in headform linear acceleration that replicated real, on-field head linear acceleration measurements from impacts to women's lacrosse players [139], [140]. However, the reported headform PLA values from the Bowman et al. impact study for 2.9 m/s impacts were much greater with the headgears on (Avg. PLA = 177.6 g for Cascade, 148.6 g for Hummingbird) than the most severe on-field values were with no headgear on the players (Avg. PLA = ~77 g). The PRA values of the Bowman et al. laboratory experiment were much closer to the reported on-

field head PRA values. The issue with trying to match experimental acceleration values with specific on-field acceleration values is that on-field head acceleration monitoring has been shown to be inherently inaccurate, especially the sensors used on the women's lacrosse players that are not mounted in any type of headgear [95], [96]. This could explain the discrepancies between the PLA and PRA values in this research and those reported by Bowman et al. Although the magnitude of PLA and PRA were much higher for both headgears in the Bowman et al. study than they were in this one, a similar finding was made that the Hummingbird headgear was able to reduce both PLA and PRA at 2.9 m/s more effectively than the Cascade headgear was [67].

Both headgears were able to significantly reduce all five concussion metrics compared to the no headgear condition for 5.0 m/s linear impactor impacts. At this impact speed, there were no concussion metrics that were statistically significantly different in value between the Cascade and the Hummingbird headgears. Currently, this study was the first to examine the impact mitigation of the women's lacrosse headgears at 5.0 m/s linear impactor impacts. However, Clark and Hoshizaki (2016) studied this impact speed on a headform with no headgear and one with a men's lacrosse helmet to determine the potential effectiveness of headgear use in women's lacrosse [68]. This impact speed was supposed to replicate shoulder-to-head impacts like it was in this study. They found that the men's lacrosse helmet was able to significantly reduce PLA of the headform at both a front and side impact location, but that it was not able to significantly reduce PRA at either of the impact locations. One possible reason for the headgears tested in this study significantly reducing the headform's PRA while the men's lacrosse helmet did not is the difference in composition and design of the headgears/helmet. Another possible explanation is that the 5.0 m/s linear impactor impacts in the Clark and Hoshizaki study did not result in nearly as severe of PLA and PRA values as this study did. For the Clark and Hoshizaki

study, PLA and PRA values for the non-helmeted headform were below 25 g and 2500 rad/s^2, respectively, for 5.0 m/s impacts. Conversely, average PLA and PRA values at the same impact speed on the headform with no headgear in this study were 195 g and 7577 rad/s^2, respectively. This highlights the importance of linear impactor testing setup and the importance of including the distance that the impactor can travel after making initial contact with the head and before bottoming out as a parameter. This parameter can greatly influence the resulting concussion metrics of an impact and may explain the differences in values, so future impact studies should include the parameter in their methodology so that impacting conditions can be repeatable across studies.

For 13.4 m/s ball impacts, the Hummingbird headgear was able to significantly reduce all concussion metrics compared to the headform with no headgear. The Cascade headgear only significantly reduced HIC, PRV, and BrIC compared to the no headgear condition. For 27.0 m/s ball impacts, both headgears were only able to significantly reduce PRA and PRV compared to the headform with no headgear. The mean PLA value for 27.0 m/s ball impacts for the Cascade and the Hummingbird headgears were both 94.6 g. This is a surprising finding considering that the ASTM F3137 standard requires that women's lacrosse headgears must be capable of all keeping 27.0 m/s ball impacts below 80 g of PLA. Before the development of the women's lacrosse headgears tested in this study, Rodowicz et al. (2014) studied how soft headgears that are commonly used in women's soccer can mitigate ball impacts at the same speeds as this study [69]. Of the metrics that were calculated for both studies, the soft headgears studied by Rodowicz et al. were only able to significantly reduce HIC at 13.4 m/s. No other metrics at either ball speed were significantly reduced. The discrepancies between the results of the Rodowicz et al. study and the results of this study likely arise from the fact that although the headgears tested

exhibit similar properties (such as a lack of a hard outer shell), they are not the same. In fact, the "headgears" tested by Rodowicz et al. are actually more of padded headbands than they are headgears. There were no statistically significant differences between concussion metrics of the Cascade and the Hummingbird headgears at either ball impact speed.

2.4.2.4 Data Grouped by Impact Location

Another data grouping method that was used in this study was grouping data by impact location, but including data from all impact speeds (of a given impact type, i.e. linear impactor or ball impact). By grouping data using this method, conclusions could be drawn about how well each headgear was able to mitigate impacts at a certain impact location across a variety of impacts that a player may experience while playing women's lacrosse. Statistical significance drawn from this data grouping method should be interpreted with caution because the sample size was still relatively small (n = 9). Therefore, the Mann-Whitney U tests did not have a high level of statistical power for these comparisons to determine statistical significance.

For linear impactor impacts, the Cascade and the Hummingbird headgears both significantly reduced most of the concussion metrics at most impact locations. Interestingly, the concussion metric/impact location combinations that the headgears were not able to significantly reduce were the same for both headgears. These included PRV and BrIC at the frontal, front boss, and RBCG impact location and HIC at the RBCG location. McIver et al. (2019) studied the impact attenuation of the Cascade and Hummingbird headgears using a variety of magnitudes of impulses administered by an impulse hammer [66]. They found that both headgears were able to significantly reduce PLA and PRA values across the variety of impulse magnitudes for each impact location tested (front, front boss, front oblique, side, rear boss, rear oblique, and rear). This finding by McIver et al. is in agreement with the findings of this study that the headgears

significantly reduced PLA and PRA at each impact location compared to the headform with no headgear. Also, McIver et al. noted that the button that holds together the rear part of the Hummingbird headgear broke during some of the rear impacts. This was observed during a rear impact on one of the Hummingbird headgears used in this study as well. Furthermore, the plastic, rear tightening component of the Hummingbird headgear broke during a rear impact on one of the headgears. In total, two Hummingbird headgears had a rear component break. These headgears were not used for further impact testing once they broke. There were no concussion metrics at any of the impact locations that were significantly different between the two headgears. This data grouping method suggests that for that on-field impacts that are similar to the impacts produced by the range of linear impactor impacts in this study, both headgears mitigate impacts most effectively at the side, rear, and RBNC locations.

For ball impacts, the only statistically significant difference for any comparison was that the Cascade had significantly lower PLA and HIC values than the headform with no headgear at the rear impact location. There were no statistically significant differences at any impact location between concussion metrics of the Hummingbird and the headform with no headgear, as well as between the Cascade and the Hummingbird headgears. To date, no laboratory studies have performed ball impact testing on these headgears, so there are no results to compare to.

2.4.3 Headgear Design Comparison

As mentioned earlier, it is not in the scope of this research to determine exactly what design attributes of each headgear cause them to result in differing concussion metric values. However, a few possible explanations based on observations of the headgears and the impacts on them are provided here. The main, significant difference in concussion metrics observed between the two headgears in this study was that the Hummingbird headgear was able to significantly

reduce PRA compared to the Cascade headgear. This difference was especially evident at lower linear impact speeds. Bowman et al. (2020) had a similar finding and hypothesized that the Hummingbird's ability to decrease PRA was a result of its lower level of coupling with the headform [67]. Similar to their study, a noticeable amount of moving and sliding of the Hummingbird headgear was observed during linear impactor impacts. This movement and sliding was not nearly as apparent for the Cascade headgear. Although both headgears fit properly on the headform, the Cascade headgear seems to have a more effective tightening method that allows the player to achieve a better and tighter fit of the headgear onto the head. The Hummingbird sliding more upon impact in a way that is less coupled with the head may cause headgear itself to rotate more than the head does. Though this reduction in PRA seems desirable, it does not result in a significant reduction in PRV compared to the Cascade headgear and may cause a higher probability of different types of head/face injuries to occur [67]. The other main difference in concussion metric reduction between the two headgears was that in general, the Hummingbird headgear was able to reduce PLA and HIC more effectively than the Cascade headgear was. This could be a result of the materials used in each headgear. Specifically, the Hummingbird headgear incorporates Windpact's Crash Cloud^{TM} energy absorption systems. According to Windpact, these systems are highly effective at dissipating impact energy and making the force of an impact less localized. They are often used in sports helmets to reduce both linear and rotational accelerations of impacts, which may be why the Hummingbird headgear generally exhibited lower PLA and PRA values than the Cascade headgear.

2.4.4 Concussion Metric Comparison

Gabler et al. (2016) studied how 15 different kinematic concussion metrics correlated with brain strain, which is a much better predictor of concussion than kinematic concussion metrics are themselves. By analyzing the 15 metrics from 660 different head impacts, a correlation coefficient between each metric and its resulting finite element analysis brain strain was developed. The coefficient of determination (R^2) of each of the kinematic concussion metrics calculated in this study to brain maximum principal strain were 0.778, 0.554, 0.549, 0.119, and 0.017, for BrIC, PRV, PRA, HIC, and PLA, respectively. These kinematic concussion metrics are correlated with brain strain, which is in turn correlated to concussion. This correlation to a correlation makes kinematic concussion metrics inherently inaccurate at predicting concussion. Consequently, caution should be used in drawing any conclusion about how the magnitude of the concussion metrics results from this study relate to concussion thresholds. The reasoning for this is two-fold: (1) the kinematic concussion metrics are merely a loose correlation to concussion and (2) the concussion thresholds themselves are kinematic metrics that are usually determined through laboratory impact reconstruction of sports impacts. Without making any comparisons of the concussion metric values from this study to the 50% probability of concussion thresholds, it can still be noted that both headgears were able to reduce the PLA, HIC, and PRA concussion metrics to a much greater extent than they were able to reduce the PRV and BrIC concussion metrics. This finding suggests that the apparent ability of these headgears to effectively reduce concussions compared to wearing no headgear might be greatly influenced by which kinematic concussion metric is being analyzed. Furthermore, it highlights the importance of incorporating rotational velocity-based kinematic concussion

metrics in headgear and helmet safety standards if it is a goal for them to reduce the likelihood of concussions.

The recent increase in awareness of the influence that rotational kinematic metrics have on concussion and brain injury has sparked research on how helmet design can be changed to reduce head rotation. Vanden Bosche et al. (2017) found that a polyethersulfone foam with anisotropic foam structure was able to reduce the PRA of oblique impacts on a bicycle helmet by about 40% [141]. PLA did not suffer and was actually reduced by around 37%. The anisotropic structure of the foam reduces its shear resistance compared to traditional isotropic foams. This reduction in shear resistance allows the outer part of the headgear to rotate more freely in relation to the head itself, which effectively reduces the amount that the head rotates. Mosleh et al. (2018) found that the shear resistance of composite foams used in headgears can be reduced to lower PRA of the head by using a more compliant matrix for the foam and by using a higher number of lower diameter column [142]. The higher number of lower diameter columns in the composite foam allows it to maintain the same density while reducing shear resistance because it is easier for the thinner columns to bend. Hansen et al. (2013) developed an angular impact mitigation system for bicycle helmets that resulted in a 34% reduction in PRA for oblique impacts by incorporating a loose, sliding layer of material between the outer shell of the helmet and the inner liner [143]. This allowed the outer shell to move and slide when impacted without the whole helmet or the head itself rotating as much.

2.4.5 Temperature Effects on Impact Mitigation

This study was the first study to investigate the effects of cold temperatures on the impact mitigation properties of women's lacrosse headgears. Furthermore, the ASTM standard for women's lacrosse headgears does not require any headgear testing to be performed with cold-

conditioned headgears, so it was not known how these headgears would behave in cold temperatures. The effects that cold temperatures had on the impact mitigation properties of the Cascade and Hummingbird headgears were established by grouping the impact data using he same methods for the headgear impact mitigation characterization and comparison section above, besides the omission of grouping by impact location since it was not desired to know which locations exhibited higher temperature dependence.

Cold temperature conditioning had little to no effect on the concussion metrics that resulted from linear impactor and ball impacts to the head. In fact, the only statistically significant difference was that cold-conditioned Cascade headgears had significantly higher HIC values than the ambient Cascade headgears for 2.2 m/s linear impactor impacts. No other comparisons between headgear temperature conditions were statistically significant for any impact speed or any concussion metric. It is noteworthy to point out that for linear impactor data grouped by impact speed and grouped all together, the mean value for all five concussion metrics was higher for the cold conditioned Cascade headgear than it was for the ambient conditioned headgear. This was also true for most metrics and impact speeds of the Hummingbird headgear. However, for these comparisons, the sample size was too small to determine statistical significance.

Since most sports headgear standards do not require testing in cold conditions, few studies have examined how cold conditioning of a headgear affects its impact mitigation properties. However, one study by Ramirez and Gupta (2018) examined how the PLA of a headform with a Riddell Revolution football helmet differed when the helmet was conditioned at an ambient temperature of 23 ˚C and at a cold temperature of -15 ˚C. They found that PLA increased by 59%, 94%, and 73%, for 2.1 m/s, 3.0 m/s, and 4.3 m/s drop impacts, respectively.

This large reduction in PLA compared to what was seen with the women's lacrosse headgears in this study may be explained by the difference in conditioning temperatures. Furthermore, it is possible that the hard exterior shell of the football helmets greatly contributes to the cold conditioning effects on impact mitigation of the helmets compared to the soft, flexible outer shells of the women's lacrosse headgears.

2.4.6 Limitations

There were several limitations to the methodology of this study. First, impact speeds were determined to replicate common and severe impacts in women's lacrosse. However, these impacts were simplified and idealized by the linear impactor and the projectile shooting machine. Consequently, the impact testing in this study may not be as representative of on-field women's lacrosse related impacts as it was intended to be. Furthermore, since the distance that the linear impactor could travel after making initial contact with the head was not provided from other studies, the impacts in this study may not have necessarily been equivalent to the impacts in previous studies. This was highlighted earlier in this discussion by pointing out the discrepancy in concussion metrics between this study and previous ones that have utilized the same impact speeds.

Another limitation was that the impact locations used in this study were based on a medium sized NOCSAE headform. Measurements for the impact locations on the NOCSAE headform were translated to the 50^{th} percentile male Hybrid III headform used in this study, but it is possible that they were slightly skewed from where they should be in relation to the NOCSAE headform. Also, the headform had to be moved around to different impact locations throughout the study. Every time the headform was moved there was a chance that it was not oriented exactly how it was for previous trials, even though the impact locations were marked,

which could have potentially affected the concussion metrics at a given location. The way in which cold conditioning was done was another limitation of the methodology of this study. Before cold-conditioned headgears were tested, their external temperature was constantly checked until it was at -0.05 ˚C. However, it was unknown what the temperature of the more inner materials was or what the internal temperature of each material was. Ideally, impact testing would have been conducted in an environment that was 0 ˚C, but this was not possible.

The sample size of impacts at each impact speed and each impact location limited the statistical analysis capabilities of this study. At a given impact speed, impact location, and temperature condition there were only three trials. This sample size was too small to have a high enough statistical power when comparing between two groups that only had three trials available, so data had to be grouped together as described earlier in this section for statistical analysis. Future impact research should ideally be conducted so that each condition has a sample size of at least thirty.

As discussed earlier in this section, the results and conclusions that can be drawn from this study are inherently limited by the limited relationship between kinematic concussion metrics and concussion itself. Future studies on the impact mitigation of women's lacrosse headgears should use finite element analysis to gain further, more accurate insight on how they are able to protect against concussion. This will be discussed in further detail in the next chapter.

Chapter 3: Material Testing

3.1 Introduction

The ability of a headgear to reduce the severity of an impact is largely dependent on the materials it is made of. Consequently, material consideration is an important part of headgear design and can drastically affect the performance of the resulting headgear. Headgears used for sports applications commonly incorporate polymer foams (i.e. thermoplastic polyurethane (TPU), polypropylene, polyethylene, etc.) that are highly elastic and energy absorbing [144], [145]. These characteristics generally allow headgears to sustain a high number of impacts without its performance diminishing and to transfer significantly less contact force to the head than the initial force of the impact.

The ability of polymer foams to effectively protect against sports-related impacts comes in part from their strain rate dependent stress-strain behavior. A material that does not exhibit strain rate dependence has a compressive stress-strain curve that is not altered by the rate of the impact. Conversely, a material that exhibits strain rate dependence, like the polymer foams used in sports headgears, has a stress-strain curve that is altered by the rate of the impact. Strain rate dependent foams generally have a stress-strain curve that essentially "shifts" as the strain rate increases, with the slope of the initial linear elastic region of the curve increasing as strain rate increases and the plateau region of the curve occurring at a greater stress level as the strain rate increases. Strain rate dependence is an important property of the polymer foams used in sports

headgears because it allows the headgear to dissipate the same amount of energy at a lower level of contact stress to the head when the strain rate is low.

Another factor that can influence the stress-strain curve of a material is temperature. The stress-strain curves of the polymer foams used in sports headgears have been shown to have "shifted" stress strain curves at different temperatures, with the curves at lower temperatures being shifted upward (greater initial slope and greater plateau region stress) [129]–[132].

The purpose of this study was to establish a general mechanical characterization of the materials that the Cascade and the Hummingbird headgears are made of. This characterization incorporated stress-strain behavior, energy dissipation, and tangent modulus behavior at multiple strain rates. A secondary purpose was to determine how cold temperatures affect the characterization of these materials.

3.2 Methodology

3.2.1 Test System Overview

Compressive material testing was done on each of the materials that the Cascade and the Hummingbird headgears are composed of. For the Cascade headgear, this included an inner black, inner gray, outer gray, outer white, and yellow material (Figure 28a). For the Hummingbird headgear, this included an inner black, inner charcoal, and outer white material (Figure 28b). Materials were named by location and color because it was not known exactly what polymers the materials were made of since that is proprietary information specific to each headgear.

Figure 28 | Tested materials of the (a) Cascade headgear and the (b) Hummingbird headgear.

Uniform test specimens of each material, shown in Figure 29, were cut out using a custom guillotine and drilling method. Although there was not a uniform diameter and thickness across all materials, each individual material did have a relatively uniform diameter and thickness for its own test specimens.

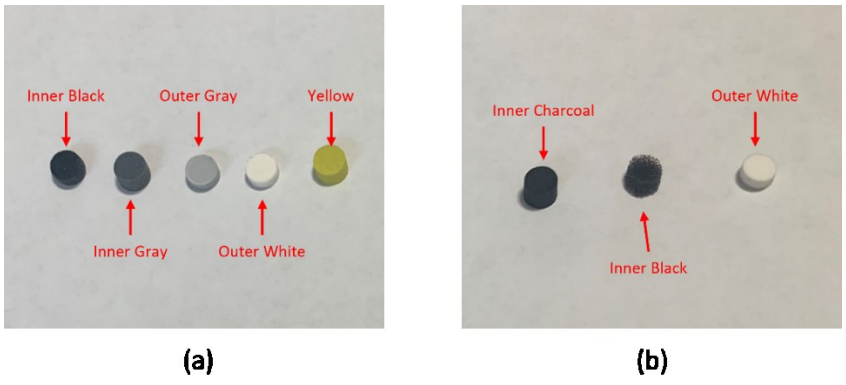

Figure 29 | A representative image of the material test specimens from the (a) Cascade headgear and the (b) Hummingbird headgear.

All materials were tested at two quasi-static strain rates, 0.01/s and1/s, and one dynamic high strain rate of about 100/s. Quasi-static rate compressive material testing was conducted using Model 100-Q-225 uniaxial test machine systems (TestResources Inc., Shakopee, MN), shown in Figure 30a. These systems use an actuator to maintain a constant compressive velocity and therefore a constant strain rate. The 100/s strain rate testing system, shown in Figure 30b, uses pressurized air to drive a striker piston into an incident bar and plate. The incident bar then compresses the test specimen against a force transducer.

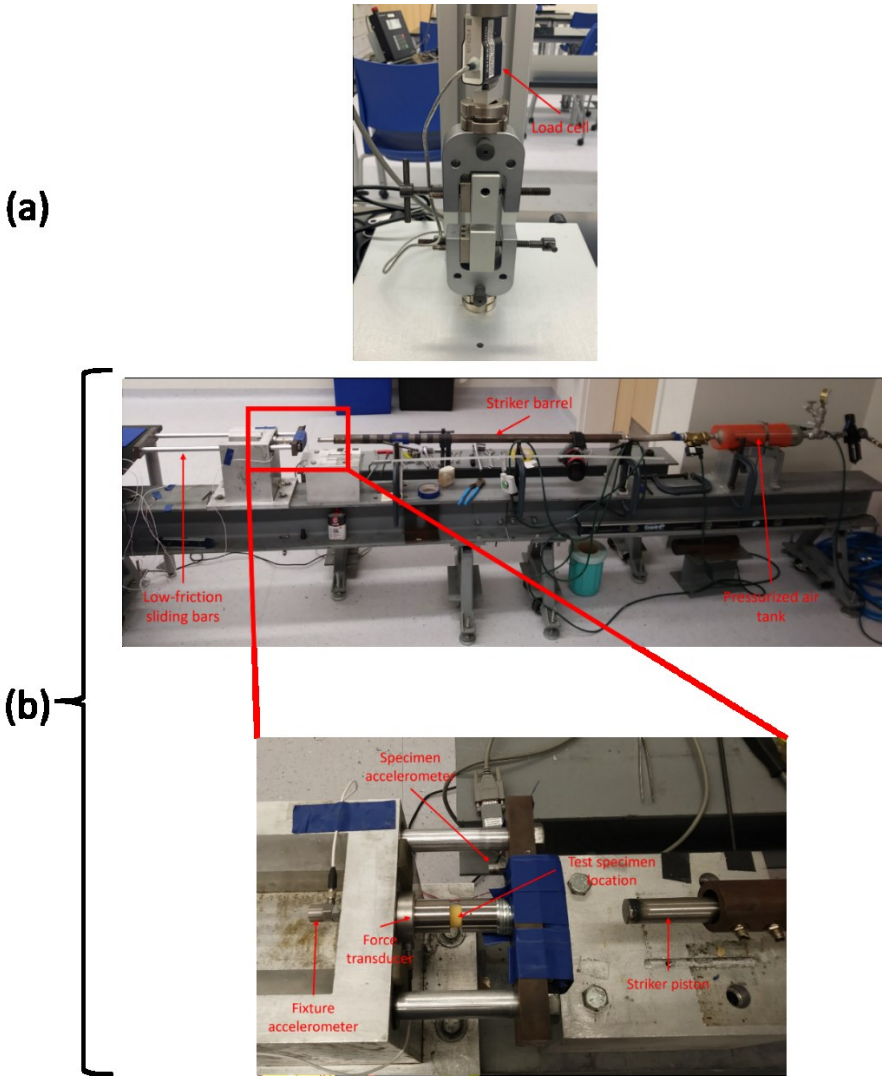

Figure 30 | Pictures of (a) the quasi-static compressive test system and (b) the high-rate compressive test system.

3.2.2 Experimental Procedure

3.2.2.1 Quasi-Static Rate Testing

Prior to quasi-static rate compressive material testing, the thickness and diameter of each test specimen was measured using a digital caliper. The original thickness of each test specimen was used to calculate the test machine velocity that was required to achieve the desired strain rate via Equation 6,

Equation 6 | Strain rate equation.

$$\dot{\varepsilon} = \frac{v}{L_0} ,$$

where $\dot{\varepsilon}$ is strain rate, v is velocity of the test machine, and L_0 is the original thickness of the test specimen. The testing velocity was adjusted accordingly before each test specimen was tested to ensure that it was being tested at the desired strain rate.

Three test specimens were tested at each of the two quasi-static strain rates for all materials. In every test, the test specimens were compressed to 75% strain. Displacement data from the uniaxial test machine and force data from the load cell were recorded at a rate of 25 Hz for the 0.01/s strain rate tests and 1 kHz for the 1/s strain rate tests.

3.2.2.2 High-Rate Testing

For high-rate testing, only the outer materials of the Cascade (outer gray and outer white) and Hummingbird (outer white) headgears were tested. Before testing, the thickness and diameter of each test specimen were measured using a digital caliper. Unlike the quasi-static rate testing, the high-rate testing does not compress the sample at a consistent strain rate since it does not use an actuator that adjusts the compressive force to maintain a constant velocity. Instead, the strain rate changes as a function of displacement (or strain) of the test, as shown in Figure 31.

Preliminary trials were conducted on each of the three material types used for high-rate testing to determine what air pressure was needed to achieve an average strain rate of roughly 100/s.

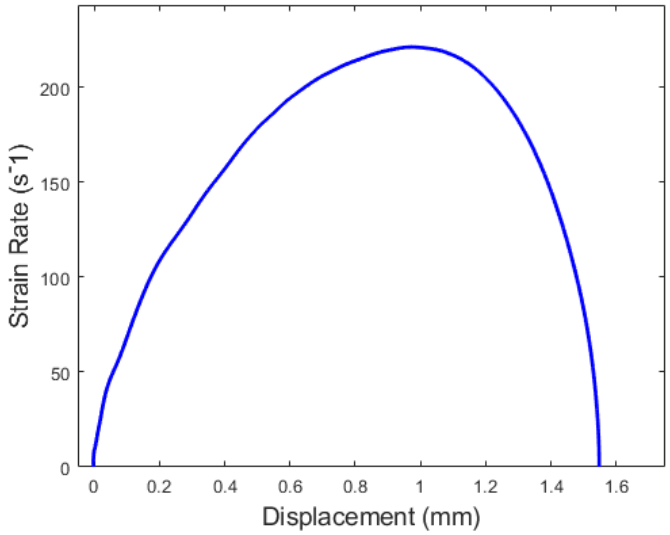

Figure 31 | An example of the strain rate as a function of displacement for the high-rate material testing.

Three test specimens of each of the three outer materials were tested for high-rate tests. The tests were not carried out to a specific strain like with the quasi-static tests since the distance of compression could not be preset. Instead, the level of compression was dependent on the material being tested. An OROS model OR-35 four channel analyzer and data acquisition system and OROS NVGate software were used to acquire data at 25 kHz. The four channels of data collected were time, specimen acceleration, fixture acceleration, and force. Data was collected in a time interval surrounding the impact of the striker rod into the incident plate/rod, triggered by a 0.5 N force transducer reading.

3.2.2.3 Cold-Conditioned Testing

The quasi-static rate and high-rate testing described above were repeated for test specimens that were cold-conditioned. Test specimens were cold-conditioned to freezing

temperature (roughly -5 ˚C) in a lab freezer (Hampton, NH) for at least one hour prior to testing to replicate the amount of time that women's lacrosse players would be in cold conditions for games or practices. Test specimen exterior temperature was checked before testing occurred. Since the exterior temperature of the test specimens was never at or below 0 ˚C when pulled from the freezer, testing was initiated as soon as possible after removal of the test specimen from the freezer instead of waiting for the exterior temperature to reach 0 ˚C like with the headgear impact testing.

3.2.3 Data Analysis

All data analysis was performed in MATLAB using custom scripts (Appendix A). Stress-strain curves were created for each test using the data acquired from testing. First, displacement data was used to calculate engineering strain via Equation 7.

Equation 7 | Engineering strain equation.

$$\varepsilon = \frac{d}{L_0}$$

where:
- ε is engineering strain
- d is displacement
- L_0 is original thickness of specimen

For the quasi-static tests, displacement data was directly recorded by the uniaxial test machine. For the high-rate tests, displacement of the test specimen was calculated by integrating the acceleration of the incident plate/rod twice. The displacement of the test fixture was calculated the same way using the fixture acceleration data and then was subtracted from the specimen displacement to negate any displacement that resulted from the movement of the fixture. Engineering stress was then calculated using Equation 8.

Equation 8 | Engineering stress equation.

$$\sigma = \frac{F}{A_0}$$

where:

σ is engineering stress
F is force
A_0 is original cross-sectional area of specimen

All stress-strain data was filtered using a low-pass filter. Three different low-pass filters were created based on the sampling rate from each strain rate's test. The order of each filter, determined through trial and error, was set so that the derivative of each stress-strain curve was as smooth as possible while not sacrificing the shape of the stress-strain curve. An example comparison of the stress-strain curve created from raw and from filtered data is shown in Figure 32a. If pseudo-strain was present in a trial, shown in Figure 32b, it was removed.

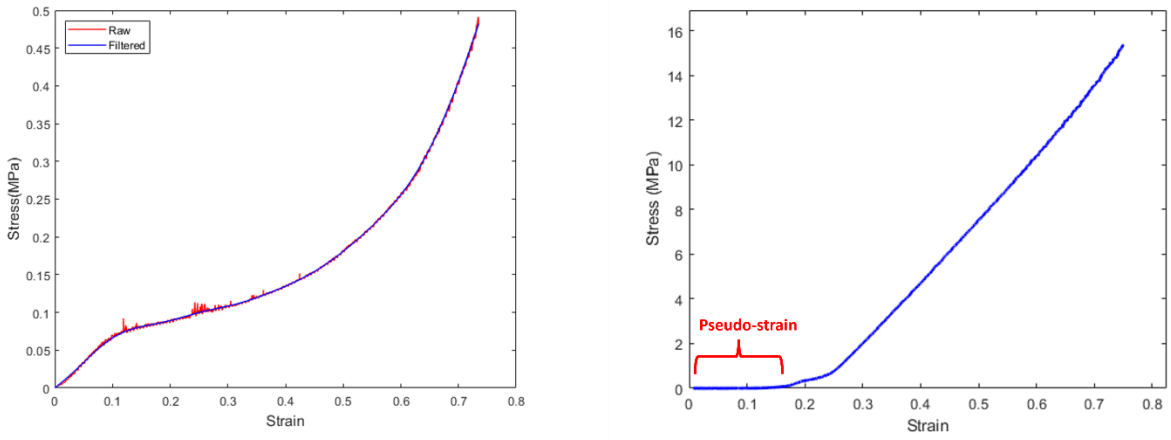

Figure 32 | An example trial (a) stress-strain data filtering and (b) pseudo-strain.

Energy dissipation per unit volume and tangent modulus were calculated from stress-strain data using Equation 9 [146] and Equation 10, respectively.

Equation 9 | Energy dissipation per unit volume equation.

$$e = \int_0^{\varepsilon} \sigma(\varepsilon) d\varepsilon$$

where: e is energy dissipation per unit volume
σ is engineering stress
ε is engineering strain

Equation 10 | Tangent modulus equation.

$$T = \frac{\sigma_{n+1} - \sigma_n}{\varepsilon_{n+1} - \varepsilon_n} = \frac{\Delta\sigma}{\Delta\varepsilon}$$

where: T is tangent modulus
σ is engineering stress
ε is engineering strain
n is the index of a stress-strain data point

3.3 Results

Averaged stress-strain curves, energy dissipation curves, and tangent modulus curves for each material at each of the tested strain rates and temperature conditions are shown in Figure 33, Figure 34, and Figure 35, respectively.

Stress-strain data for each plot was truncated at the minimum-maximum strain value from all trials incorporated in the plot to compare to a uniform compression level across the conditions being analyzed (since some trials had pseudo-strain). Accordingly, only the available data up to the strain truncation point of each plot was used in the creation of the averaged energy dissipation plots and the averaged tangent modulus plots. The data in those plots were then also truncated to the minimum-maximum value of the available x-axis data.

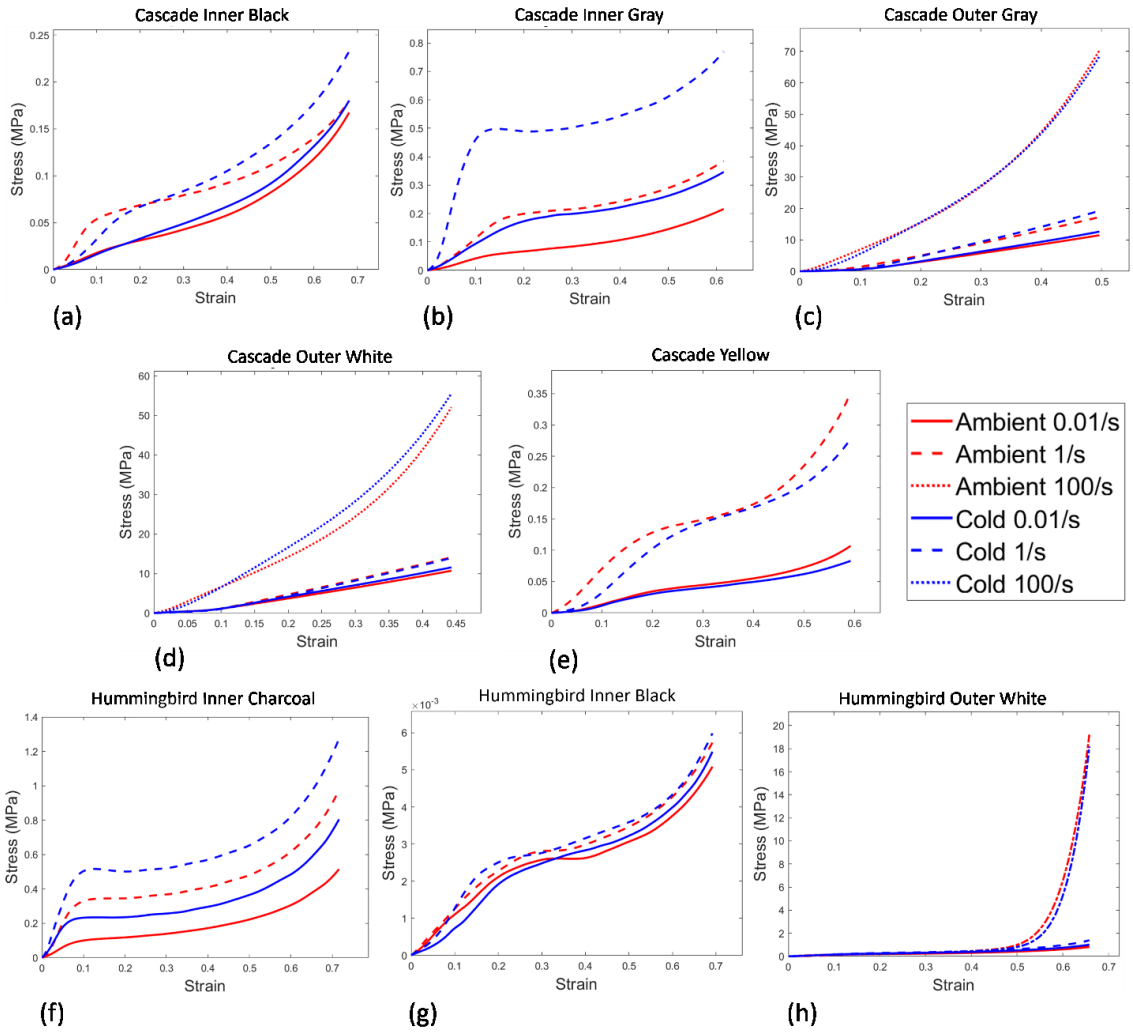

Figure 33 | Average stress-strain curves for the Cascade (a) Inner Black, (b) Inner Gray, (c) Outer Gray, (d) Outer White, and (e) Yellow materials and the Hummingbird (f) Inner Charcoal, (g) Inner Black, and (h) Outer White materials. Note, only the outer materials were tested at 100/s strain rate.

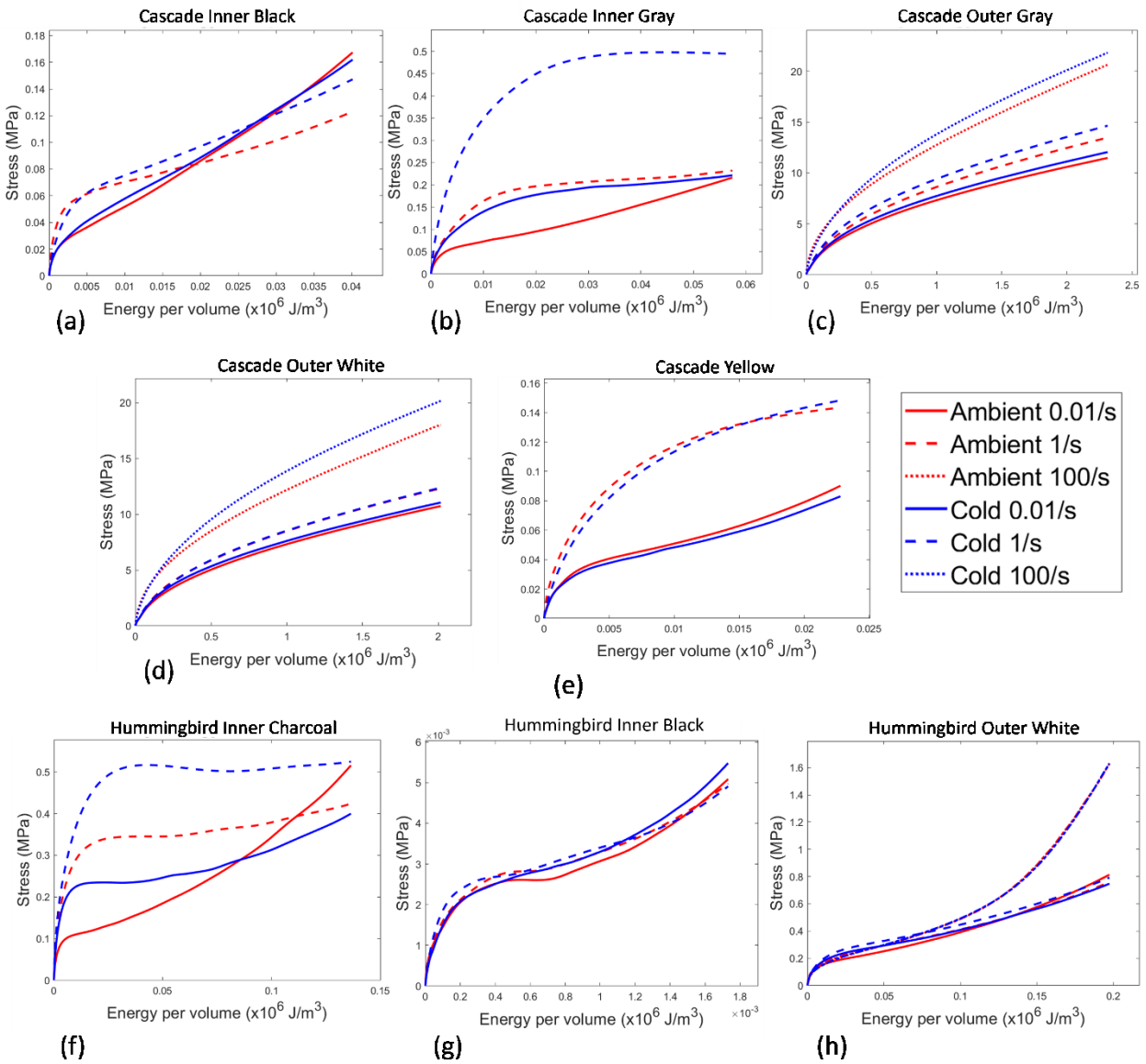

Figure 34 | Average energy dissipation curves for the Cascade (a) Inner Black, (b) Inner Gray, (c) Outer Gray, (d) Outer White, and (e) Yellow materials and the Hummingbird (f) Inner Charcoal, (g) Inner Black, and (h) Outer White materials. Note, only the outer materials were tested at 100/s strain rate.

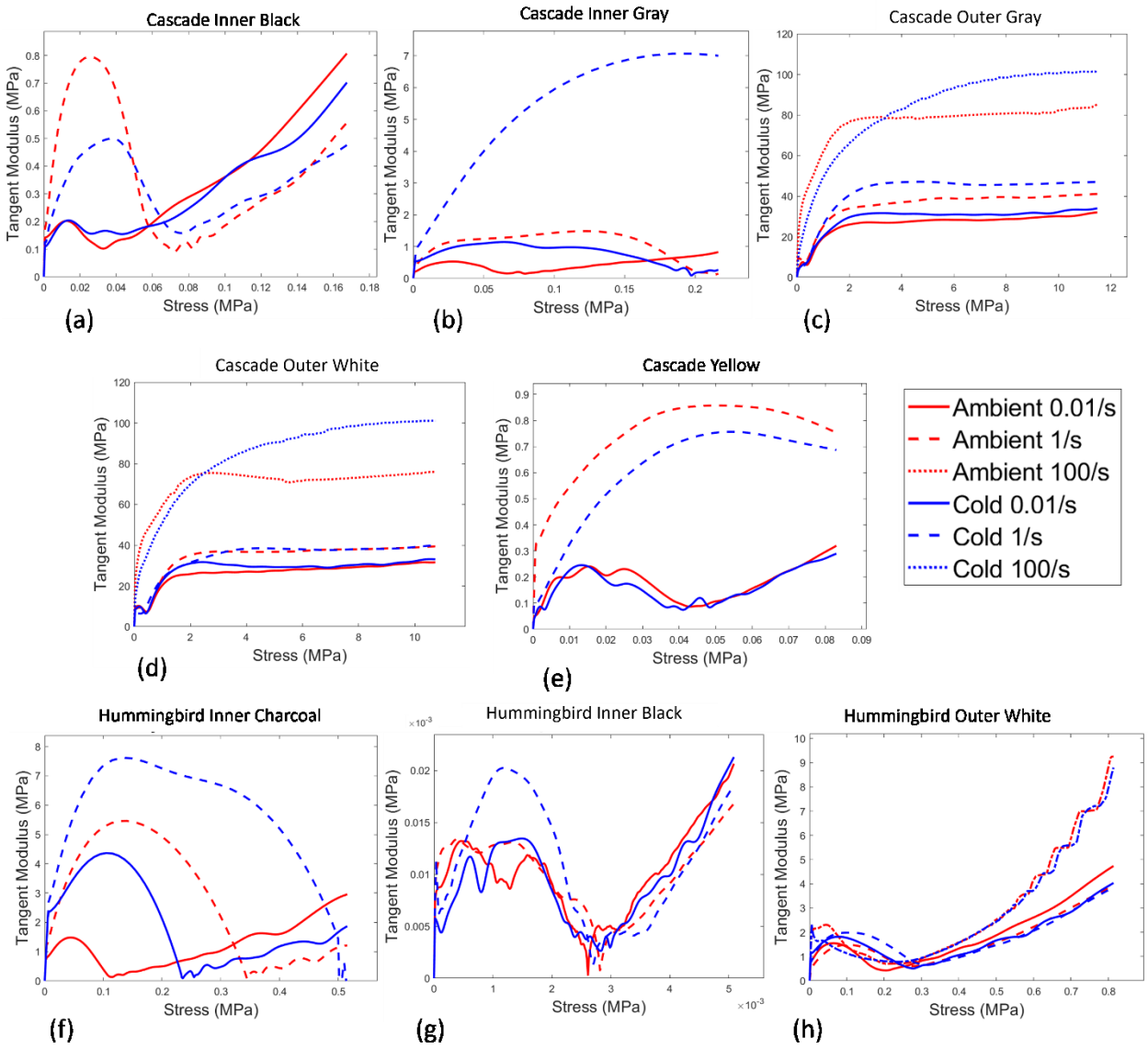

Figure 35 | Average tangent modulus curves for the Cascade (a) Inner Black, (b) Inner Gray, (c) Outer Gray, (d) Outer White, and (e) Yellow materials and the Hummingbird (f) Inner Charcoal, (g) Inner Black, and (h) Outer White materials. Note, only the outer materials were tested at 100/s strain rate.

A stress comparison and tangent modulus comparison between temperatures of each material can be found in Table 3, Table 4, Table 5, Table 6, Table 7, Table 8, Table 9, Table 10. These tables consist of a stress and tangent modulus values at each of the three regions of interest in the stress-strain curve: the initial linear elastic region, the plateau region, and the densification

region. An exception to this was the Cascade Outer materials in which there was no identifiable plateau region, so a "middle value" was recorded near the middle of the material's stress-strain curve. Values at these regions are reported for each temperature condition at each testing strain rate. These tables, along with Figure 33 and Figure 35, can be used to characterize the strain rate hardening and temperature hardening of the materials.

Table 3 | Cascade Inner Black material stress and tangent modulus at regions of interest. Percent difference refers to the change in stress or tangent modulus value from 0.01/s strain rate to 1/s strain rate. Percentages below the cold values show the change in value from the ambient condition to the cold condition.

		Stress (MPA)			Tangent Modulus (MPA)		
Strain	Temperature Condition	0.01/s Rate	1/s Rate	Difference (%)	0.01/s Rate	1/s Rate	Difference (%)
Linear Region	Ambient	0.008	0.026	225	0.188	0.795	324
	Cold	0.007 -19%	0.011 -59%	63	0.166 -12%	0.327 -59%	97
Plateau Region	Ambient	0.043	0.079	86	0.135	0.124	-8
	Cold	0.049 15%	0.084 6%	71	0.164 22%	0.182 57%	11
Densification Region	Ambient	0.118	0.140	19	0.444 4%	0.351	-21
	Cold	0.131 11%	0.177 26%	35	0.461	0.526 50%	14

Table 4 | Cascade Inner Gray material stress and tangent modulus at regions of interest. Percent difference refers to the change in stress or tangent modulus value from 0.01/s strain rate to 1/s strain rate. Percentages below the cold values show the change in value from the ambient condition to the cold condition.

		Stress (MPA)			Tangent Modulus (MPA)		
Strain	Temperature Condition	0.01/s Rate	1/s Rate	Difference (%)	0.01/s Rate	1/s Rate	Difference (%)
Linear Region	Ambient	0.016	0.044	169	0.476	1.227	158
	Cold	0.039 137%	0.213 380%	445	1.056 122%	7.018 472%	565
Plateau Region	Ambient	0.084	0.215	157	0.176	0.130	-26
	Cold	0.199 137%	0.502 133%	153	0.131 -26%	0.331 155%	154
Densification Region	Ambient	0.172	0.324	89	0.585	0.752	28
	Cold	0.293 71%	0.667 106%	128	0.688 17%	1.216 62%	77

Table 5 | Cascade Outer Gray material stress and tangent modulus at regions of interest. Unless denoted otherwise, percent difference refers to the change in stress or tangent modulus value from 0.01/s strain rate to 1/s strain rate. Percentages below the cold values show the change in value from the ambient condition to the cold condition.

		Stress (MPA)			Tangent Modulus (MPA)		
Strain	Temperature Condition	0.01/s Rate	1/s Rate	Difference (%)	0.01/s Rate	1/s Rate	Difference (%)
Linear Region	Ambient	0.261	0.416	59	7.229	9.047	25
	Cold	0.201 -23%	0.257 -38%	28	5.920 -18%	5.700 -37%	-4
Middle Region	Ambient	5.723	8.893	55	28.344	39.233	38
	Cold	6.262 9%	9.354 5%	49	30.928 9%	46.045 17%	49
Densification Region	Ambient	10.804	16.277	51	30.598	45.213	48
	Cold	11.858 10%	18.057 11%	52	34.842 14%	55.143 22%	58
Strain	Temperature Condition	100/s	% Difference (0.01/s to 100/s)	% Difference (1/s to 100/s)	100/s	% Difference (0.01/s to 100/s)	% Difference (1/s to 100/s)
Linear Region	Ambient	2.963	1035%	612%	78.982	993%	773%
	Cold	1.616 -45%	704%	529%	61.102 -23%	932%	972%
Middle Region	Ambient	26.913	370%	203%	138.135	387%	252%
	Cold	27.170 1%	334%	190%	132.037 -4%	327%	187%
Densification Region	Ambient	63.634	489%	291%	299.985	880%	563%
	Cold	61.999 -3%	423%	243%	284.895 -5%	718%	417%

Table 6 | Cascade Outer White material stress and tangent modulus at regions of interest. Unless denoted otherwise, percent difference refers to the change in stress or tangent modulus value from 0.01/s strain rate to 1/s strain rate. Percentages below the cold values show the change in value from the ambient condition to the cold condition.

		Stress (MPA)			Tangent Modulus (MPA)		
Strain	Temperature Condition	0.01/s Rate	1/s Rate	Difference (%)	0.01/s Rate	1/s Rate	Difference (%)
Linear Region	Ambient	0.451	0.427	-5	7.205	7.188	0
	Cold	0.424 -6%	0.322 -25%	-24	6.449 -11%	6.996 -3%	8
Middle Region	Ambient	5.053	6.543	29	27.499	37.614	37
	Cold	5.593 11%	6.301 -4%	13	29.255 6%	37.817 1%	29
Densification Region	Ambient	10.170	13.394	32	31.512	40.907	30
	Cold	10.978 8%	13.190 -2%	20	33.110 5%	42.317 3%	28
Strain	Temperature Condition	100/s	% Difference (0.01/s to 100/s)	% Difference (1/s to 100/s)	100/s	% Difference (0.01/s to 100/s)	% Difference (1/s to 100/s)
Linear Region	Ambient	2.982	561%	599%	75.353	946%	948%
	Cold	2.235 -25%	428%	594%	72.762 -3%	1028%	940%
Middle Region	Ambient	18.746	271%	187%	98.440	258%	162%
	Cold	22.030 18%	294%	250%	114.349 16%	291%	202%
Densification Region	Ambient	47.381	366%	254%	255.423	711%	524%
	Cold	51.127 8%	366%	288%	237.568 -7%	618%	461%

Table 7 | Cascade Yellow material stress and tangent modulus at regions of interest. Percent difference refers to the change in stress or tangent modulus value from 0.01/s strain rate to 1/s strain rate. Percentages below the cold values show the change in value from the ambient condition to the cold condition.

		Stress (MPA)			Tangent Modulus (MPA)		
Strain	Temperature Condition	0.01/s Rate	1/s Rate	Difference (%)	0.01/s Rate	1/s Rate	Difference (%)
Linear Region	Ambient	0.004	0.028	675	0.133	0.777	483
	Cold	0.003 -7%	0.008 -72%	138	0.076 -43%	0.274 -65%	258
Plateau Region	Ambient	0.045	0.149	234	0.089	0.190	114
	Cold	0.040 -10%	0.144 -3%	259	0.078 -12%	0.276 45%	253
Densification Region	Ambient	0.088	0.289	228	0.368	1.234	236
	Cold	0.072 -15%	0.238 -18%	230	0.236 -36%	0.774 -37%	229

Table 8 | Hummingbird Inner Charcoal material stress and tangent modulus at regions of interest. Percent difference refers to the change in stress or tangent modulus value from 0.01/s strain rate to 1/s strain rate. Percentages below the cold values show the change in value from the ambient condition to the cold condition.

		Stress (MPA)			Tangent Modulus (MPA)		
Strain	Temperature Condition	0.01/s Rate	1/s Rate	Difference (%)	0.01/s Rate	1/s Rate	Difference (%)
Linear Region	Ambient	0.061	0.202	229	1.358	4.891	260
	Cold	0.178 189%	0.318 57%	79	3.061 125%	6.538 34%	114
Plateau Region	Ambient	0.155	0.388	151	0.319	0.502	57
	Cold	0.273 76%	0.546 40%	100	0.524 64%	0.531 6%	1
Densification Region	Ambient	0.376	0.729	94	1.621	2.613	61
	Cold	0.584 55%	0.965 32%	65	2.511 55%	3.442 32%	37

Table 9 | Hummingbird Inner Black material stress and tangent modulus at regions of interest. Percent difference refers to the change in stress or tangent modulus value from 0.01/s strain rate to 1/s strain rate. Percentages below the cold values show the change in value from the ambient condition to the cold condition.

		Stress (MPA)			Tangent Modulus (MPA)		
Strain	Temperature Condition	0.01/s Rate	1/s Rate	Difference (%)	0.01/s Rate	1/s Rate	Difference (%)
Linear Region	Ambient	5.47E-04	6.34E-04	16	1.32E-02	1.24E-02	-6
	Cold	2.67E-04 -51%	4.34E-04 -32%	62	6.69E-03 -49%	1.17E-02 -6%	76
Plateau Region	Ambient	2.58E-03	2.81E-03	9	2.67E-03	1.32E-03	-51
	Cold	2.48E-03 -4%	2.76E-03 -2%	11	4.46E-03 67%	2.79E-03 112%	-37
Densification Region	Ambient	4.37E-03	4.95E-03	13	1.46E-02	1.59E-02	9
	Cold	4.63E-03 6%	5.07E-03 2%	10	1.56E-0 6%2	1.84E-02 16%	19

Table 10 | Hummingbird Outer White material stress and tangent modulus at regions of interest. Unless denoted otherwise, percent difference refers to the change in stress or tangent modulus value from 0.01/s strain rate to 1/s strain rate. Percentages below the cold values show the change in value from the ambient condition to the cold condition.

		Stress (MPA)			Tangent Modulus (MPA)		
Strain	Temperature Condition	0.01/s Rate	1/s Rate	Difference (%)	0.01/s Rate	1/s Rate	Difference (%)
Linear Region	Ambient	0.063	0.036	-42	1.551	1.087	-30
	Cold	0.077 23%	0.071 95%	-8	1.817 17%	1.933 78%	6
Plateau Region	Ambient	0.239	0.286	20	0.548	0.614	12
	Cold	0.308 29%	0.357 24%	16	0.656 20%	0.799 30%	22
Densification Region	Ambient	0.773	0.821	6	4.322	3.998	-8
	Cold	0.961 24%	1.306 59%	36	5.449 26%	8.855 121%	63
Strain	Temperature Condition	100/s	% Difference (0.01/s to 100/s)	% Difference (1/s to 100/s)	100/s	% Difference (0.01/s to 100/s)	% Difference (1/s to 100/s)
Linear Region	Ambient	0.100	59%	175%	1.425	-8%	31%
	Cold	0.079 -21%	2%	11%	1.259 -12%	-31%	-35%
Plateau Region	Ambient	0.315	32%	10%	1.023	87%	67%
	Cold	0.302 -4%	-2%	-15%	0.957 -6%	46%	20%
Densification Region	Ambient	16.553	2041%	1916%	273.568	6229%	6743%
	Cold	15.288 -8%	1491%	1071%	296.666 8%	5345%	3250%

All eight materials exhibited strain rate hardening to some extent. The Cascade Inner Black (Table 3), Inner Gray (Table 4), and Yellow (Table 7) materials all exhibited a substantial increase in tangent modulus from 0.01/s testing to 1/s testing, especially in the linear region. For the Cascade outer materials (Table 5 and Table 6), the strain rate hardening effect was not as prominent between 0.01/s and 1/s testing, but this effect was larger in the densification region. Comparing to 100/s strain rate testing, these outer materials (Table 5 and Table 6) exhibited substantial strain rate hardening, and the hardening was greatest in the linear region. The Hummingbird Inner Charcoal material (Table 8) also had significant strain rate hardening, with the hardening having a greater effect in the linear region. The Hummingbird Inner Black (Table 9) and Outer White (Table 10) materials showed little to no strain rate hardening between 0.01/s

strain rate and 1/s strain rate testing. However, the Outer White material did substantially harden at 100/s, with the hardening effect being greatest in the densification region of the stress-strain curve.

Cold temperature hardening was not as consistent or as prominent as strain rate hardening was across the materials but was still prevalent in some cases (Table 3, Table 4, Table 5, Table 6, Table 7, Table 8, Table 9, and Table 10). The Hummingbird Inner Charcoal material (Table 8) and the Cascade Inner Gray material (Table 4) exhibited substantial cold hardening. The Hummingbird Outer White material (Table 10) also cold hardened, but this effect was only prominent at the 0.01/s and 1/s strain rates. At a 1/s strain rate, the Cascade Inner Black (Table 3) material had a much greater densification region tangent modulus at cold temperature than at ambient temperature. All other materials showed little to no cold temperature hardening.

Energy dissipation comparisons between temperature conditions can be made from Figure 34. For a given energy dissipation value on the energy dissipation plots, the energy is dissipated at a lower stress for the ambient condition when compared to the cold condition for the Cascade Inner Gray, Outer Gray, and Outer White materials and for the Hummingbird Inner Charcoal material (until around 8×10^4 J/m^3). The same energy is dissipated at higher stresses for the cold condition of the Cascade Inner Black material at 1/s strain rate beyond about 5×10^3 J/m^3. Ambient and cold conditioned materials dissipated the same energy at about the same stress for all other materials (Cascade Yellow material and Hummingbird Inner Black and Outer White materials).

3.4 Discussion

The purpose of this study was to characterize the materials used in the Cascade and Hummingbird headgears in terms of their stress-strain behavior, energy dissipation, and tangent modulus, and to determine how cold conditioning affects these characterizations. These characterizations were acquired through compressive testing of the materials at different strain rates and at ambient and cold temperatures.

Of the materials that were tested in this study, most exhibited the linear elastic, plateau, and densification regions that are characteristic of polymer foams. The exceptions to this were the two outer materials of the Cascade headgear. At quasi-static strain rates (0.01/s and 1/s), these materials had a linear region spanning from around 0.1 strain until the truncation strain value. For high-rate impacts, these materials exhibited a linear or even slightly exponential stress-strain curve shape from zero strain until the end of the test. This is likely because the Cascade Outer Gray and Outer White materials may not be foams. Solid foams have pockets of air trapped within them. Although no microscopy was performed in this study to examine the microstructure of the materials used in these headgears, it did not appear that the Cascade outer materials were constructed as foams.

3.4.1 Strain Rate Hardening and Energy Dissipation

All tested materials strain-rate hardened to some extent. The extent of the strain rate hardening was usually greatest in the linear region of the stress-strain curve, except for the Hummingbird Outer White material in which it was greatest in the densification region when comparing the 100/s strain rate curve to the other strain rate curves. This finding that the greatest strain rate hardening is usually in the linear elastic region of the stress-strain curve is consistent

with previous studies that have tested polymer foams at various strain rates [147]–[151]. This phenomenon is a result of what is happening within the foam during the linear elastic region of the stress-strain curve. When foams first start to deform, their cell walls begin to bend, causing the initial spike in stress [152]. The key to low levels of stress in this stage of deformation is for the cell walls and molecules of the foam to easily slide past each other [153]. As strain rate increases, the cell walls and molecules of the foam do not as easily slide past each other while the foam deforms, causing an increase in the stress required for a given strain. During the plateau region of the stress-strain curve, the cell structures within the foam continuously collapse [152]. This stage occurs after most cell wall bending has occurred, which is why the stress required to further compress the foam remains relatively constant. Since this is the case, an increase in strain rate does not have nearly as much of an effect on the tangent modulus (hardening) in the plateau region of the curve. This is evident in most of the materials tested but is especially clear in Cascade Inner Black and Inner Gray materials and the Hummingbird Inner Charcoal and Inner Black materials.

The apparent strain rate hardening of the materials that the Cascade headgear and the Hummingbird headgear are made of is characteristic of materials used in sports headgear. Strain rate hardening of the materials within headgears allows them to protect against both minor (lower strain rate) and more severe (higher strain rate) impacts without sacrificing the performance for minor impacts. This becomes more evident when analyzing the energy dissipation curves of the materials used in the women's lacrosse headgears. The energy dissipation curves, which are the areas under the stress-strain curves, can be interpreted as follows: at a given energy dissipation value (x-axis), the material transmits a certain stress (y-axis). In the case of a head impact, this transmitted stress is either passed on to another material

or area in the helmet or is transmitted as contact stress to the head. The energy values on the x-axis of each energy dissipation curve are essentially the kinetic energies that would need to be dissipated from certain impacts. The materials in the headgears follow different stress-strain curves and consequently exhibit different energy dissipation capabilities for different strain rates (impact severity).

Figure 36 below of the untruncated energy dissipation curve of the Hummingbird Inner Charcoal material further shows the importance of the strain rate hardening characteristic of the materials used in the women's lacrosse helmets. In the case of low severity impacts where the material will not deform at a fast rate (i.e., low strain rate), it will follow the 0.01/s energy dissipation curve. This is ideal for these low severity impacts because it is not likely that they need a high level of energy to be dissipated, so the material will transmit less stress to neighboring materials or to the head of the player. Conversely, for high severity impacts in which the deformation of the material happens at a faster rate (i.e., higher strain rate), the material will follow the 1/s curve. This is ideal for the higher severity impacts because they are likely to need higher levels of energy to be dissipated. Figure 36 highlights that at a certain level of energy needed to be dissipated, the 1/s strain rate curve starts to become more favorable for dissipating energy at a lower contact stress. By following a different curve for different severities of impacts, the headgear is better optimized to effectively protect against both minor and more severe impacts.

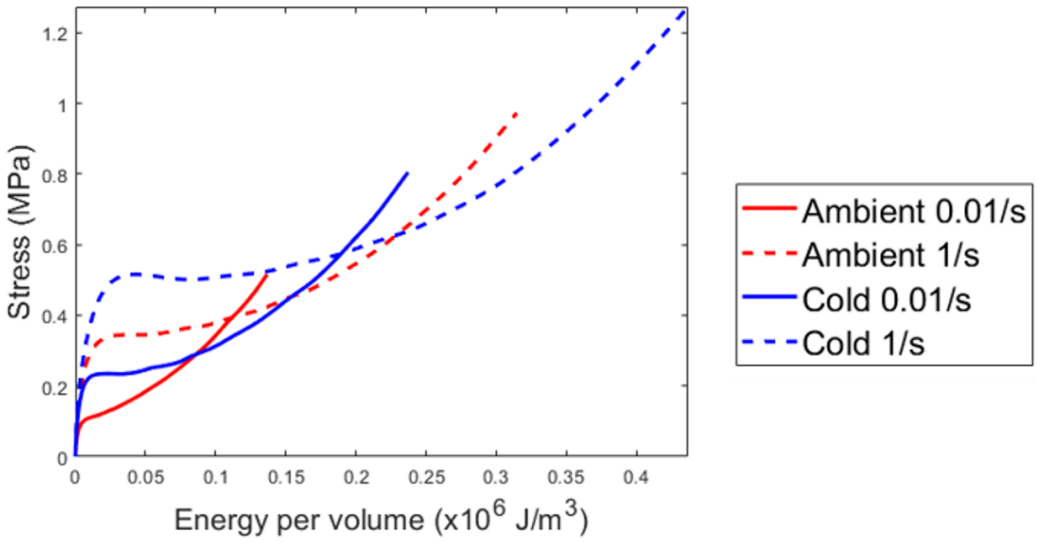

Figure 36 | Untruncated energy dissipation curve for the Hummingbird Inner Charcoal material.

3.4.2 Temperature Effects

The Cascade Inner Gray and the Hummingbird Inner Charcoal materials were the only materials that showed any noteworthy cold temperature effects on their mechanical characterization. For these materials, cold temperature increased the tangent modulus of the material and made it so that it dissipated energy at higher stresses compared to at ambient temperature.

Previous studies that have tested polymers commonly used is sports helmets have found that there is a clear temperature dependence on the material's stress-strain curve, with the initial modulus being greater and the rest of the curve "shifting" upwards at cold temperatures [129]–[132]. However, it should be noted that the temperature effect becomes much less significant as the conditioning temperatures become closer. In fact, one study that performed compression testing on different temperature conditions of polymer foams commonly used in athletic shoe insoles (which are similar shock absorbing materials to helmet liners) found that some foams had

stress-strain curves that barely differed between 0 ˚C (cold) and 20 ˚C (ambient) conditioning. Smaller temperature-based fluctuations in the mechanical characterizations of the materials tested in this study could be a result of the of the cold temperature conditioning not being close to the glass transition temperature of the polymers used in sports headgears, which is usually around -50 ˚C to -40 ˚C. Zhang et al. (2004) saw distinctly different stress-strain curves for the -40 ˚C temperature conditioned thermoplastic polyurethane (TPU) that they tested, pointing out that it was likely a result of the TPU being at or very close to its glass transition temperature. It is possible that that the foam liner of the football helmet tested by Ramirez and Gupta that was mentioned in Chapter 2 may have been near its glass transition temperature when conditioned to -15 ˚C. This may be why the materials of the helmet were not able to dissipate energy as well and ultimately allowed much higher levels of PLA at a cold temperature than at an ambient temperature.

3.4.3 Material Testing Comparison to Headgear Impact Testing

Caution should be used in drawing any comparisons between the material testing performed in this study and the headgear impact testing study described in the last chapter. The strain rate that impacts conducted in Chapter 2 cause on each material within each headgear is not known and was not used to conduct material testing on the headgear materials. Furthermore, material testing did not capture the behavior of the materials are able to work as a whole system to dissipate energy. Therefore, the material testing conditions did not replicate a real sport impact or how the headgears are able to dissipate energy as an entire system. Overall, the material testing is too unrelated to the whole headgear testing to draw any specific or detailed conclusions comparing quantitative results from the two test methods (example: comparing energy dissipated by all of the materials of the headgears and then comparing that to a calculated energy

dissipation by the headgear during headgear impact testing). The only comparisons that will be made are that the apparent strain rate hardening of the the materials of both headgears may have helped contribute to the ability of the headgears to mitigate impacts of various severities and that the apparent low effect of temperature on the mechanical characterizations of the materials may partially explain the lack of significant differences between the impact mitigation properties of cold and ambient conditioned headgears.

The purpose of this study was to characterize the mechanical behavior of the materials used in women's lacrosse headgears at multiple strain rates and at ambient and cold temperatures. By doing so, these characterizations can be used as inputs into FEA software as the strain rate and temperature dependent material properties of the materials used in the headgears. Using FEA, future studies can more accurately study the mechanical behavior of the materials at different strain rates and can even use the materials in a whole-headgear model for simulation of head impacts to a head and brain model protected by the headgears. This would allow for determination of brain strains from women's lacrosse impacts with and without the headgears and at cold and ambient temperatures. It would also allow for the study of how the materials/headgears can affect the safety of players that are not wearing the headgears and if cold temperatures influence the effect.

3.4.4 Limitations

There were several limitations to the material testing study described in this chapter. One limitation was that foams are inherently difficult to uniformly cut. Consequently, some materials had surfaces that were slightly tilted and not flat. This could have caused shear forces to act on the materials instead of just compression. Another limitation was the method of cold conditioning the test specimens. Test specimens were frozen in a research grade freezer at ~ -0.5

˚C temperatures for at least four hours before being tested. The specimens were then taken out of the freezing condition right before testing and then tested as soon as possible. Because of the small size of the specimens, they may have quickly warmed up in the quick amount of time in which the necessary steps were carried out to begin the testing. Ideally, a cold temperature control chamber would have been built around the specimen in the two test apparatuses used in this study to ensure a constant and controlled cold temperature condition. A third limitation was that only the outer headgear materials were tested at the high-rate (~100/s) strain rate since they are the materials that are the first line of defense against impacts. However, it may be beneficial to know the behavior of the other materials at higher strain rates so that more inputs can be provided for the material properties in an FEA model. Lastly, the sample size of the material tests in this study was three per strain rate and temperature combination. Consequently, there may have been some outliers that affected the material characterizations. Future work should include a higher sample size of test specimens.

Chapter 4: Conclusion

The purpose of this study was to characterize the impact mitigation properties of women's lacrosse headgears across a variety of impact types and severities that players may experience during competition and to characterize the mechanical properties of the materials that the headgears are made of. The effect of cold temperature on these characterizations was also analyzed.

Impact testing results showed that both the Cascade and the Hummingbird headgear were able to significantly reduce the PLA, HIC, PRA, PRV, and BrIC of all linear impactor impact speeds, but the reductions were more much more subtle for the rotational velocity based metrics (PRV and BrIC) than they were for the other metrics. For ball impacts, both headgears were able to significantly reduce PRV and PRA (and BrIC for the Cascade), but not PLA or HIC_{15} (and BrIC for the Hummingbird). In general, these reductions of concussion metrics for the ball impacts were not as large as they were for the linear impactor impacts. Material testing results depicted that the material of both headgears strain rate harden, which is characteristic of polymers used in sports headgears and is important to the ability of the headgears to effectively mitigate impacts and optimize player safety across a variety of impact severities. Cold conditioning of the materials showed that freezing temperatures did not significantly affect the material characterizations of most of the materials used in the headgears, which may explain why cold conditioning of the headgears for impact testing did not result in a significant change in any of the concussion metrics.

The results from impact testing suggest that the headgears can effectively protect against skull fracture because of their ability to substantially reduce PLA and HIC_{15}, but their ability to effectively protect against concussion is more ambiguous because of the loose correlation between kinematic concussion metrics and concussion itself. The material characterizations acquired in this research can be used in future FEA studies to gain further insight on the ability of the headgears to reduce concussion risks at ambient and cold temperatures through the analysis of brain strains that are closely related to concussion.

Appendices

Appendix A: MATLAB Scripts

*** Many of the scripts had some changes to them that were done depending on what groups of data were being analyzed or depending on what the desired result of the script was. Therefore, this section of the appendix does not show every single line of code that was used for this thesis, but it is representative of the core of the scripts that were used to process data.

Mann-Whitney U Test Script (grouped by impact location)

```
clc
clear

%% Selecting concussion metric
list = {'Linear Acceleration','Rotational Velocity','Rotational
Acceleration','HIC','BrIC'};
[indx,tf] = listdlg('PromptString',{'Select the metric to
analyze'},'SelectionMode','single','ListString',list);

%% Reading in data
data = readtable('Cascade Data','Sheet',2);

first = data(1:36,:);
first_PLA = table2array(first(:,5));
first_PRV = table2array(first(:,6));
first_PRA = table2array(first(:,7));
first_HIC = table2array(first(:,8));
first_BrIC = table2array(first(:,9));

data = readtable('Hummingbird Data','Sheet',2);
second = data(1:36,:);
second_PLA = table2array(second(:,5));
second_PRV = table2array(second(:,6));
second_PRA = table2array(second(:,7));
second_HIC = table2array(second(:,8));
second_BrIC = table2array(second(:,9));

%% Setting variables
if indx == 1
```

```
    metric = 'PLA';
    first_metric = first_PLA;
    second_metric = second_PLA;
elseif indx == 2
    metric = 'PRV';
    first_metric = first_PRV;
    second_metric = second_PRV;
elseif indx == 3
    metric = 'PRA';
    first_metric = first_PRA;
    second_metric = second_PRA;
elseif indx == 4
    metric = 'HIC';
    first_metric = first_HIC;
    second_metric = second_HIC;
elseif indx == 5
    metric = 'BrIC';
    first_metric = first_BrIC;
    second_metric = second_BrIC;
end

%% Separating by impact location
first_metric_F = first_metric(1:6,1);
first_metric_FB = first_metric(7:12,1);
first_metric_R = first_metric(13:18,1);
first_metric_RBCG = first_metric(19:24,1);
first_metric_RBNC = first_metric(25:30,1);
first_metric_S = first_metric(31:36,1);

second_metric_F = second_metric(1:6,1);
second_metric_FB = second_metric(7:12,1);
second_metric_R = second_metric(13:18,1);
second_metric_RBCG = second_metric(19:24,1);
second_metric_RBNC = second_metric(25:30,1);
second_metric_S = second_metric(31:36,1);

% %% Chi squared test for normal distribution
% [first_metric_F_chi,first_metric_F_chi_p] = chi2gof(first_metric_F);
% [second_metric_F_chi,second_metric_F_chi_p] = chi2gof(second_metric_F);

%% Mann-Whitney Test
p_value_F = ranksum(first_metric_F,second_metric_F);
p_value_FB = ranksum(first_metric_FB,second_metric_FB);
p_value_R = ranksum(first_metric_R,second_metric_R);
p_value_RBCG = ranksum(first_metric_RBCG,second_metric_RBCG);
p_value_RBNC = ranksum(first_metric_RBNC,second_metric_RBNC);
p_value_S = ranksum(first_metric_S,second_metric_S);

Results = [mean(first_metric_F),mean(second_metric_F),p_value_F;...
           mean(first_metric_FB),mean(second_metric_FB),p_value_FB;...
           mean(first_metric_R),mean(second_metric_R),p_value_R;...
           mean(first_metric_RBCG),mean(second_metric_RBCG),p_value_RBCG;...
           mean(first_metric_RBNC),mean(second_metric_RBNC),p_value_RBNC;...
           mean(first_metric_S),mean(second_metric_S),p_value_S];

clear 'tf';
```

Quasi-Static Material Testing Post-Processing Script

```
clear all;
clear allvars;
clc;

%% Selecting and loading in raw CSV data
[file,path] = uigetfile('*.csv','Select a CSV file','C:\Material Testing\CSV
Exports');
addpath(path);
raw_data = readtable(file);

%% User input for sample cross-sectional area and thickness
prompt = {'Enter sample cross-sectional area (m^2):','Enter sample thickness
(mm):'};
dlgtitle = 'Sample Dimensions';
dims = [1 35];
user_input = inputdlg(prompt,dlgtitle,dims);
user_input = array2table(user_input);

sample_cross_sectional_area = user_input(1,1);
sample_cross_sectional_area = table2array(sample_cross_sectional_area);
sample_cross_sectional_area = str2double(sample_cross_sectional_area);
sample_thickness = user_input(2,1);
sample_thickness = table2array(sample_thickness);
sample_thickness = str2double(sample_thickness);

%% Clipping relevant force data
force_data = raw_data(:,2);
force_length = size(force_data);
force_length = force_length(1,1);
force_data = table2array(force_data);

i = 1;
for index = 1:force_length-1;
    row_value = isnan(force_data(i,1));
    if row_value == 0
        trimmed_force_data(i,:) = force_data(i,:);
        i = i+1;
    else end
end

%% Clipping relevant displacement data
displacement_data = raw_data(:,5);
displacement_data = table2array(displacement_data);

i = 1;
for index = 1:force_length-1; %force length still works here
    row_value = isnan(displacement_data(i,1));
    if row_value == 0
        trimmed_displacement_data(i,:) = displacement_data(i,:);
        i = i+1;
    else end
end
```

```
%% Calculating stress, strain, and energy dissipation
stress_Pa = trimmed_force_data./sample_cross_sectional_area;
stress_MPa = stress_Pa./1e6;

strain = trimmed_displacement_data./sample_thickness;

energy_dissipation = cumtrapz(strain,stress_MPa);

true_strain = log(1+strain);

true_stress = stress_MPa.*(1+strain);

true_energy_dissipation = cumtrapz(true_strain,true_stress);

current_trial_max_stress = max(stress_MPa);
current_trial_max_strain = max(strain);
current_trial_max_energy_dissipation = max(energy_dissipation);

%% Plotting graphs before pseudo-strain is removed
figure

z = plot(strain,stress_MPa,'b');
title('Stress-Strain Curve');
xlabel('Strain');
ylabel('Stress (MPa)');
xlim([0 (current_trial_max_strain*1.1)]);
ylim([0 (current_trial_max_stress*1.1)]);

%% Finding starting point to eliminate pseudo-strai
[x,y,r]=MagnetGInput(z,1);

%% Removing pseudo-strain
starting_number = find(strain == x);

strain = strain(starting_number:end);
% strain = smooth(strain);
strain_to_subtract = strain(1,1);
strain = strain - strain_to_subtract;

stress_MPa = stress_MPa(starting_number:end);
% stress_MPa = smooth(stress_MPa);
stress_to_subtract = stress_MPa(1,1);
stress_MPa = stress_MPa - stress_to_subtract;

energy_dissipation = energy_dissipation(starting_number:end);
% energy_dissipation = smooth(energy_dissipation);
energy_to_subtract = energy_dissipation(1,1);
energy_dissipation = energy_dissipation - energy_to_subtract;

true_strain = true_strain(starting_number:end);
% true_strain = smooth(true_strain);
true_strain_to_subtract = true_strain(1,1);
true_strain = true_strain - true_strain_to_subtract;
```

```
true_stress = true_stress(starting_number:end);
% true_stress = smooth(true_stress);
true_stress_to_subtract = true_stress(1,1);
true_stress = true_stress - true_stress_to_subtract;

true_energy_dissipation = true_energy_dissipation(starting_number:end);
% true_energy_dissipation = smooth(true_energy_dissipation);
true_energy_dissipation_to_subtract = true_energy_dissipation(1,1);
true_energy_dissipation = true_energy_dissipation -
true_energy_dissipation_to_subtract;

%% Filtering data
cutoff_frequency = 0.1;
sampling_frequency = 25;                                                % for
0.01/s strain rate
% sampling_frequency = 1000;                                              %
for 1/s strain rate
nyquist_frequency = 0.5*sampling_frequency;
norm_cutoff_frequency = cutoff_frequency/nyquist_frequency;
lpfilter = fir1(500,norm_cutoff_frequency,'low');                       % for
0.01/s strain rate
% lpfilter = fir1(50,norm_cutoff_frequency,'low');                        %
for 1/s strain rate

filtered_stress = filtfilt(lpfilter,1,true_stress);
filtered_strain = filtfilt(lpfilter,1,true_strain);
filtered_energy = filtfilt(lpfilter,1,true_energy_dissipation);

filtered_eng_stress = filtfilt(lpfilter,1,stress_MPa);
filtered_eng_strain = filtfilt(lpfilter,1,strain);
filtered_eng_energy = cumtrapz(filtered_eng_strain,filtered_eng_stress);

%% Starting stress and strain at zero point (since filter slightly skewed it)
filtered_eng_stress(1,1) = [0];
filtered_eng_strain(1,1) = [0];

%% Raw vs filtered stress strain curve
figure
plot(strain,stress_MPa,'r','DisplayName','Raw');
xlabel('Strain');
ylabel('Stress(MPa)');
hold on
plot(filtered_eng_strain,filtered_eng_stress,'b','DisplayName','Filtered');
legend('Location','eastoutside');
hold off

%% Setting new axes limits
eng_and_true_strain = [filtered_eng_strain;filtered_strain];
eng_and_true_stress = [filtered_eng_stress;filtered_stress];
eng_and_true_energy = [filtered_eng_energy;filtered_energy];

current_trial_max_stress = max(eng_and_true_stress);
current_trial_max_strain = max(eng_and_true_strain);
current_trial_max_energy_dissipation = max(eng_and_true_energy);
```

```
%% Points for eng and true labels
eng_strain_end_point = filtered_eng_strain(end,:);
eng_stress_end_point = filtered_eng_stress(end,:);
eng_energy_end_point = filtered_eng_energy(end,:);
true_strain_end_point = filtered_strain(end,:);
true_stress_end_point = filtered_stress(end,:);
true_energy_end_point = filtered_energy(end,:);

%% Plotting new stress-strain and energy dissipation graphs
figure
tiledlayout(2,1);

nexttile
plot(filtered_eng_strain,filtered_eng_stress,'b');
text(eng_strain_end_point,eng_stress_end_point,'Engineering');
hold on
plot(filtered_strain,filtered_stress,'r');
text(true_strain_end_point,true_stress_end_point,'True');
title('Stress-Strain Curve');
xlabel('Strain');
ylabel('Stress (MPa)');
xlim([0 (current_trial_max_strain*1.25)]);
ylim([0 (current_trial_max_stress*1.25)]);
hold off

nexttile
plot(filtered_eng_energy,filtered_eng_stress,'b');
text(eng_energy_end_point,eng_stress_end_point,'Engineering');
hold on
plot(filtered_energy,filtered_stress,'r');
text(true_energy_end_point,true_stress_end_point,'True');
title('Energy Dissipation Curve');
xlabel('Energy per volume (x10^6 J/m^3)');
ylabel('Stress (MPa)');
xlim([0 (current_trial_max_energy_dissipation*1.25)]);
ylim([0 (current_trial_max_stress*1.25)]);

%% Saving stress-strain and energy dissipation graphs
file = file(1:end-4);
saving_file_name = fullfile(path,file);
image_ending = ' (Stress Strain & Energy Dissipation Plots)';
image_file_name = append(saving_file_name,image_ending);
saveas(gcf,image_file_name,'svg');

%% Modulus calculation using forward difference method
lengthForLoop = length(filtered_eng_stress) - 1;
i=1;
for i = 1:lengthForLoop
    first_stress = filtered_eng_stress(i);
    second_stress = filtered_eng_stress(i+1);
    first_strain = filtered_eng_strain(i);
    second_strain = filtered_eng_strain(i+1);
```

```
    derivative_value = (second_stress - first_stress)/(second_strain -
first_strain);

    Modulus_data(i,:) = derivative_value;

    i = i+1;
end

max_filtered_eng_stress = max(filtered_eng_stress);
Peak_modulus = max(Modulus_data);
Modulus_data = [0;Modulus_data];

%% Plotting tangent modulus
figure
plot(filtered_eng_stress,Modulus_data,'r');
title('Modulus Plot');
title('Tangent Modulus Curve');
xlabel('Stress (MPa)');
ylabel('Tangent Modulus (MPa)');
xlim([0 (max_filtered_eng_stress*1.1)]);
ylim([0 (Peak_modulus*1.1)]);

%% Saving tangent modulus graph
file = file(1:end-4);
image_ending = ' (Tangent Modulus Plot)';
image_file_name = append(saving_file_name,image_ending);
saveas(gcf,image_file_name,'svg');

%% Calculating peak data
processed_data =
[filtered_eng_strain,filtered_eng_stress,filtered_eng_energy,filtered_strain,
filtered_stress,filtered_energy];
peak_data = processed_data(end,:);
peak_data = [peak_data, Peak_modulus];
peak_data = array2table(peak_data);
peak_data.Properties.VariableNames = {'Peak Strain','Peak Stress (MPa)','Peak
Energy Dissipation (x10^6 J/m^3)','Peak True Strain','Peak True Stress
(MPa)','Peak True Energy Dissipation (x10^6 J/m^3)','Peak Tangent Modulus'};

%% Saving peak stress-strain curve and energy dissipation curve data
peaks_ending = ' (Peak Data)';
peaks_file_name = append(saving_file_name,peaks_ending);
writetable(peak_data,peaks_file_name);

%% Saving processed data for use in plotting all three curves on one
coordinate system
processed_data = array2table(processed_data);
processed_data.Properties.VariableNames = {'Strain','Stress (MPa)','Energy
Dissipation (x10^6 J/m^3)','True Strain','True Stress (MPa)','True Energy
Dissipation (x10^6 J/m^3)'};
csv_ending = ' (Processed Data).csv';
processed_data_file_name = append(saving_file_name,csv_ending);
writetable(processed_data,processed_data_file_name);

%% Saving tangent modulus data
```

```
tangent_modulus_data = [filtered_eng_stress,Modulus_data];
tangent_modulus_data = array2table(tangent_modulus_data);
tangent_modulus_data.Properties.VariableNames = {'Stress (MPa)','Tangent
Modulus (MPa)'};
csv_ending = ' (Modulus Data).csv';
tangent_modulus_data_file_name = append(saving_file_name,csv_ending);
writetable(tangent_modulus_data,tangent_modulus_data_file_name);

%% Opening other processed data if 3rd trial, then plotting all together
number = '3';
check_for_third_trial = contains(file,number);
if check_for_third_trial == 1
    % opening data and converting to array
    [file_trial_1,path_trial_1] = uigetfile('*.csv','Select Trial 1 Processed
CSV file',path);
    [file_trial_2,path_trial_2] = uigetfile('*.csv','Select Trial 2 Processed
CSV file',path);
    [file_trial_3,path_trial_3] = uigetfile('*.csv','Select Trial 3 Processed
CSV file',path);

    trial_1 = readtable(file_trial_1);
    strain_1 = trial_1(:,1);
    strain_1 = table2array(strain_1);
    trial_2 = readtable(file_trial_2);
    strain_2 = trial_2(:,1);
    strain_2 = table2array(strain_2);
    trial_3 = readtable(file_trial_3);
    strain_3 = trial_3(:,1);
    strain_3 = table2array(strain_3);

    % finding which trial should be used as the x-axis for the graph
    max_strain_1 = max(strain_1);
    max_strain_2 = max(strain_2);
    max_strain_3 = max(strain_3);
    all_trials_strain = [max_strain_1; max_strain_2; max_strain_3];
    all_trials_max_strain = max(all_trials_strain);
    trial_to_use_for_strain = find(all_trials_strain ==
all_trials_max_strain);

    strain_1 = transpose(strain_1);
    strain_2 = transpose(strain_2);
    strain_3 = transpose(strain_3);

    % finding stress and length of stress
    stress_1 = trial_1(:,2);
    stress_1 = table2array(stress_1);
    length_stress_1 = length(stress_1);
    stress_2 = trial_2(:,2);
    stress_2 = table2array(stress_2);
    length_stress_2 = length(stress_2);
    stress_3 = trial_3(:,2);
    stress_3 = table2array(stress_3);
    length_stress_3 = length(stress_3);

    max_stress_1 = max(stress_1);
    max_stress_2 = max(stress_2);
```

```
max_stress_3 = max(stress_3);
all_trials_stress = [max_stress_1; max_stress_2; max_stress_3];
all_trials_max_stress = max(all_trials_stress);

stress_1 = transpose(stress_1);
stress_2 = transpose(stress_2);
stress_3 = transpose(stress_3);

%energy dissipation
energy_1 = trial_1(:,3);
energy_1 = table2array(energy_1);
energy_2 = trial_2(:,3);
energy_2 = table2array(energy_2);
energy_3 = trial_3(:,3);
energy_3 = table2array(energy_3);

max_energy_1 = max(energy_1);
max_energy_2 = max(energy_2);
max_energy_3 = max(energy_3);
all_trials_energy = [max_energy_1; max_energy_2; max_energy_3];
all_trials_max_energy = max(all_trials_energy);

figure
plot(strain_1,stress_1,'r','DisplayName','Trial 1');
title('Combined Stress-Strain Curves');
xlabel('Strain');
ylabel('Stress (MPa)');
xlim([0 (all_trials_max_strain*1.1)]);
ylim([0 (all_trials_max_stress*1.1)]);
hold on
plot(strain_2,stress_2,'g','DisplayName','Trial 2');
plot(strain_3,stress_3,'b','DisplayName','Trial 3');
legend('Location','north');
hold off


% Saving graphs to appropriate folder
file = file(1:end-4);
saving_file_name = fullfile(path,file);
summary_plot_ending = 'All Trials Stress-Strain Curve';
summary_plot_file_name = append(saving_file_name,summary_plot_ending);
saveas(gcf,summary_plot_file_name,'svg');

% Summary Energy Dissipation Plot
figure
plot(energy_1,stress_1,'r','DisplayName','Trial 1');
title('Combined Energy Dissipation Curves');
xlabel('Energy per volume (x10^6 J/m^3)');
ylabel('Stress (MPa)');
xlim([0 (all_trials_max_energy*1.1)]);
ylim([0 (all_trials_max_stress*1.1)]);
hold on
plot(energy_2,stress_2,'g','DisplayName','Trial 2');
plot(energy_3,stress_3,'b','DisplayName','Trial 3');
legend('Location','north');
```

```
    hold off

    % saving summary energy dissipation figure
    summary_plot_energy_ending = 'All Trials Energy Dissipation Curve';
    summary_plot_energy_file_name =
append(saving_file_name,summary_plot_energy_ending);
    saveas(gcf,summary_plot_energy_file_name,'svg');

    % opening modulus processed data files (not actual 6 trials, same 3
trials as above but just new numbers)
    [file_trial_4,path_trial_4] = uigetfile('*.csv','Select Trial 1 Modulus
Data',path);
    [file_trial_5,path_trial_5] = uigetfile('*.csv','Select Trial 2 Modulus
Data',path);
    [file_trial_6,path_trial_6] = uigetfile('*.csv','Select Trial 3 Modulus
Data',path);

    trial_4 = readtable(file_trial_4);
    m_stress_4 = trial_4(:,1);
    m_stress_4 = table2array(m_stress_4);
    modulus_4 = trial_4(:,2);
    modulus_4 = table2array(modulus_4);

    trial_5 = readtable(file_trial_5);
    m_stress_5 = trial_5(:,1);
    m_stress_5 = table2array(m_stress_5);
    modulus_5 = trial_5(:,2);
    modulus_5 = table2array(modulus_5);

    trial_6 = readtable(file_trial_6);
    m_stress_6 = trial_6(:,1);
    m_stress_6 = table2array(m_stress_6);
    modulus_6 = trial_6(:,2);
    modulus_6 = table2array(modulus_6);

    % finding which trial should be used as the x-axis for the tangent
modulus plot
    max_m_stress_1 = max(m_stress_4);
    max_m_stress_2 = max(m_stress_5);
    max_m_stress_3 = max(m_stress_6);
    all_trials_m_stress = [max_m_stress_1; max_m_stress_2; max_m_stress_3];
    all_trials_max_m_stress = max(all_trials_m_stress);

    % finding which trial should be used as the y-axis for the tangent
modulus plot
    max_modulus_1 = max(modulus_4);
    max_modulus_2 = max(modulus_5);
    max_modulus_3 = max(modulus_6);
    all_trials_modulus = [max_modulus_1; max_modulus_2; max_modulus_3];
    all_trials_max_modulus = max(all_trials_modulus);

    % Summary tangent modulus plot
    figure
    plot(m_stress_4,modulus_4,'r','DisplayName','Trial 1');
    title('Combined Tangent Modulus Curves');
```

```
    xlabel('Stress (MPa)');
    ylabel('Tangent Modulus (MPa)');
    xlim([0 (all_trials_max_m_stress*1.1)]);
    ylim([0 (all_trials_max_modulus*1.1)]);
    hold on
    plot(m_stress_5,modulus_5,'g','DisplayName','Trial 2');
    plot(m_stress_6,modulus_6,'b','DisplayName','Trial 3');
    legend('Location','north');
    hold off

    % saving summary tangent modulus figure
    summary_plot_energy_ending = 'All Trials Tangent Modulus Curve';
    summary_plot_energy_file_name =
append(saving_file_name,summary_plot_energy_ending);
    saveas(gcf,summary_plot_energy_file_name,'svg');

end
```

Pneumatic High Rate Material Testing Post-Processing Script

```
clc
clear

%% Opening file ------------------------------------------------------------
[file,path] = uigetfile('*.xlsx','Select Excel file','C:\Material Testing\CSV
Exports\Pneumatic Excel Files');
addpath(path);
data = readtable(file);
data = table2array(data);
% data = str2double(data);

%% User input for sample cross-sectional area and thickness
prompt = {'Enter sample cross-sectional area (m^2):','Enter sample thickness
(mm):'};
dlgtitle = 'Sample Dimensions';
dims = [1 35];
user_input = inputdlg(prompt,dlgtitle,dims);
user_input = array2table(user_input);

sample_cross_sectional_area = user_input(1,1);
sample_cross_sectional_area = table2array(sample_cross_sectional_area);
sample_cross_sectional_area = str2double(sample_cross_sectional_area);
sample_thickness = user_input(2,1);
sample_thickness = table2array(sample_thickness);
sample_thickness = str2double(sample_thickness);
sample_thickness = sample_thickness/1000;

%% Reading in time, acceleration, and force data --------------------------
time = data(1:end,1);
accel1 = data(1:end,2);
accel2 = data(1:end,4);
force = data(1:end,6);
```

```
% %% Plotting force
% figure
% plot(time,force)
% xlabel('Time (s)');
% ylabel('Force (N)');

%% Plotting acceleration to define region of interest --------------------
figure
subplot(2,1,1)
plot(time,force);
xlabel('Time (s)')
ylabel('Force (N)');

subplot(2,1,2)
z = plot(time,accel2,'r');
title('Select starting and end point for ROI');
xlabel('Time (s)');
ylabel('Acceleration (m/s^2)');

%% Slecting region of interest -------------------------------------------
[ROI_points,y,r]=MagnetGInput(z,2);

%% Trimming data ---------------------------------------------------------
start_ROI = ROI_points(1,1);
start_point = find(time == start_ROI);
end_ROI = ROI_points(1,2);
end_point = find(time == end_ROI);

time = time(start_point:end_point,1);
accel1 = accel1(start_point:end_point,1);
accel2 = accel2(start_point:end_point,1);
force = force(start_point:end_point,1);

%% Integration for displacement ------------------------------------------
velocity_1 = cumtrapz(time,accel1);
displacement_1 = cumtrapz(time,velocity_1);         %fixture displacement
velocity_2 = cumtrapz(time,accel2);
displacement_2 = cumtrapz(time,velocity_2);

%% Stress, strain, and strain rate calculation ----------------------------
----------------
eng_stress = force/sample_cross_sectional_area;
%units in N/m^2)
eng_stress = eng_stress/1e+6;
eng_strain = displacement_2/sample_thickness;
eng_strain_rate = gradient(eng_strain,time);

true_stress = eng_stress.*(1+eng_strain);               %units in N/m^2)
true_strain = log(1+eng_strain);
true_strain_rate = gradient(true_strain,time);

modified_eng_strain = (displacement_2-displacement_1)/sample_thickness;
%to compensate for the movement of the force gauge
modified_eng_strain_rate = gradient(modified_eng_strain, time);         %to
compensate for the movement of the force gauge
```

```
modified_true_stress = eng_stress.*(1+modified_eng_strain);              %to
compensate for the movement of the force gauge
modified_true_strain = log(1+modified_eng_strain);                       %to
compensate for the movement of the force gauge
modified_true_strain_rate = gradient(modified_true_strain,time);         %to
compensate for the movement of the force gauge

%% Filtering data
cutoff_frequency = 0.1;
time_interval = time(2,1) - time(1,1);
sampling_frequency = 1/time_interval;
nyquist_frequency = 0.5*sampling_frequency;
norm_cutoff_frequency = cutoff_frequency/nyquist_frequency;
lpfilter = fir1(25,norm_cutoff_frequency,'low');
filtered_eng_stress = filtfilt(lpfilter,1,eng_stress);

%% Finding maximum stress for truncation point
max_filtered_eng_stress = max(filtered_eng_stress);
truncation_point = find(filtered_eng_stress == max_filtered_eng_stress);

truncated_filtered_eng_stress = filtered_eng_stress(1:truncation_point,1);
truncated_modified_eng_strain = modified_eng_strain(1:truncation_point,1);
truncated_modified_eng_strain_rate =
modified_eng_strain_rate(1:truncation_point,1);
truncated_displacement_1 = displacement_1(1:truncation_point,1);
truncated_displacement_2 = displacement_2(1:truncation_point,1);

%% Getting rid of beginning negative strain
negative_truncation_index = find(truncated_modified_eng_strain < 0, 1);
empty_check = isempty(negative_truncation_index);

if empty_check == 0

    truncated_modified_eng_strain_negative_start =
truncated_modified_eng_strain(negative_truncation_index:end,1);

    positive_truncated_modified_eng_strain =
truncated_modified_eng_strain_negative_start(truncated_modified_eng_strain_ne
gative_start > 0);
    positive_truncation_index = find(truncated_modified_eng_strain ==
positive_truncated_modified_eng_strain(1,1));

    positive_truncated_modified_eng_strain_rate =
truncated_modified_eng_strain_rate(positive_truncation_index:end,1);

    positive_truncated_displacement_1 =
truncated_displacement_1(positive_truncation_index:end,1);
    positive_truncated_displacement_2 =
truncated_displacement_2(positive_truncation_index:end,1);

    positive_truncated_filtered_eng_stress =
truncated_filtered_eng_stress(positive_truncation_index:end,1);

    lengthforloop = length(positive_truncated_filtered_eng_stress) - 1;
    c = 1;
```

```
    for c = 1:lengthforloop
        first = positive_truncated_filtered_eng_stress(c);
        second = positive_truncated_filtered_eng_stress(c+1);

        delta_stress = second-first;

        delta_stress_data(c,:) = delta_stress;

        c = c+1;
    end

    lengthforloop = length(delta_stress_data);
    i = 1;
    for i = 1:lengthforloop

        stress_boolean = delta_stress_data < 0;              % creates a
boolean check for negative values (0 if positive, 1 if negative)
        truncated_stress_boolean = stress_boolean(i:end,1);
        truncated_stress_boolean_sum = sum(truncated_stress_boolean);
        stress_truncation_sum(i,:) = truncated_stress_boolean_sum;
    end

    lengthforloop = length(stress_truncation_sum);
    i = 1;
    for i = 1:lengthforloop
        if stress_truncation_sum(i,1) > 0;
            stress_truncation_boolean(i,:) = 0;
        elseif stress_truncation_sum(i,1) == 0;
            stress_truncation_boolean(i,:) = 1;
        end
    end

    stress_truncation_index = find(stress_truncation_boolean == 1, 1);

    positive_truncated_filtered_eng_stress =
positive_truncated_filtered_eng_stress(stress_truncation_index:end,1);
    positive_truncated_filtered_eng_stress =
positive_truncated_filtered_eng_stress -
positive_truncated_filtered_eng_stress(1,1);

    positive_truncated_modified_eng_strain =
positive_truncated_modified_eng_strain(stress_truncation_index:end,1);
    positive_truncated_modified_eng_strain =
positive_truncated_modified_eng_strain -
positive_truncated_modified_eng_strain(1,1);

    positive_truncated_modified_eng_strain_rate =
positive_truncated_modified_eng_strain_rate(stress_truncation_index:end,1);
    positive_truncated_modified_eng_strain_rate =
positive_truncated_modified_eng_strain_rate -
positive_truncated_modified_eng_strain_rate(1,1);

    positive_truncated_displacement_1 =
positive_truncated_displacement_1(stress_truncation_index:end,1);
```

```
    positive_truncated_displacement_2 =
positive_truncated_displacement_2(stress_truncation_index:end,1);

elseif empty_check == 1

    lengthforloop = length(truncated_filtered_eng_stress) - 1;
    c = 1;
    for c = 1:lengthforloop
        first = truncated_filtered_eng_stress(c);
        second = truncated_filtered_eng_stress(c+1);

        delta_stress = second-first;

        delta_stress_data(c,:) = delta_stress;

        c = c+1;
    end

    lengthforloop = length(delta_stress_data);
    i = 1;
    for i = 1:lengthforloop

        stress_boolean = delta_stress_data < 0;              % creates a
boolean check for negative values (0 if positive, 1 if negative)
        truncated_stress_boolean = stress_boolean(i:end,1);
        truncated_stress_boolean_sum = sum(truncated_stress_boolean);
        stress_truncation_sum(i,:) = truncated_stress_boolean_sum;
    end

    lengthforloop = length(stress_truncation_sum);
    i = 1;
    for i = 1:lengthforloop
        if stress_truncation_sum(i,1) > 0;
            stress_truncation_boolean(i,:) = 0;
        elseif stress_truncation_sum(i,1) == 0;
            stress_truncation_boolean(i,:) = 1;
        end
    end

    stress_truncation_index = find(stress_truncation_boolean == 1, 1);

    positive_truncated_filtered_eng_stress =
truncated_filtered_eng_stress(stress_truncation_index:end,1);
    positive_truncated_filtered_eng_stress =
positive_truncated_filtered_eng_stress -
positive_truncated_filtered_eng_stress(1,1);

    positive_truncated_modified_eng_strain =
truncated_modified_eng_strain(stress_truncation_index:end,1);
    positive_truncated_modified_eng_strain =
positive_truncated_modified_eng_strain -
positive_truncated_modified_eng_strain(1,1);
```

```
    positive_truncated_modified_eng_strain_rate =
truncated_modified_eng_strain_rate(stress_truncation_index:end,1);
    positive_truncated_modified_eng_strain_rate =
positive_truncated_modified_eng_strain_rate -
positive_truncated_modified_eng_strain_rate(1,1);

    positive_truncated_displacement_1 =
truncated_displacement_1(stress_truncation_index:end,1);
    positive_truncated_displacement_2 =
truncated_displacement_2(stress_truncation_index:end,1);

end

%% Modulus calculation using forward difference method
lengthForLoop = length(positive_truncated_modified_eng_strain) - 1;
i=1;
for i = 1:lengthForLoop

    first_stress = positive_truncated_filtered_eng_stress(i);
    second_stress = positive_truncated_filtered_eng_stress(i+1);
    first_strain = positive_truncated_modified_eng_strain(i);
    second_strain = positive_truncated_modified_eng_strain(i+1);

    derivative_value = (second_stress - first_stress)/(second_strain -
first_strain);

    Modulus_data(i,:) = derivative_value;

    i = i+1;

end

Modulus_data = [0;Modulus_data];

%% Strain rate information
avg_strain_rate = mean(positive_truncated_modified_eng_strain_rate);
max_strain_rate = max(positive_truncated_modified_eng_strain_rate);

%% Calculating energy dissipation
energy_dissipation =
cumtrapz(positive_truncated_modified_eng_strain,positive_truncated_filtered_e
ng_stress);

%% Maximums for plotting axes
stress_strain_x_axis = max(positive_truncated_modified_eng_strain)*1.1;
stress_strain_y_axis = max(positive_truncated_filtered_eng_stress)*1.1;

energy_x_axis = max(energy_dissipation)*1.1;
energy_y_axis = stress_strain_y_axis;

tangent_modulus_x_axis = stress_strain_y_axis;
tangent_modulus_y_axis = max(Modulus_data)*1.1;
```

```
strain_rate_x_axis = max((positive_truncated_displacement_2-
positive_truncated_displacement_1)*1000)*1.1;
strain_rate_y_axis = max(positive_truncated_modified_eng_strain_rate)*1.1;

%% Plotting stress-strain and energy dissipation curves
figure
tiledlayout(2,1)

nexttile
plot(positive_truncated_modified_eng_strain,positive_truncated_filtered_eng_s
tress,'b');
title('Stress-Strain Curve');
xlabel('Strain');
ylabel('Stress (MPa)');
xlim([0 stress_strain_x_axis]);
ylim([0 stress_strain_y_axis]);

nexttile
plot(energy_dissipation,positive_truncated_filtered_eng_stress,'r');
title('Engergy Dissipation Curve');
xlabel('Energy per volume (x10^6 J/m^3)');
ylabel('Stress (MPa)');
xlim([0 energy_x_axis]);
ylim([0 energy_y_axis]);

file_name = file(1:end-5);
saving_file_name = fullfile(path,file_name);
stress_strain_energy_ending = ' (Stress-Strain & Energy Dissipation Plots)';
stress_strain_energy_file_name =
append(saving_file_name,stress_strain_energy_ending);
saveas(gcf,stress_strain_energy_file_name,'svg');

%% Plotting strain rate vs. displacement
figure
plot((positive_truncated_displacement_2-
positive_truncated_displacement_1)*1000,positive_truncated_modified_eng_strai
n_rate,'b');
title('Strain Rate vs Displacement');
xlabel('Displacement (mm)');
ylabel('Strain Rate (s^-1)');
xlim([0 strain_rate_x_axis]);
ylim([0 strain_rate_y_axis]);

saving_file_name = fullfile(path,file_name);
strain_rate_ending = ' (Strain Rate vs Displacement Plot)';
strain_rate_file_name = append(saving_file_name,strain_rate_ending);
saveas(gcf,strain_rate_file_name,'svg');

%% Plotting tangent modulus curve
figure
plot(positive_truncated_filtered_eng_stress,Modulus_data,'b');
title('Tangent Modulus Curve');
xlabel('Stress (MPa)');
ylabel('Tangent Modulus (MPa)');
xlim([0 tangent_modulus_x_axis]);
```

```
ylim([0 tangent_modulus_y_axis]);

saving_file_name = fullfile(path,file_name);
tangent_modulus_ending = ' (Tangent Modulus Plot)';
tangent_modulus_file_name = append(saving_file_name,tangent_modulus_ending);
saveas(gcf,tangent_modulus_file_name,'svg');

%% Saving processed data
processed_data = [positive_truncated_modified_eng_strain,
positive_truncated_filtered_eng_stress, energy_dissipation, Modulus_data];
processed_data = array2table(processed_data);
processed_data.Properties.VariableNames = {'Eng Strain', 'Eng Stress (MPa)',
'Energy Dissipation (x10^6 J/m^3)', 'Tangent Modulus (MPa)'};
csv_ending = ' (Processed Data).csv';
processed_data_file_name = append(saving_file_name,csv_ending);
writetable(processed_data,processed_data_file_name);

% %% Saving modulus data
% tangent_modulus_data = [positive_truncated_filtered_eng_stress,
Modulus_data];
% tangent_modulus_data = array2table(tangent_modulus_data);
% tangent_modulus_data.Properties.VariableNames = {'Stress (MPa)', 'Tangent
Modulus (MPa)'};
% csv_ending = ' (Modulus Data).csv';
% tangent_modulus_data_file_name = append(saving_file_name,csv_ending);
% writetable(tangent_modulus_data,tangent_modulus_data_file_name);

%% Saving text file of average and max strain rate
strain_rate_info = [avg_strain_rate,max_strain_rate];
strain_rate_info = array2table(strain_rate_info);
strain_rate_info.Properties.VariableNames = {'Avg Strain Rate', 'Max Strain
Rate'};
strain_rate_info_ending = ' (Strain Rate Info)';
strain_rate_info_file_name =
append(saving_file_name,strain_rate_info_ending);
writetable(strain_rate_info, strain_rate_info_file_name);

%% Opening other processed data if 3rd trial, then plotting all together
number = '3';
check_for_third_trial = contains(file,number);
if check_for_third_trial == 1
    % opening data and converting to array
    [file_trial_1,path_trial_1] = uigetfile('*.csv','Select Trial 1 Processed
CSV file',path);
    [file_trial_2,path_trial_2] = uigetfile('*.csv','Select Trial 2 Processed
CSV file',path);
    [file_trial_3,path_trial_3] = uigetfile('*.csv','Select Trial 3 Processed
CSV file',path);

    trial_1 = readtable(file_trial_1);
    strain_1 = trial_1(:,1);
    strain_1 = table2array(strain_1);
    trial_2 = readtable(file_trial_2);
    strain_2 = trial_2(:,1);
    strain_2 = table2array(strain_2);
    trial_3 = readtable(file_trial_3);
```

```
    strain_3 = trial_3(:,1);
    strain_3 = table2array(strain_3);

    % finding which trial should be used as the x-axis for the graph
    max_strain_1 = max(strain_1);
    max_strain_2 = max(strain_2);
    max_strain_3 = max(strain_3);
    all_trials_strain = [max_strain_1; max_strain_2; max_strain_3];
    all_trials_max_strain = max(all_trials_strain);
    trial_to_use_for_strain = find(all_trials_strain ==
all_trials_max_strain);

    strain_1 = transpose(strain_1);
    strain_2 = transpose(strain_2);
    strain_3 = transpose(strain_3);

    % finding stress and length of stress
    stress_1 = trial_1(:,2);
    stress_1 = table2array(stress_1);
    length_stress_1 = length(stress_1);
    stress_2 = trial_2(:,2);
    stress_2 = table2array(stress_2);
    length_stress_2 = length(stress_2);
    stress_3 = trial_3(:,2);
    stress_3 = table2array(stress_3);
    length_stress_3 = length(stress_3);

    max_stress_1 = max(stress_1);
    max_stress_2 = max(stress_2);
    max_stress_3 = max(stress_3);
    all_trials_stress = [max_stress_1; max_stress_2; max_stress_3];
    all_trials_max_stress = max(all_trials_stress);

    stress_1 = transpose(stress_1);
    stress_2 = transpose(stress_2);
    stress_3 = transpose(stress_3);

    %energy dissipation
    energy_1 = trial_1(:,3);
    energy_1 = table2array(energy_1);
    energy_2 = trial_2(:,3);
    energy_2 = table2array(energy_2);
    energy_3 = trial_3(:,3);
    energy_3 = table2array(energy_3);

    max_energy_1 = max(energy_1);
    max_energy_2 = max(energy_2);
    max_energy_3 = max(energy_3);
    all_trials_energy = [max_energy_1; max_energy_2; max_energy_3];
    all_trials_max_energy = max(all_trials_energy);

    figure
    plot(strain_1,stress_1,'r','DisplayName','Trial 1');
    title('Combined Stress-Strain Curves');
    xlabel('Strain');
```

```
    ylabel('Stress (MPa)');
    xlim([0 (all_trials_max_strain*1.1)]);
    ylim([0 (all_trials_max_stress*1.1)]);
    hold on
    plot(strain_2,stress_2,'g','DisplayName','Trial 2');
    plot(strain_3,stress_3,'b','DisplayName','Trial 3');
    legend('Location','north');
    hold off


    % Saving graphs to appropriate folder
    saving_file_name = saving_file_name(1:end-8);
    summary_plot_ending = 'All Trials Stress-Strain Curve';
    summary_plot_file_name = append(saving_file_name,summary_plot_ending);
    saveas(gcf,summary_plot_file_name,'svg');

    % Summary Energy Dissipation Plot
    figure
    plot(energy_1,stress_1,'r','DisplayName','Trial 1');
    title('Combined Energy Dissipation Curves');
    xlabel('Energy per volume (x10^6 J/m^3)');
    ylabel('Stress (MPa)');
    xlim([0 (all_trials_max_energy*1.1)]);
    ylim([0 (all_trials_max_stress*1.1)]);
    hold on
    plot(energy_2,stress_2,'g','DisplayName','Trial 2');
    plot(energy_3,stress_3,'b','DisplayName','Trial 3');
    legend('Location','north');
    hold off

    % saving summary energy dissipation figure
    summary_plot_energy_ending = 'All Trials Energy Dissipation Curve';
    summary_plot_energy_file_name =
append(saving_file_name,summary_plot_energy_ending);
    saveas(gcf,summary_plot_energy_file_name,'svg');

    m_stress_1 = trial_1(:,2);
    m_stress_1 = table2array(m_stress_1);
    modulus_1 = trial_1(:,4);
    modulus_1 = table2array(modulus_1);

    m_stress_2 = trial_2(:,2);
    m_stress_2 = table2array(m_stress_2);
    modulus_2 = trial_2(:,4);
    modulus_2 = table2array(modulus_2);

    m_stress_3 = trial_3(:,2);
    m_stress_3 = table2array(m_stress_3);
    modulus_3 = trial_3(:,4);
    modulus_3 = table2array(modulus_3);

    % finding which trial should be used as the x-axis for the tangent
modulus plot
    max_m_stress_1 = max(m_stress_1);
    max_m_stress_2 = max(m_stress_2);
```

```
    max_m_stress_3 = max(m_stress_3);
    all_trials_m_stress = [max_m_stress_1; max_m_stress_2; max_m_stress_3];
    all_trials_max_m_stress = max(all_trials_m_stress);

    % finding which trial should be used as the y-axis for the tangent
modulus plot
    max_modulus_1 = max(modulus_1);
    max_modulus_2 = max(modulus_2);
    max_modulus_3 = max(modulus_3);
    all_trials_modulus = [max_modulus_1; max_modulus_2; max_modulus_3];
    all_trials_max_modulus = max(all_trials_modulus);

    % Summary tangent modulus plot
    figure
    plot(m_stress_1,modulus_1,'r','DisplayName','Trial 1');
    title('Combined Tangent Modulus Curves');
    xlabel('Stress (MPa)');
    ylabel('Tangent Modulus (MPa)');
    xlim([0 (all_trials_max_m_stress*1.1)]);
    ylim([0 (all_trials_max_modulus*1.1)]);
    hold on
    plot(m_stress_2,modulus_2,'g','DisplayName','Trial 2');
    plot(m_stress_3,modulus_3,'b','DisplayName','Trial 3');
    legend('Location','north');
    hold off

    % saving summary tangent modulus figure
    summary_plot_energy_ending = 'All Trials Tangent Modulus Curve';
    summary_plot_energy_file_name =
append(saving_file_name,summary_plot_energy_ending);
    saveas(gcf,summary_plot_energy_file_name,'svg');

end
```

Material Testing Data Averaging Script

```
clear all;
clear allvars;
clc;

%% Opening files for comparison
[file1,path] = uigetfile('*.csv','Select AMBIENT 0.01s processed CSV file
1','C:\Material Testing\CSV Exports');
addpath(path);
[file2,path] = uigetfile('*.csv','Select AMBIENT 0.01s processed CSV file
2',path);
[file3,path] = uigetfile('*.csv','Select AMBIENT 0.01s processed CSV file
3',path);

Cascade = 'Cascade';
Hummingbird = 'Hummingbird';
check_for_cascade = contains(path,Cascade);
```

```
if check_for_cascade == 1
    [file4,path] = uigetfile('*.csv','Select AMBIENT 1s processed CSV file
1','C:\Material Testing\CSV Exports\Ambient\Cascade 1s');
    addpath(path);
    [file5,path] = uigetfile('*.csv','Select AMBIENT 1s processed CSV file
2',path);
    [file6,path] = uigetfile('*.csv','Select AMBIENT 1s processed CSV file
3',path);

    [file7,path] = uigetfile('*.csv','Select COLD 0.01s processed CSV file
1','C:\Material Testing\CSV Exports\Cold\Cascade 0.01s');
    addpath(path);
    [file8,path] = uigetfile('*.csv','Select COLD 0.01s processed CSV file
2',path);
    [file9,path] = uigetfile('*.csv','Select COLD 0.01s processed CSV file
3',path);

    [file10,path] = uigetfile('*.csv','Select COLD 1s processed CSV file
1','C:\Material Testing\CSV Exports\Cold\Cascade 1s');
    addpath(path);
    [file11,path] = uigetfile('*.csv','Select COLD 1s processed CSV file
2',path);
    [file12,path] = uigetfile('*.csv','Select COLD 1s processed CSV file
3',path);

    [file13,path] = uigetfile('*.csv','Select AMBIENT 100s processed CSV file
1','C:\Material Testing\CSV Exports\Pneumatic Excel Files\Ambient\Cascade
100s');
    addpath(path);
    [file14,path] = uigetfile('*.csv','Select AMBIENT 100s processed CSV file
2',path);
    [file15,path] = uigetfile('*.csv','Select AMBIENT 100s processed CSV file
3',path);

    [file16,path] = uigetfile('*.csv','Select COLD 100s processed CSV file
1','C:\Material Testing\CSV Exports\Pneumatic Excel Files\Cold\Cascade
100s');
    addpath(path);
    [file17,path] = uigetfile('*.csv','Select COLD 100s processed CSV file
2',path);
    [file18,path] = uigetfile('*.csv','Select COLD 100s processed CSV file
3',path);

else
    [file4,path] = uigetfile('*.csv','Select AMBIENT 1s processed CSV file
1','C:\Material Testing\CSV Exports\Ambient\Hummingbird 1s');
    addpath(path);
    [file5,path] = uigetfile('*.csv','Select AMBIENT 1s processed CSV file
2',path);
    [file6,path] = uigetfile('*.csv','Select AMBIENT 1s processed CSV file
3',path);

    [file7,path] = uigetfile('*.csv','Select COLD 0.01s processed CSV file
1','C:\Material Testing\CSV Exports\Cold\Hummingbird 0.01s');
    addpath(path);
```

```
    [file8,path] = uigetfile('*.csv','Select COLD 0.01s processed CSV file
2',path);
    [file9,path] = uigetfile('*.csv','Select COLD 0.01s processed CSV file
3',path);

    [file10,path] = uigetfile('*.csv','Select COLD 1s processed CSV file
1','C:\Material Testing\CSV Exports\Cold\Hummingbird 1s');
    addpath(path);
    [file11,path] = uigetfile('*.csv','Select COLD 1s processed CSV file
2',path);
    [file12,path] = uigetfile('*.csv','Select COLD 1s processed CSV file
3',path);

    [file13,path] = uigetfile('*.csv','Select AMBIENT 100s processed CSV file
1','C:\Material Testing\CSV Exports\Pneumatic Excel Files\Ambient\Hummingbird
100s');
    addpath(path);
    [file14,path] = uigetfile('*.csv','Select AMBIENT 100s processed CSV file
2',path);
    [file15,path] = uigetfile('*.csv','Select AMBIENT 100s processed CSV file
3',path);

    [file16,path] = uigetfile('*.csv','Select COLD 100s processed CSV file
1','C:\Material Testing\CSV Exports\Pneumatic Excel Files\Cold\Hummingbird
100s');
    addpath(path);
    [file17,path] = uigetfile('*.csv','Select COLD 100s processed CSV file
2',path);
    [file18,path] = uigetfile('*.csv','Select COLD 100s processed CSV file
3',path);

end

%% Reading in processed data and modulus data
trial1 = readtable(file1);
trial2 = readtable(file2);
trial3 = readtable(file3);
trial4 = readtable(file4);
trial5 = readtable(file5);
trial6 = readtable(file6);
trial7 = readtable(file7);
trial8 = readtable(file8);
trial9 = readtable(file9);
trial10 = readtable(file10);
trial11 = readtable(file11);
trial12 = readtable(file12);
trial13 = readtable(file13);
trial14 = readtable(file14);
trial15 = readtable(file15);
trial16 = readtable(file16);
trial17 = readtable(file17);
trial18 = readtable(file18);


%% Converting table data to array data
```

```
trial1 = table2array(trial1);
trial2 = table2array(trial2);
trial3 = table2array(trial3);
trial4 = table2array(trial4);
trial5 = table2array(trial5);
trial6 = table2array(trial6);
trial7 = table2array(trial7);
trial8 = table2array(trial8);
trial9 = table2array(trial9);
trial10 = table2array(trial10);
trial11 = table2array(trial11);
trial12 = table2array(trial12);
trial13 = table2array(trial13);
trial14 = table2array(trial14);
trial15 = table2array(trial15);
trial16 = table2array(trial16);
trial17 = table2array(trial17);
trial18 = table2array(trial18);


%% Strain
strain1 = trial1(:,1);
strain2 = trial2(:,1);
strain3 = trial3(:,1);
strain4 = trial4(:,1);
strain5 = trial5(:,1);
strain6 = trial6(:,1);
strain7 = trial7(:,1);
strain8 = trial8(:,1);
strain9 = trial9(:,1);
strain10 = trial10(:,1);
strain11 = trial11(:,1);
strain12 = trial12(:,1);
strain13 = trial13(:,1);
strain14 = trial14(:,1);
strain15 = trial15(:,1);
strain16 = trial16(:,1);
strain17 = trial17(:,1);
strain18 = trial18(:,1);

maxstrain1 = max(strain1);
maxstrain2 = max(strain2);
maxstrain3 = max(strain3);
maxstrain4 = max(strain4);
maxstrain5 = max(strain5);
maxstrain6 = max(strain6);
maxstrain7 = max(strain7);
maxstrain8 = max(strain8);
maxstrain9 = max(strain9);
maxstrain10 = max(strain10);
maxstrain11 = max(strain11);
maxstrain12 = max(strain12);
maxstrain13 = max(strain13);
maxstrain14 = max(strain14);
maxstrain15 = max(strain15);
maxstrain16 = max(strain16);
```

```
maxstrain17 = max(strain17);
maxstrain18 = max(strain18);

alltrialsstrain =
[maxstrain1;maxstrain2;maxstrain3;maxstrain4;maxstrain5;maxstrain6;maxstrain7
;maxstrain8;maxstrain9;maxstrain10;maxstrain11;maxstrain12;maxstrain13;maxstr
ain14;maxstrain15;maxstrain16;maxstrain17;maxstrain18];
alltrialsmaxstrain = max(alltrialsstrain);

%% Stress
stress1 = trial1(:,2);
stress2 = trial2(:,2);
stress3 = trial3(:,2);
stress4 = trial4(:,2);
stress5 = trial5(:,2);
stress6 = trial6(:,2);
stress7 = trial7(:,2);
stress8 = trial8(:,2);
stress9 = trial9(:,2);
stress10 = trial10(:,2);
stress11 = trial11(:,2);
stress12 = trial12(:,2);
stress13 = trial13(:,2);
stress14 = trial14(:,2);
stress15 = trial15(:,2);
stress16 = trial16(:,2);
stress17 = trial17(:,2);
stress18 = trial18(:,2);

maxstress1 = max(stress1);
maxstress2 = max(stress2);
maxstress3 = max(stress3);
maxstress4 = max(stress4);
maxstress5 = max(stress5);
maxstress6 = max(stress6);
maxstress7 = max(stress7);
maxstress8 = max(stress8);
maxstress9 = max(stress9);
maxstress10 = max(stress10);
maxstress11 = max(stress11);
maxstress12 = max(stress12);
maxstress13 = max(stress13);
maxstress14 = max(stress14);
maxstress15 = max(stress15);
maxstress16 = max(stress16);
maxstress17 = max(stress17);
maxstress18 = max(stress18);

alltrialsstress =
[maxstress1;maxstress2;maxstress3;maxstress4;maxstress5;maxstress6;maxstress7
;maxstress8;maxstress9;maxstress10;maxstress11;maxstress12;maxstress13;maxstr
ess14;maxstress15;maxstress16;maxstress17;maxstress18];
alltrialsmaxstress = max(alltrialsstress);

%% Finding minimum max strain of all 6 trials
minimum_overall_strain = min(alltrialsstrain);
```

```
strain_interval = minimum_overall_strain/300;
xq = 0:strain_interval:minimum_overall_strain;

%% Interpolating stress-strain curves
int_results_trial_1 = interp1(strain1,stress1,xq);
i = 1;
for i = 1:length(int_results_trial_1)
    if int_results_trial_1(1,i) < 0
        int_results_trial_1(1,i) = 0;
        i = i+1;
    else
        int_results_trial_1(1,i) = int_results_trial_1(1,i);
    end
end

int_results_trial_2 = interp1(strain2,stress2,xq);
i = 1;
for i = 1:length(int_results_trial_2)
    if int_results_trial_2(1,i) < 0
        int_results_trial_2(1,i) = 0;
        i = i+1;
    else
        int_results_trial_2(1,i) = int_results_trial_2(1,i);
    end
end

int_results_trial_3 = interp1(strain3,stress3,xq);
i = 1;
for i = 1:length(int_results_trial_3)
    if int_results_trial_3(1,i) < 0
        int_results_trial_3(1,i) = 0;
        i = i+1;
    else
        int_results_trial_2(1,i) = int_results_trial_2(1,i);
    end
end

int_results_trial_4 = interp1(strain4,stress4,xq);
i = 1;
for i = 1:length(int_results_trial_4)
    if int_results_trial_4(1,i) < 0
        int_results_trial_4(1,i) = 0;
        i = i+1;
    else
        int_results_trial_4(1,i) = int_results_trial_4(1,i);
    end
end

int_results_trial_5 = interp1(strain5,stress5,xq);
i = 1;
for i = 1:length(int_results_trial_5)
    if int_results_trial_5(1,i) < 0
        int_results_trial_5(1,i) = 0;
        i = i+1;
    else
        int_results_trial_5(1,i) = int_results_trial_5(1,i);
```

```
    end
end

int_results_trial_6 = interp1(strain6,stress6,xq);
i = 1;
for i = 1:length(int_results_trial_6)
    if int_results_trial_6(1,i) < 0
        int_results_trial_6(1,i) = 0;
        i = i+1;
    else
        int_results_trial_6(1,i) = int_results_trial_6(1,i);
    end
end

int_results_trial_7 = interp1(strain7,stress7,xq);
i = 1;
for i = 1:length(int_results_trial_7)
    if int_results_trial_7(1,i) < 0
        int_results_trial_7(1,i) = 0;
        i = i+1;
    else
        int_results_trial_7(1,i) = int_results_trial_7(1,i);
    end
end

int_results_trial_8 = interp1(strain8,stress8,xq);
i = 1;
for i = 1:length(int_results_trial_8)
    if int_results_trial_8(1,i) < 0
        int_results_trial_8(1,i) = 0;
        i = i+1;
    else
        int_results_trial_8(1,i) = int_results_trial_8(1,i);
    end
end

int_results_trial_9 = interp1(strain9,stress9,xq);
i = 1;
for i = 1:length(int_results_trial_9)
    if int_results_trial_9(1,i) < 0
        int_results_trial_9(1,i) = 0;
        i = i+1;
    else
        int_results_trial_9(1,i) = int_results_trial_9(1,i);
    end
end

int_results_trial_10 = interp1(strain10,stress10,xq);
i = 1;
for i = 1:length(int_results_trial_10)
    if int_results_trial_10(1,i) < 0
        int_results_trial_10(1,i) = 0;
        i = i+1;
    else
        int_results_trial_10(1,i) = int_results_trial_10(1,i);
    end
```

```
end

int_results_trial_11 = interp1(strain11,stress11,xq);
i = 1;
for i = 1:length(int_results_trial_11)
    if int_results_trial_11(1,i) < 0
        int_results_trial_11(1,i) = 0;
        i = i+1;
    else
        int_results_trial_11(1,i) = int_results_trial_11(1,i);
    end
end

int_results_trial_12 = interp1(strain12,stress12,xq);
i = 1;
for i = 1:length(int_results_trial_12)
    if int_results_trial_12(1,i) < 0
        int_results_trial_12(1,i) = 0;
        i = i+1;
    else
        int_results_trial_12(1,i) = int_results_trial_12(1,i);
    end
end

int_results_trial_13 = interp1(strain13,stress13,xq);
i = 1;
for i = 1:length(int_results_trial_13)
    if int_results_trial_13(1,i) < 0
        int_results_trial_13(1,i) = 0;
        i = i+1;
    else
        int_results_trial_13(1,i) = int_results_trial_13(1,i);
    end
end

int_results_trial_14 = interp1(strain14,stress14,xq);
i = 1;
for i = 1:length(int_results_trial_14)
    if int_results_trial_14(1,i) < 0
        int_results_trial_14(1,i) = 0;
        i = i+1;
    else
        int_results_trial_14(1,i) = int_results_trial_14(1,i);
    end
end

int_results_trial_15 = interp1(strain15,stress15,xq);
i = 1;
for i = 1:length(int_results_trial_15)
    if int_results_trial_15(1,i) < 0
        int_results_trial_15(1,i) = 0;
        i = i+1;
    else
        int_results_trial_15(1,i) = int_results_trial_15(1,i);
    end
end
```

```
int_results_trial_16 = interp1(strain16,stress16,xq);
i = 1;
for i = 1:length(int_results_trial_16)
    if int_results_trial_16(1,i) < 0
        int_results_trial_16(1,i) = 0;
        i = i+1;
    else
        int_results_trial_16(1,i) = int_results_trial_16(1,i);
    end
end

int_results_trial_17 = interp1(strain17,stress17,xq);
i = 1;
for i = 1:length(int_results_trial_17)
    if int_results_trial_17(1,i) < 0
        int_results_trial_17(1,i) = 0;
        i = i+1;
    else
        int_results_trial_17(1,i) = int_results_trial_17(1,i);
    end
end

int_results_trial_18 = interp1(strain18,stress18,xq);
i = 1;
for i = 1:length(int_results_trial_18)
    if int_results_trial_18(1,i) < 0
        int_results_trial_18(1,i) = 0;
        i = i+1;
    else
        int_results_trial_18(1,i) = int_results_trial_18(1,i);
    end
end

average_curve_1 =
(int_results_trial_1+int_results_trial_2+int_results_trial_3)/3;          %
AMBIENT 0.01/s
average_curve_2 =
(int_results_trial_4+int_results_trial_5+int_results_trial_6)/3;          %
AMBIENT 1/s
average_curve_3 =
(int_results_trial_7+int_results_trial_8+int_results_trial_9)/3;          %
COLD 0.01/s
average_curve_4 =
(int_results_trial_10+int_results_trial_11+int_results_trial_12)/3;       %
COLD 1/s
average_curve_5 =
(int_results_trial_13+int_results_trial_14+int_results_trial_15)/3;       %
AMBIENT 100/s
average_curve_6 =
(int_results_trial_16+int_results_trial_17+int_results_trial_18)/3;       %
COLD 100/s

average_curves =
[average_curve_1,average_curve_2,average_curve_3,average_curve_4,average_curv
e_5,average_curve_6];
```

```
max_average_curves = max(average_curves);

average_curve_1(1,1) = 0;
average_curve_2(1,1) = 0;
average_curve_3(1,1) = 0;
average_curve_4(1,1) = 0;
average_curve_5(1,1) = 0;
average_curve_6(1,1) = 0;

%% Calculating energy dissipation from average curves
average_curve_1 = transpose(average_curve_1);
average_curve_2 = transpose(average_curve_2);
average_curve_3 = transpose(average_curve_3);
average_curve_4 = transpose(average_curve_4);
average_curve_5 = transpose(average_curve_5);
average_curve_6 = transpose(average_curve_6);
xq = transpose(xq);

avg_energy_curve_1 = cumtrapz(xq,average_curve_1);
avg_energy_curve_2 = cumtrapz(xq,average_curve_2);
avg_energy_curve_3 = cumtrapz(xq,average_curve_3);
avg_energy_curve_4 = cumtrapz(xq,average_curve_4);
avg_energy_curve_5 = cumtrapz(xq,average_curve_5);
avg_energy_curve_6 = cumtrapz(xq,average_curve_6);

avg_energy_curve_1 = transpose(avg_energy_curve_1);
avg_energy_curve_2 = transpose(avg_energy_curve_2);
avg_energy_curve_3 = transpose(avg_energy_curve_3);
avg_energy_curve_4 = transpose(avg_energy_curve_4);
avg_energy_curve_5 = transpose(avg_energy_curve_5);
avg_energy_curve_6 = transpose(avg_energy_curve_6);

average_curve_1 = transpose(average_curve_1);
average_curve_2 = transpose(average_curve_2);
average_curve_3 = transpose(average_curve_3);
average_curve_4 = transpose(average_curve_4);
average_curve_5 = transpose(average_curve_5);
average_curve_6 = transpose(average_curve_6);
xq = transpose(xq);

%% Interpolation for energy dissipation curve
max_avg_energy_curve_1 = max(avg_energy_curve_1);
max_avg_energy_curve_2 = max(avg_energy_curve_2);
max_avg_energy_curve_3 = max(avg_energy_curve_3);
max_avg_energy_curve_4 = max(avg_energy_curve_4);
max_avg_energy_curve_5 = max(avg_energy_curve_5);
max_avg_energy_curve_6 = max(avg_energy_curve_6);

max_avg_energy_curves =
[max_avg_energy_curve_1;max_avg_energy_curve_2;max_avg_energy_curve_3;max_avg
_energy_curve_4;max_avg_energy_curve_5;max_avg_energy_curve_6];
minimum_max_avg_energy = min(max_avg_energy_curves);

energy_interval = minimum_max_avg_energy/300;
```

```
energy_xq = 0:energy_interval:minimum_max_avg_energy;

int_avg_energy_curve_1 =
interp1(avg_energy_curve_1,average_curve_1,energy_xq);
int_avg_energy_curve_2 =
interp1(avg_energy_curve_2,average_curve_2,energy_xq);
int_avg_energy_curve_3 =
interp1(avg_energy_curve_3,average_curve_3,energy_xq);
int_avg_energy_curve_4 =
interp1(avg_energy_curve_4,average_curve_4,energy_xq);
int_avg_energy_curve_5 =
interp1(avg_energy_curve_5,average_curve_5,energy_xq);
int_avg_energy_curve_6 =
interp1(avg_energy_curve_6,average_curve_6,energy_xq);

%% Calculating tangent modulus from average curves
lengthForLoop = length(xq)-1;
i=1;
for i =1:lengthForLoop
    first_stress = average_curve_1(i);
    second_stress = average_curve_1(i+1);
    first_strain = xq(i);
    second_strain = xq(i+1);

    derivative_value_1 = (second_stress - first_stress)/(second_strain -
first_strain);

    avg_modulus_data_1(1,i) = derivative_value_1;

    i = i+1;
end

avg_modulus_data_1 = [0,avg_modulus_data_1];

i=1;
for i =1:lengthForLoop
    first_stress = average_curve_2(i);
    second_stress = average_curve_2(i+1);
    first_strain = xq(i);
    second_strain = xq(i+1);

    derivative_value_2 = (second_stress - first_stress)/(second_strain -
first_strain);

    avg_modulus_data_2(1,i) = derivative_value_2;

    i = i+1;
end

avg_modulus_data_2 = [0,avg_modulus_data_2];

i=1;
for i =1:lengthForLoop
    first_stress = average_curve_3(i);
```

```
    second_stress = average_curve_3(i+1);
    first_strain = xq(i);
    second_strain = xq(i+1);

    derivative_value_3 = (second_stress - first_stress)/(second_strain -
first_strain);

    avg_modulus_data_3(1,i) = derivative_value_3;

    i = i+1;
end

avg_modulus_data_3 = [0,avg_modulus_data_3];

i=1;
for i =1:lengthForLoop
    first_stress = average_curve_4(i);
    second_stress = average_curve_4(i+1);
    first_strain = xq(i);
    second_strain = xq(i+1);

    derivative_value_4 = (second_stress - first_stress)/(second_strain -
first_strain);

    avg_modulus_data_4(1,i) = derivative_value_4;

    i = i+1;
end

avg_modulus_data_4 = [0,avg_modulus_data_4];

i=1;
for i =1:lengthForLoop
    first_stress = average_curve_5(i);
    second_stress = average_curve_5(i+1);
    first_strain = xq(i);
    second_strain = xq(i+1);

    derivative_value_5 = (second_stress - first_stress)/(second_strain -
first_strain);

    avg_modulus_data_5(1,i) = derivative_value_5;

    i = i+1;
end

avg_modulus_data_5 = [0,avg_modulus_data_5];

i=1;
for i =1:lengthForLoop
    first_stress = average_curve_6(i);
    second_stress = average_curve_6(i+1);
    first_strain = xq(i);
    second_strain = xq(i+1);
```

```
    derivative_value_6 = (second_stress - first_stress)/(second_strain -
first_strain);

    avg_modulus_data_6(1,i) = derivative_value_6;

    i = i+1;
end

avg_modulus_data_6 = [0,avg_modulus_data_6];

%% Interpolating for tangent modulus curve
max_avg_stress_1 = max(average_curve_1);
max_avg_stress_2 = max(average_curve_2);
max_avg_stress_3 = max(average_curve_3);
max_avg_stress_4 = max(average_curve_4);
max_avg_stress_5 = max(average_curve_5);
max_avg_stress_6 = max(average_curve_6);

max_avg_stress =
[max_avg_stress_1;max_avg_stress_2;max_avg_stress_3;max_avg_stress_4;max_avg_
stress_5;max_avg_stress_6];
minimum_max_avg_stress = min(max_avg_stress);
stress_interval = minimum_max_avg_stress/300;

stress_xq = 0:stress_interval:minimum_max_avg_stress;

int_avg_modulus_curve_1 =
interp1(average_curve_1,avg_modulus_data_1,stress_xq);
int_avg_modulus_curve_2 =
interp1(average_curve_2,avg_modulus_data_2,stress_xq);
int_avg_modulus_curve_3 =
interp1(average_curve_3,avg_modulus_data_3,stress_xq);
int_avg_modulus_curve_4 =
interp1(average_curve_4,avg_modulus_data_4,stress_xq);
int_avg_modulus_curve_5 =
interp1(average_curve_5,avg_modulus_data_5,stress_xq);
int_avg_modulus_curve_6 =
interp1(average_curve_6,avg_modulus_data_6,stress_xq);

%% Formatting axes
all_avg_stress_curves =
[average_curve_1,average_curve_2,average_curve_3,average_curve_4,average_curv
e_5,average_curve_6];
max_all_avg_stress_curves = max(all_avg_stress_curves);

all_avg_energy_curves =
[int_avg_energy_curve_1,int_avg_energy_curve_2,int_avg_energy_curve_3,int_avg
_energy_curve_4,int_avg_energy_curve_5,int_avg_energy_curve_6];
max_all_avg_energy_curves = max(all_avg_energy_curves);

all_avg_modulus_curves =
[int_avg_modulus_curve_1,int_avg_modulus_curve_2,int_avg_modulus_curve_3,int_
avg_modulus_curve_4,int_avg_modulus_curve_5,int_avg_modulus_curve_6];
max_all_avg_modulus_curves = max(all_avg_modulus_curves);
```

```
max_xq = max(xq);
max_energy_xq = max(energy_xq);
max_stress_xq = max(stress_xq);

stress_strain_x_axis = max_xq*1.1;
stress_strain_y_axis = max_all_avg_stress_curves*1.1;

energy_x_axis = max_energy_xq*1.1;
energy_y_axis = max_all_avg_energy_curves*1.1;

modulus_x_axis = max_stress_xq*1.1;
modulus_y_axis = max_all_avg_modulus_curves*1.1;

%% Plotting
saving_path = uigetdir('C:\Material Testing\CSV Exports\Overall Material
Comparison','Select folder of material that was processed.');
x0 = 10;
y0 = 10;
width = 1300;
height = 1000;

figure

subplot(2,2,1)
plot(xq,average_curve_1,'r','Linewidth',2,'DisplayName','Ambient 0.01/s');
x = xlabel('Strain');
x.FontSize = 16;
y = ylabel('Stress (MPa)');
y.FontSize = 16;
t = title('Summary Stress-Strain Plot');
t.FontSize = 18;
xlim([0 stress_strain_x_axis]);
ylim([0 stress_strain_y_axis]);
hold on
plot(xq,average_curve_2,'r--','Linewidth',2,'DisplayName','Ambient 1/s');
plot(xq,average_curve_5,'r-.','Linewidth',2,'DisplayName','Ambient 100s');
plot(xq,average_curve_3,'b','Linewidth',2,'DisplayName','Cold 0.01/s');
plot(xq,average_curve_4,'b--','Linewidth',2,'DisplayName','Cold 1/s');
plot(xq,average_curve_6,'b-.','Linewidth',2,'DisplayName','Cold 100s');
% legend('Location','eastoutside');
hold off

% stress_strain_ending = 'Summary Stress-Strain Plot';
% saving_figure_name = fullfile(saving_path,stress_strain_ending);
% saving_figure_name = char(saving_figure_name);
% saveas(gcf,saving_figure_name,'svg');

subplot(2,2,2)
plot(energy_xq,int_avg_energy_curve_1,'r','Linewidth',2,'DisplayName','Ambien
t 0.01/s')
x = xlabel('Energy per volume (x10^6 J/m^3)');
x.FontSize = 16;
y = ylabel('Stress (MPa)');
y.FontSize = 16;
```

```
t = title('Summary Energy Dissipation Plot');
t.FontSize = 18;
xlim([0 energy_x_axis]);
ylim([0 energy_y_axis]);
hold on
plot(energy_xq,int_avg_energy_curve_2,'r--
','Linewidth',2,'DisplayName','Ambient 1/s');
plot(energy_xq,int_avg_energy_curve_5,'r-
.','Linewidth',2,'DisplayName','Ambient 100/s');
plot(energy_xq,int_avg_energy_curve_3,'b','Linewidth',2,'DisplayName','Cold
0.01/s');
plot(energy_xq,int_avg_energy_curve_4,'b--','Linewidth',2,'DisplayName','Cold
1/s');
plot(energy_xq,int_avg_energy_curve_6,'b-.','Linewidth',2,'DisplayName','Cold
100/s');
% legend('Location','eastoutside');
hold off

% energy_dissipation_ending = 'Summary Energy Dissipation Plot';
% saving_figure_name = fullfile(saving_path,energy_dissipation_ending);
% saving_figure_name = char(saving_figure_name);
% saveas(gcf,saving_figure_name,'svg');

subplot(2,2,3)
plot(stress_xq,int_avg_modulus_curve_1,'r','Linewidth',2,'DisplayName','Ambie
nt 0.01/s');
x = xlabel('Stress (MPa)');
x.FontSize = 16;
y = ylabel('Tangent Modulus (MPa)');
y.FontSize = 16;
t = title('Summary Elastic Modulus Plot');
t.FontSize = 18;xlim([0 modulus_x_axis]);
xlim([0 modulus_x_axis]);
ylim([0 modulus_y_axis]);
hold on
plot(stress_xq,int_avg_modulus_curve_2,'r--
','Linewidth',2,'DisplayName','Ambient 1/s');
plot(stress_xq,int_avg_modulus_curve_5,'r-
.','Linewidth',2,'DisplayName','Ambient 100/s');
plot(stress_xq,int_avg_modulus_curve_3,'b','Linewidth',2,'DisplayName','Cold
0.01/s');
plot(stress_xq,int_avg_modulus_curve_4,'b--
','Linewidth',2,'DisplayName','Cold 1/s');
plot(stress_xq,int_avg_modulus_curve_6,'b-
.','Linewidth',2,'DisplayName','Cold 100/s');
% legend('Location','eastoutside');
hold off

subplot(2,2,4)
plot(nan, nan, 'r','Linewidth',2);
axis off
hold on
plot(nan, nan, 'r--','Linewidth',2);
plot(nan, nan, 'r:','Linewidth',2);
plot(nan, nan, 'b','Linewidth',2);
plot(nan, nan, 'b--','Linewidth',2);
```

```
plot(nan, nan, 'b:','Linewidth',2);
leg =legend('Ambient 0.01/s','Ambient 1/s','Ambient 100/s','Cold
0.01/s','Cold 1/s','Cold 100/s');
leg.Location = 'west';
leg.FontSize = 18;
hold off

s = sgtitle('Summary Plots for Hummingbird Outer White Material');
s.FontSize = 32;
set(gcf,'position',[x0,y0,width,height]);

% tangent_modulus_ending = 'Summary Tangent Modulus Plot';
% saving_figure_name = fullfile(saving_path,tangent_modulus_ending);
% saving_figure_name = char(saving_figure_name);
% saveas(gcf,saving_figure_name,'svg');

%% Saving Plots
% figure_ending = 'Summary Figure';
% saving_figure_name = fullfile(saving_path,figure_ending);
% saving_figure_name = char(saving_figure_name);
% saveas(gcf,saving_figure_name,'png');

%% Stress comparison
ambient_01s_max = average_curve_1(1,end);
ambient_1s_max = average_curve_2(1,end);
ambient_100s_max = average_curve_5(1,end);
ambient_1s_max = average_curve_2(1,end);
cold_01s_max = average_curve_3(1,end);
cold_1s_max = average_curve_4(1,end);
cold_100s_max = average_curve_6(1,end);

stress_comparison_results = [ambient_01s_max, cold_01s_max;...
                             ambient_1s_max, cold_1s_max;...
                             ambient_100s_max, cold_100s_max];

%% Finding index for strain values of interest

% 0.1 strain
dist = abs(xq - 0.1);
minDist = min(dist);
strain_01_index = (dist == minDist);
strain_01_index = find(strain_01_index == 1);
closest_strain_01 = xq(strain_01_index);

% 0.25 strain
dist = abs(xq - 0.25);
minDist = min(dist);
strain_025_index = (dist == minDist);
strain_025_index = find(strain_025_index == 1);
closest_strain_025 = xq(strain_025_index);

% 0.3 strain
dist = abs(xq - 0.3);
minDist = min(dist);
strain_03_index = (dist == minDist);
```

```
strain_03_index = find(strain_03_index == 1);
closest_strain_03 = xq(strain_03_index);

% 0.4 strain
dist = abs(xq - 0.4);
minDist = min(dist);
strain_04_index = (dist == minDist);
strain_04_index = find(strain_04_index == 1);
closest_strain_04 = xq(strain_04_index);

% 0.5 strain
dist = abs(xq - 0.5);
minDist = min(dist);
strain_05_index = (dist == minDist);
strain_05_index = find(strain_05_index == 1);
closest_strain_05 = xq(strain_05_index);

test = find(strain_01_index == 1);

%% Finding stress, energy dissipation, and elastic modulus at strain values
of interest

% Ambient 0.01/s
ambient_01s_stress_at_01 = average_curve_1(strain_01_index);
ambient_01s_energy_at_01 = avg_energy_curve_1(strain_01_index);
ambient_01s_modulus_at_01 = avg_modulus_data_1(strain_01_index);

ambient_01s_stress_at_025 = average_curve_1(strain_025_index);
ambient_01s_energy_at_025 = avg_energy_curve_1(strain_025_index);
ambient_01s_modulus_at_025 = avg_modulus_data_1(strain_025_index);

ambient_01s_stress_at_03 = average_curve_1(strain_03_index);
ambient_01s_energy_at_03 = avg_energy_curve_1(strain_03_index);
ambient_01s_modulus_at_03 = avg_modulus_data_1(strain_03_index);

ambient_01s_stress_at_04 = average_curve_1(strain_04_index);
ambient_01s_energy_at_04 = avg_energy_curve_1(strain_04_index);
ambient_01s_modulus_at_04 = avg_modulus_data_1(strain_04_index);

ambient_01s_stress_at_05 = average_curve_1(strain_05_index);
ambient_01s_energy_at_05 = avg_energy_curve_1(strain_05_index);
ambient_01s_modulus_at_05 = avg_modulus_data_1(strain_05_index);

% Ambient 1/s
ambient_1s_stress_at_01 = average_curve_2(strain_01_index);
ambient_1s_energy_at_01 = avg_energy_curve_2(strain_01_index);
ambient_1s_modulus_at_01 = avg_modulus_data_2(strain_01_index);

ambient_1s_stress_at_025 = average_curve_2(strain_025_index);
ambient_1s_energy_at_025 = avg_energy_curve_2(strain_025_index);
ambient_1s_modulus_at_025 = avg_modulus_data_2(strain_025_index);

ambient_1s_stress_at_03 = average_curve_2(strain_03_index);
ambient_1s_energy_at_03 = avg_energy_curve_2(strain_03_index);
```

```
ambient_1s_modulus_at_03 = avg_modulus_data_2(strain_03_index);

ambient_1s_stress_at_04 = average_curve_2(strain_04_index);
ambient_1s_energy_at_04 = avg_energy_curve_2(strain_04_index);
ambient_1s_modulus_at_04 = avg_modulus_data_2(strain_04_index);

ambient_1s_stress_at_05 = average_curve_2(strain_05_index);
ambient_1s_energy_at_05 = avg_energy_curve_2(strain_05_index);
ambient_1s_modulus_at_05 = avg_modulus_data_2(strain_05_index);

% Cold 0.01/s
cold_01s_stress_at_01 = average_curve_3(strain_01_index);
cold_01s_energy_at_01 = avg_energy_curve_3(strain_01_index);
cold_01s_modulus_at_01 = avg_modulus_data_3(strain_01_index);

cold_01s_stress_at_025 = average_curve_3(strain_025_index);
cold_01s_energy_at_025 = avg_energy_curve_3(strain_025_index);
cold_01s_modulus_at_025 = avg_modulus_data_3(strain_025_index);

cold_01s_stress_at_03 = average_curve_3(strain_03_index);
cold_01s_energy_at_03 = avg_energy_curve_3(strain_03_index);
cold_01s_modulus_at_03 = avg_modulus_data_3(strain_03_index);

cold_01s_stress_at_04 = average_curve_3(strain_04_index);
cold_01s_energy_at_04 = avg_energy_curve_3(strain_04_index);
cold_01s_modulus_at_04 = avg_modulus_data_3(strain_04_index);

cold_01s_stress_at_05 = average_curve_3(strain_05_index);
cold_01s_energy_at_05 = avg_energy_curve_3(strain_05_index);
cold_01s_modulus_at_05 = avg_modulus_data_3(strain_05_index);

% Cold 1/s
cold_1s_stress_at_01 = average_curve_4(strain_01_index);
cold_1s_energy_at_01 = avg_energy_curve_4(strain_01_index);
cold_1s_modulus_at_01 = avg_modulus_data_4(strain_01_index);

cold_1s_stress_at_025 = average_curve_4(strain_025_index);
cold_1s_energy_at_025 = avg_energy_curve_4(strain_025_index);
cold_1s_modulus_at_025 = avg_modulus_data_4(strain_025_index);

cold_1s_stress_at_03 = average_curve_4(strain_03_index);
cold_1s_energy_at_03 = avg_energy_curve_4(strain_03_index);
cold_1s_modulus_at_03 = avg_modulus_data_4(strain_03_index);

cold_1s_stress_at_04 = average_curve_4(strain_04_index);
cold_1s_energy_at_04 = avg_energy_curve_4(strain_04_index);
cold_1s_modulus_at_04 = avg_modulus_data_4(strain_04_index);

cold_1s_stress_at_05 = average_curve_4(strain_05_index);
cold_1s_energy_at_05 = avg_energy_curve_4(strain_05_index);
cold_1s_modulus_at_05 = avg_modulus_data_4(strain_05_index);

% Ambient 100/s
ambient_100s_stress_at_01 = average_curve_5(strain_01_index);
```

```
ambient_100s_energy_at_01 = avg_energy_curve_5(strain_01_index);
ambient_100s_modulus_at_01 = avg_modulus_data_5(strain_01_index);

ambient_100s_stress_at_025 = average_curve_5(strain_025_index);
ambient_100s_energy_at_025 = avg_energy_curve_5(strain_025_index);
ambient_100s_modulus_at_025 = avg_modulus_data_5(strain_025_index);

ambient_100s_stress_at_05 = average_curve_5(strain_05_index);
ambient_100s_energy_at_05 = avg_energy_curve_5(strain_05_index);
ambient_100s_modulus_at_05 = avg_modulus_data_5(strain_05_index);

% Cold 100/s
cold_100s_stress_at_01 = average_curve_6(strain_01_index);
cold_100s_energy_at_01 = avg_energy_curve_6(strain_01_index);
cold_100s_modulus_at_01 = avg_modulus_data_6(strain_01_index);

cold_100s_stress_at_025 = average_curve_6(strain_025_index);
cold_100s_energy_at_025 = avg_energy_curve_6(strain_025_index);
cold_100s_modulus_at_025 = avg_modulus_data_6(strain_025_index);

cold_100s_stress_at_05 = average_curve_6(strain_05_index);
cold_100s_energy_at_05 = avg_energy_curve_6(strain_05_index);
cold_100s_modulus_at_05 = avg_modulus_data_6(strain_05_index);

%% Finding percent differences

% 0.10 strain
ambient_01_percent_difference = [(((ambient_1s_stress_at_01 -
ambient_01s_stress_at_01)/ambient_01s_stress_at_01)*100),
(((ambient_1s_energy_at_01 -
ambient_01s_energy_at_01)/ambient_01s_energy_at_01)*100),
(((ambient_1s_modulus_at_01 -
ambient_01s_modulus_at_01)/ambient_01s_modulus_at_01)*100)];
cold_01_percent_difference = [(((cold_1s_stress_at_01 -
cold_01s_stress_at_01)/cold_01s_stress_at_01)*100), (((cold_1s_energy_at_01 -
cold_01s_energy_at_01)/cold_01s_energy_at_01)*100), (((cold_1s_modulus_at_01
- cold_01s_modulus_at_01)/cold_01s_modulus_at_01)*100)];

% 0.25 strain
ambient_025_percent_difference = [(((ambient_1s_stress_at_025 -
ambient_01s_stress_at_025)/ambient_01s_stress_at_025)*100),
(((ambient_1s_energy_at_025 -
ambient_01s_energy_at_025)/ambient_01s_energy_at_025)*100),
(((ambient_1s_modulus_at_025 -
ambient_01s_modulus_at_025)/ambient_01s_modulus_at_025)*100)];
cold_025_percent_difference = [(((cold_1s_stress_at_025 -
cold_01s_stress_at_025)/cold_01s_stress_at_025)*100),
(((cold_1s_energy_at_025 -
cold_01s_energy_at_025)/cold_01s_energy_at_025)*100),
(((cold_1s_modulus_at_025 -
cold_01s_modulus_at_025)/cold_01s_modulus_at_025)*100)];

% 0.50 strain
ambient_05_percent_difference = [(((ambient_1s_stress_at_05 -
ambient_01s_stress_at_05)/ambient_01s_stress_at_05)*100),
```

```
(((ambient_1s_energy_at_05 -
ambient_01s_energy_at_05)/ambient_01s_energy_at_05)*100),
(((ambient_1s_modulus_at_05 -
ambient_01s_modulus_at_05)/ambient_01s_modulus_at_05)*100)];
cold_05_percent_difference = [(((cold_1s_stress_at_05 -
cold_01s_stress_at_05)/cold_01s_stress_at_05)*100), (((cold_1s_energy_at_05 -
cold_01s_energy_at_05)/cold_01s_energy_at_05)*100), (((cold_1s_modulus_at_05
- cold_01s_modulus_at_05)/cold_01s_modulus_at_05)*100)];

Stress_Energy_Modulus_Results =
[ambient_01s_stress_at_01,ambient_1s_stress_at_01,
ambient_01_percent_difference(1,1),
ambient_01s_energy_at_01,ambient_1s_energy_at_01,
ambient_01_percent_difference(1,2),
ambient_01s_modulus_at_01,ambient_1s_modulus_at_01,
ambient_01_percent_difference(1,3);...
                                cold_01s_stress_at_01,cold_1s_stress_at_01,
cold_01_percent_difference(1,1), cold_01s_energy_at_01,cold_1s_energy_at_01,
cold_01_percent_difference(1,2),
cold_01s_modulus_at_01,cold_1s_modulus_at_01,
cold_01_percent_difference(1,3);...

ambient_01s_stress_at_025,ambient_1s_stress_at_025,
ambient_025_percent_difference(1,1),
ambient_01s_energy_at_025,ambient_1s_energy_at_025,
ambient_025_percent_difference(1,2),
ambient_01s_modulus_at_025,ambient_1s_modulus_at_025,
ambient_025_percent_difference(1,3);...

cold_01s_stress_at_025,cold_1s_stress_at_025,
cold_025_percent_difference(1,1),
cold_01s_energy_at_025,cold_1s_energy_at_025,
cold_025_percent_difference(1,2),
cold_01s_modulus_at_025,cold_1s_modulus_at_025,
cold_025_percent_difference(1,3);...

ambient_01s_stress_at_05,ambient_1s_stress_at_05,
ambient_05_percent_difference(1,1),
ambient_01s_energy_at_05,ambient_1s_energy_at_05,
ambient_05_percent_difference(1,2),
ambient_01s_modulus_at_05,ambient_1s_modulus_at_05,
ambient_05_percent_difference(1,3);...
                                cold_01s_stress_at_05,cold_1s_stress_at_05,
cold_05_percent_difference(1,1), cold_01s_energy_at_05,cold_1s_energy_at_05,
cold_05_percent_difference(1,2),
cold_01s_modulus_at_05,cold_1s_modulus_at_05,
cold_05_percent_difference(1,3)];

Rate_100s_Results = [ambient_100s_stress_at_01, ambient_100s_energy_at_01,
ambient_100s_modulus_at_01;...
                     cold_100s_stress_at_01, cold_100s_energy_at_01,
cold_100s_modulus_at_01;...
                     ambient_100s_stress_at_025, ambient_100s_energy_at_025,
ambient_100s_modulus_at_025;...
                     cold_100s_stress_at_025, cold_100s_energy_at_025,
cold_100s_modulus_at_025;...
```

```
                    ambient_100s_stress_at_05, ambient_100s_energy_at_05,
ambient_100s_modulus_at_05;...
                    cold_100s_stress_at_05, cold_100s_energy_at_05,
cold_100s_modulus_at_05];
```

Appendix B. Impact Testing Results Tables

Table 11 | Ambient temperature linear impactor testing averaged results at all three tested impact speeds and all six tested impact locations.

	Impact Speed	2.2 m/s			2.9 m/s			5.0 m/s		
Impact Location	Metric	Cascade	Hummingbird	No Headgear	Cascade	Hummingbird	No Headgear	Cascade	Hummingbird	No Headgear
Frontal	PLA (g)	32.3	23.4	79.6	50.6	37.5	112.9	119.3	90.9	193.9
	PRV (rad/s)	15.9	12.0	14.2	20.4	17.7	19.2	34.9	27.0	34.2
	PRA (rad/s^2)	980.4	646.5	2228.8	1654.2	1298.2	2942.6	3776.9	2031.1	4876.3
	HIC	17.9	5.8	72.5	53.6	17.8	168.4	349.1	158.4	553.8
	BrIC	0.28	0.21	0.25	0.36	0.31	0.34	0.62	0.48	0.61
Front Boss	PLA (g)	20.9	20.9	69.9	43.5	35.4	116.7	121.4	119.3	222.2
	PRV (rad/s)	13.0	12.1	15.6	18.5	19.6	20.3	30.1	33.3	32.9
	PRA (rad/s^2)	1829.9	898.1	4011.3	2482.8	1524.7	5453.8	4830.2	3207.2	9232.2
	HIC	8.9	7.9	68.5	36.7	27.2	172.4	267.7	297.4	801.3
	BrIC	0.30	0.23	0.32	0.40	0.37	0.42	0.60	0.61	0.67
Rear	PLA (g)	25.9	18.8	79.6	50.4	34.7	119.6	64.8	117.0	159.2
	PRV (rad/s)	11.9	8.5	14.2	14.1	9.9	18.5	15.4	18.7	29.6
	PRA (rad/s^2)	1225.9	771.1	2492.4	1441.9	1185.7	3447.7	2161.4	2183.2	5629.2
	HIC	8.3	3.7	74.2	16.3	12.6	206.6	39.2	162.7	242.5
	BrIC	0.21	0.15	0.25	0.25	0.18	0.33	0.27	0.33	0.47
RBCG	PLA (g)	23.4	20.0	75.5	46.3	40.6	101.5	134.2	132.5	182.1
	PRV (rad/s)	13.9	11.4	15.3	18.3	15.9	20.0	28.7	26.8	31.7
	PRA (rad/s^2)	1430.7	1321.7	3543.8	2495.9	2522.1	4831.4	6001.0	6114.5	8187.6
	HIC	11.8	8.2	67.1	38.6	29.8	158.3	341.1	281.1	111.1
	BrIC	0.25	0.21	0.30	0.34	0.29	0.40	0.56	0.51	0.62
RBNC	PLA (g)	17.5	18.1	58.8	26.7	19.6	91.9	94.3	79.7	191.0
	PRV (rad/s)	10.2	10.6	17.6	14.7	14.4	22.8	28.9	29.6	36.5
	PRA (rad/s^2)	1366.2	911.9	4039.9	2135.3	1421.4	5589.0	5491.6	5549.5	9265.4
	HIC	6.3	3.6	49.1	16.3	9.4	128.1	157.0	115.8	603.1
	BrIC	0.17	0.18	0.36	0.25	0.25	0.48	0.53	0.52	0.77
Side	PLA (g)	20.3	19.7	69.7	30.5	24.4	104.6	98.0	82.0	222.1
	PRV (rad/s)	10.5	10.6	15.9	14.7	14.5	20.1	25.8	26.5	30.6
	PRA (rad/s^2)	1590.9	1488.7	3694.2	2380.3	2099.9	4975.2	5050.3	4948.0	8273.7
	HIC	8.1	7.0	69.9	21.5	15.2	155.5	207.5	134.5	608.5
	BrIC	0.17	0.18	0.26	0.23	0.24	0.33	0.40	0.42	0.50

Table 12 | Ambient temperature ball impact testing averaged results at all three tested impact speeds and all six tested impact locations.

	Impact Speed	13.4 m/s			27.0 m/s		
Impact Location	Metric	Cascade	Hummingbird	No Headgear	Cascade	Hummingbird	No Headgear
Frontal	PLA	28.6	15.4	30.8	58.1	48.5	74.2
	PRV	3.0	2.7	3.9	5.7	5.9	7.1
	PRA	476.8	465.4	589.2	767.2	953.1	1386.8
	HIC	3.6	1.7	6.1	19.3	11.3	45.4
	BrIC	0.05	0.05	0.07	0.10	0.11	0.13
Front Boss	PLA	36.8	28.6	36.9	113.9	100.8	84.7
	PRV	5.0	6.0	7.0	8.4	8.9	12.5
	PRA	997.8	1040.2	1797.0	2158.3	2074.3	3450.7
	HIC	4.3	3.2	8.0	46.1	37.8	51.8
	BrIC	0.11	0.13	0.14	0.17	0.18	0.23
Rear	PLA	70.9	56.1	82.4	59.9	81.9	94.2
	PRV	3.2	3.6	4.3	6.2	6.5	8.5
	PRA	971.9	750.3	989.7	1359.9	1187.3	3153.1
	HIC	37.9	18.3	80.5	65.2	102.4	151.6
	BrIC	0.06	0.07	0.08	0.12	0.12	0.15
RBCG	PLA	53.8	70.1	59.7	119.8	129.2	117.4
	PRV	4.6	4.9	6.2	9.0	10.5	11.5
	PRA	1269.2	1099.4	1513.5	2460.5	2728.0	3023.9
	HIC	7.3	7.2	11.8	48.3	99.6	85.3
	BrIC	0.11	0.09	0.12	0.17	0.19	0.21
RBNC	PLA	23.9	17.3	37.6	104.9	119.4	93.0
	PRV	4.6	5.0	7.4	10.1	10.8	14.1
	PRA	1166.9	1202.4	1781.0	2727.2	2822.9	3647.9
	HIC	3.1	1.5	7.6	37.0	35.8	24.2
	BrIC	0.07	0.08	0.15	0.19	0.20	0.28
Side	PLA	28.3	21.3	42.5	108.0	88.0	97.3
	PRV	5.5	4.9	5.4	11.6	10.1	10.8
	PRA	1493.8	1281.7	1218.4	3335.8	2845.3	2806.7
	HIC	3.0	2.2	8.9	41.3	46.4	24.7
	BrIC	0.09	0.08	0.09	0.18	0.16	0.17

Table 13 | Cold temperature linear impactor testing averaged results at all three tested impact speeds and all six tested impact locations.

	Impact Speed	2.2 m/s		2.9 m/s		5.0 m/s	
Impact Location	Metric	Cascade	Hummingbird	Cascade	Hummingbird	Cascade	Hummingbird
Frontal	PLA (g)	35.68	19.94	53.10	37.57	120.16	85.89
	PRV (rad/s)	13.42	11.49	19.41	16.83	35.21	30.54
	PRA (rad/s^2)	1127.22	687.77	1678.22	1366.45	3660.60	2598.02
	HIC	23.16	6.61	58.64	16.53	368.55	186.31
	BrIC	0.24	0.20	0.35	0.30	0.62	0.54
Front Boss	PLA (g)	22.99	27.90	47.46	44.71	140.15	124.19
	PRV (rad/s)	13.50	13.98	18.60	19.65	31.47	32.78
	PRA (rad/s^2)	1099.28	1192.33	2087.40	2005.79	5463.15	4344.41
	HIC	9.01	12.63	38.89	39.02	320.30	301.80
	BrIC	0.28	0.26	0.37	0.38	0.65	0.62
Rear	PLA (g)	34.20	15.85	41.13	31.66	71.65	99.84
	PRV (rad/s)	12.57	8.86	15.03	10.46	19.80	17.66
	PRA (rad/s^2)	1410.92	777.32	1701.89	1222.43	3326.87	2085.98
	HIC	13.96	4.28	23.22	12.56	89.43	133.32
	BrIC	0.23	0.16	0.27	0.19	0.36	0.32
RBCG	PLA (g)	29.65	22.91	47.72	33.87	135.74	133.37
	PRV (rad/s)	13.84	13.55	17.63	18.64	29.47	26.63
	PRA (rad/s^2)	1882.59	1763.27	2816.78	2755.15	5982.80	6173.45
	HIC	16.40	9.49	41.63	21.31	321.28	289.00
	BrIC	0.27	0.25	0.35	0.34	0.59	0.51
RBNC	PLA (g)	19.50	16.98	29.58	23.41	103.80	65.83
	PRV (rad/s)	10.38	11.10	14.37	15.34	29.90	27.63
	PRA (rad/s^2)	1749.07	1567.66	2425.37	2274.65	6008.98	4993.54
	HIC	8.21	5.69	19.60	12.04	193.97	82.38
	BrIC	0.17	0.18	0.25	0.25	0.56	0.47
Side	PLA (g)	21.82	21.18	32.32	26.30	88.15	63.36
	PRV (rad/s)	12.73	10.73	16.65	14.34	28.76	26.38
	PRA (rad/s^2)	2416.96	1699.58	3119.50	2474.51	6186.58	5065.47
	HIC	9.55	6.89	21.90	14.79	142.00	92.35
	BrIC	0.21	0.17	0.27	0.23	0.44	0.41

Table 14 | Cold temperature ball impact testing averaged results at all three tested impact speeds and all six tested impact locations.

	Impact Speed	13.4 m/s			27.0 m/s		
Impact Location	Metric	Cascade	Hummingbird	No Headgear	Cascade	Hummingbird	No Headgear
Frontal	PLA	24.8	15.3	31.4	70.1	59.0	80.5
	PRV	2.8	2.7	3.7	6.2	5.5	7.1
	PRA	437.9	468.9	543.6	701.8	969.5	1191.2
	HIC	3.6	1.6	6.0	29.2	16.3	42.6
	BrIC	0.05	0.05	0.07	0.11	0.10	0.13
Front Boss	PLA	34.9	23.9	37.7	125.4	91.2	86.5
	PRV	4.6	5.9	6.8	7.7	9.3	11.9
	PRA	857.4	1260.6	1768.5	1863.5	2106.4	3259.1
	HIC	4.3	2.6	8.4	53.7	36.1	55.1
	BrIC	0.10	0.13	0.14	0.16	0.17	0.23
Rear	PLA	67.9	43.4	93.3	90.4	78.5	111.6
	PRV	3.3	3.2	4.1	5.9	6.5	7.7
	PRA	827.1	676.2	956.6	1639.8	2371.2	2312.3
	HIC	59.1	3.3	40.9	118.8	151.4	96.3
	BrIC	0.06	0.06	0.08	0.12	0.13	0.15
RBCG	PLA	58.7	68.7	61.8	152.1	160.9	130.4
	PRV	4.7	4.6	5.9	8.4	9.5	11.3
	PRA	1291.1	1108.8	1479.1	2396.7	2573.7	3047.2
	HIC	7.1	9.3	9.7	68.5	65.7	60.0
	BrIC	0.11	0.09	0.11	0.16	0.19	0.21
RBNC	PLA	36.9	43.9	56.2	98.2	98.0	101.7
	PRV	4.3	4.8	7.3	9.3	10.5	14.0
	PRA	1149.4	1203.5	1823.3	2542.3	2859.7	3580.8
	HIC	4.2	2.5	8.9	40.3	31.2	39.2
	BrIC	0.07	0.08	0.15	0.17	0.20	0.28
Side	PLA	34.2	34.4	43.3	76.0	77.5	112.5
	PRV	6.0	5.6	5.3	11.7	10.1	10.3
	PRA	1671.0	1517.5	1239.8	3390.8	2936.9	2637.3
	HIC	4.8	3.2	9.1	25.3	27.8	32.1
	BrIC	0.10	0.09	0.08	0.19	0.16	0.16

Appendix C. Impact Testing Mann-Whitney U-Test Results

Table 15 | Linear impactor headgear comparison Mann-Whitney U test results with all data together. Red p-values indicate statistical significance ($p < 0.05$).

Metric	Cascade Mean	Hummingbird Mean	No Headgear Mean	Cascade - No Headgear p-value	Hummingbird - No Headgear p-value	Cascade - Hummingbird p-value
PLA	56.7	51.9	125.1	3.60E-10	4.560E-10	0.194
PRV	18.9	17.7	22.7	7.34E-04	1.481E-04	0.242
PRA	2684.8	2229.1	5150.8	4.02E-09	3.430E-11	0.025
HIC	89.2	72.1	239.5	8.27E-08	2.292E-08	0.065
BrIC	0.34	0.32	0.43	1.78E-03	3.998E-05	0.175

Table 16 | Linear impactor headgear comparison Mann-Whitney U test results with data grouped by impact speed. Red p-values indicate statistical significance ($p < 0.05$).

Metric	Impact Speed	Cascade Mean	Hummingbird Mean	No Headgear Mean	Cascade - No Headgear p-value	Hummingbird - No Headgear p-value	Cascade - Hummingbird p-value
PLA	2.2	23.4	20.1	72.2	3.23E-07	3.23E-07	0.091
	2.9	41.3	32.0	107.9	3.23E-07	3.23E-07	0.005
	5	105.3	103.6	195.1	3.23E-07	3.23E-07	0.812
PRV	2.2	12.5	10.9	15.5	1.21E-04	3.23E-07	0.038
	2.9	16.8	15.3	20.2	1.38E-04	1.18E-05	0.150
	5	27.3	27.0	32.6	6.71E-04	8.18E-05	0.558
PRA	2.2	1404.0	1006.4	3335.1	3.23E-07	3.23E-07	0.001
	2.9	2098.4	1675.3	4540.0	3.23E-07	3.23E-07	0.017
	5	4551.9	4005.6	7577.4	1.21E-04	9.33E-05	0.438
HIC	2.2	10.2	6.0	66.9	3.22E-07	3.23E-07	1.77E-4
	2.9	30.5	18.7	164.9	3.23E-07	3.23E-07	0.009
	5	226.9	191.6	486.7	0.005	2.26E-03	0.200
BrIC	2.2	0.23	0.19	0.29	0.002	2.84E-07	0.071
	2.9	0.30	0.27	0.38	0.009	2.15E-05	0.233
	5	0.50	0.48	0.61	0.022	1.33E-03	0.333

Table 17 | Linear impactor headgear comparison Mann-Whitney U test results with data grouped by impact location. Red p-values indicate statistical significance ($p < 0.05$).

Impact Location	Metric	Cascade Mean	Hummingbird Mean	No Headgear Mean	Cascade - No Headgear p-value	Hummingbird - No Headgear p-value	Cascade - Hummingbird p-value
Frontal	PLA	67.4	50.6	128.8	0.050	0.001	0.258
	PRV	23.8	18.9	22.6	0.258	0.258	0.258
	PRA	2137.1	1325.3	3349.3	0.050	1.65E-04	0.258
	HIC	140.2	60.6	264.9	0.050	0.008	0.094
	BrIC	0.42	0.34	0.40	0.253	0.245	0.246
Front Boss	PLA	61.9	58.5	136.3	0.014	0.040	0.796
	PRV	20.5	21.7	23.0	0.258	0.436	0.730
	PRA	3047.7	1876.7	6232.4	0.004	4.11E-05	0.050
	HIC	104.4	110.8	347.4	0.050	0.050	0.666
	BrIC	0.43	0.40	0.47	0.249	0.246	0.591
Rear	PLA	47.0	56.8	119.5	4.11E-05	0.019	0.730
	PRV	13.8	12.4	20.7	0.011	0.011	0.258
	PRA	1609.7	1380.0	3856.4	4.11E-05	4.11E-05	0.340
	HIC	21.3	59.7	174.4	4.11E-05	0.019	0.730
	BrIC	0.24	0.22	0.35	0.010	0.019	0.248
RBCG	PLA	68.0	64.4	119.7	0.050	0.050	0.489
	PRV	20.3	18.0	22.3	0.258	0.258	0.258
	PRA	3309.2	3319.4	5520.9	0.050	0.050	0.931
	HIC	130.5	106.4	112.1	0.258	0.258	0.297
	BrIC	0.38	0.34	0.44	0.248	0.057	0.247
RBNC	PLA	46.2	39.1	113.9	0.024	0.004	0.489
	PRV	17.9	18.2	25.6	0.050	0.050	0.796
	PRA	2997.7	2627.6	6298.1	0.008	0.024	0.489
	HIC	59.9	43.0	260.1	0.050	0.006	0.258
	BrIC	0.32	0.32	0.54	0.045	0.045	0.699
Side	PLA	49.6	42.0	132.1	0.006	0.004	0.387
	PRV	17.0	17.2	22.2	0.050	0.050	0.863
	PRA	3007.2	2845.6	5647.7	0.031	0.014	0.340
	HIC	79.0	52.2	278.0	0.050	0.006	0.258
	BrIC	0.27	0.28	0.36	0.047	0.047	0.348

Table 18 | Ball impact headgear comparison Mann-Whitney U test results with all data together. Red p-values indicate statistical significance ($p < 0.05$).

Metric	Cascade Mean	Hummingbird Mean	No Headgear Mean	Cascade - No Headgear p-value	Hummingbird - No Headgear p-value	Cascade - Hummingbird p-value
PLA	67.5	64.7	70.9	0.481	0.371	0.461
PRV	6.4	6.6	8.2	0.017	0.017	0.510
PRA	1598.8	1537.5	2113.2	0.019	0.007	0.740
HIC	26.4	30.6	42.2	0.054	0.071	0.547
BrIC	0.12	0.12	0.15	0.033	0.061	0.722

Table 19 | Ball impact headgear comparison Mann-Whitney U test results with data grouped by impact speed. Red p-values indicate statistical significance ($p < 0.05$).

Metric	Impact Speed	Cascade Mean	Hummingbird Mean	No Headgear Mean	Cascade - No Headgear p-value	Hummingbird - No Headgear p-value	Cascade - Hummingbird p-value
PLA	13.4	40.4	34.8	48.3	0.069	0.018	0.117
	27.0	94.6	94.6	93.5	0.624	0.646	0.692
PRV	13.4	4.3	4.5	5.7	0.013	0.011	0.402
	27.0	8.5	8.8	10.8	0.010	0.006	0.537
PRA	13.4	1062.7	973.2	1314.8	0.052	0.017	0.304
	27.0	2134.8	2101.8	2911.5	0.006	0.005	0.788
HIC	13.4	9.9	5.7	20.5	0.001	0.001	0.056
	27.0	42.9	55.5	63.8	0.261	0.669	0.496
BrIC	13.4	0.08	0.08	0.11	0.012	0.040	0.898
	27.0	0.16	0.16	0.20	0.062	0.063	0.544

Table 20 | Ball impact headgear comparison Mann-Whitney U test results with data grouped by impact location. Red p-values indicate statistical significance ($p < 0.05$).

Impact Location	Metric	Cascade Mean	Hummingbird Mean	No Headgear Mean	Cascade - No Headgear p-value	Hummingbird - No Headgear p-value	Cascade - Hummingbird p-value
Frontal	PLA	43.3	31.9	52.5	0.180	0.180	0.310
	PRV	4.4	4.3	5.5	0.180	0.180	0.485
	PRA	622.0	709.3	988.0	0.180	0.180	0.699
	HIC	11.4	6.5	25.7	0.180	0.180	0.180
	BrIC	0.08	0.08	0.10	0.165	0.169	1.000
Front Boss	PLA	75.3	64.7	60.8	0.485	1.000	0.180
	PRV	6.7	7.4	9.7	0.180	0.180	0.240
	PRA	1578.0	1557.3	2623.9	0.180	0.180	0.818
	HIC	25.2	20.5	29.9	0.180	0.180	0.240
	BrIC	0.14	0.16	0.19	0.188	0.154	0.262
Rear	PLA	65.4	69.0	88.3	0.026	0.093	1.000
	PRV	4.7	5.0	6.4	0.180	0.180	0.394
	PRA	1165.9	968.8	2071.4	0.310	0.065	0.180
	HIC	51.6	60.3	116.0	0.041	0.132	1.000
	BrIC	0.09	0.10	0.12	0.167	0.251	0.407
RBCG	PLA	86.8	99.6	88.5	0.818	0.310	0.589
	PRV	6.8	7.7	8.9	0.180	0.180	0.180
	PRA	1864.9	1913.7	2268.7	0.180	0.310	0.818
	HIC	27.8	53.4	48.6	0.180	0.589	0.589
	BrIC	0.14	0.14	0.17	0.162	0.180	1.000
RBNC	PLA	66.0	68.4	65.3	1.000	1.000	0.699
	PRV	7.3	7.9	10.8	0.180	0.180	0.180
	PRA	1947.0	2012.7	2714.5	0.180	0.180	0.310
	HIC	20.1	18.7	15.9	1.000	0.699	0.394
	BrIC	0.13	0.14	0.21	0.165	0.154	0.331
Side	PLA	68.2	54.6	69.9	0.937	0.310	0.240
	PRV	8.6	7.5	8.1	0.310	0.180	0.180
	PRA	2414.8	2063.5	2012.6	0.180	0.485	0.180
	HIC	22.1	24.3	16.8	0.937	0.937	0.818
	BrIC	0.14	0.12	0.13	0.600	0.245	0.229

Table 21 | Linear impactor temperature comparison Mann-Whitney U test results with all data together. Red p-values indicate statistical significance ($p < 0.05$).

	Cascade			Hummingbird		
Metric	Ambient Mean	Cold Mean	p-value	Ambient Mean	Cold Mean	p-value
PLA (g)	56.7	59.7	0.459	51.9	49.7	0.929
PRV (rad/s)	18.9	19.6	0.625	17.7	18.1	0.643
PRA (rad/s2)	2684.8	3008.0	0.190	2229.1	2502.7	0.148
HIC	89.2	95.5	0.289	72.1	69.3	0.811
BrIC	0.34	0.36	0.538	0.32	0.32	0.721

Table 22 | Linear impactor temperature comparison Mann-Whitney U test results with data grouped by impact speed. Red p-values indicate statistical significance ($p < 0.05$).

		Cascade			Hummingbird		
Metric	Impact Speed	Ambient Mean	Cold Mean	p-value	Ambient Mean	Cold Mean	p-value
PLA (g)	2.2	23.4	27.3	0.056	20.1	20.8	0.716
	2.9	41.3	41.9	0.692	32.0	32.9	0.887
	5	105.3	109.9	0.558	103.6	95.4	0.351
PRV (rad/s)	2.2	12.5	12.7	0.558	10.9	11.6	0.235
	2.9	16.8	16.9	0.937	15.3	15.9	0.537
	5	27.3	29.1	0.248	27.0	26.9	0.862
PRA (rad/s2)	2.2	1404.0	1614.3	0.248	1006.4	1281.3	0.079
	2.9	2098.4	2304.9	0.289	1675.3	2016.5	0.150
	5	4551.9	5104.8	0.141	4005.6	4210.1	0.692
HIC	2.2	10.2	13.4	0.048	6.0	7.6	0.184
	2.9	30.5	34.0	0.200	18.7	19.4	0.862
	5	226.9	239.3	0.669	191.6	180.9	0.496
BrIC	2.2	0.23	0.23	0.874	0.19	0.21	0.566
	2.9	0.30	0.31	0.525	0.27	0.28	0.775
	5	0.50	0.54	0.235	0.48	0.48	0.912

Table 23 | Ball impact temperature comparison Mann-Whitney U test results with all data together. Red p-values indicate statistical significance ($p < 0.05$).

	Cascade			Hummingbird		
Metric	Ambient Mean	Cold Mean	p-value	Ambient Mean	Cold Mean	p-value
PLA (g)	67.5	72.5	0.517	64.7	66.2	0.996
PRV (rad/s)	6.4	6.3	0.951	6.6	6.5	0.577
PRA (rad/s2)	1598.8	1564.1	0.791	1537.5	1671.1	0.440
HIC	26.4	34.9	0.290	30.6	29.2	0.770
BrIC	0.12	0.12	0.843	0.12	0.12	0.946

Table 24 | Ball impact temperature comparison Mann-Whitney U test results with data grouped by impact speed. Red p-values indicate statistical significance ($p < 0.05$).

		Cascade			Hummingbird		
Metric	Impact Speed	Ambient Mean	Cold Mean	p-value	Ambient Mean	Cold Mean	p-value
PLA (g)	13.4	40.4	42.9	0.457	34.8	38.3	0.477
	27.0	94.6	102.0	0.646	94.6	94.2	0.646
PRV (rad/s)	13.4	4.3	4.3	0.740	4.5	4.5	0.558
	27.0	8.5	8.2	0.788	8.8	8.6	0.477
PRA (rad/s2)	13.4	1062.7	1039.0	0.764	973.2	1039.2	0.420
	27.0	2134.8	2089.2	0.692	2101.8	2302.9	0.496
HIC	13.4	9.9	13.9	0.229	5.7	3.8	0.975
	27.0	42.9	56.0	0.438	55.5	54.7	0.537
BrIC	13.4	0.08	0.08	0.923	0.08	0.08	0.711
	27.0	0.16	0.15	0.351	0.16	0.16	0.632

References

[1] K. Blennow *et al.*, "Traumatic brain injuries," *Nature Reviews Disease Primers 2016 2:1*, vol. 2, no. 1, pp. 1–19, Nov. 2016, doi: 10.1038/nrdp.2016.84.`

[2] D. F. Meaney and D. H. Smith, "Biomechanics of Concussion," *Clinics in Sports Medicine*, vol. 30, pp. 19–31, 2011, doi: 10.1016/j.csm.2010.08.009.

[3] G. Teasdale and B. Jennett, "ASSESSMENT OF COMA AND IMPAIRED CONSCIOUSNESS: A Practical Scale," *The Lancet*, vol. 304, no. 7872, pp. 81–84, Jul. 1974, doi: 10.1016/S0140-6736(74)91639-0.

[4] S. Budday *et al.*, "Mechanical characterization of human brain tissue," *Acta Biomaterialia*, vol. 48, pp. 319–340, Jan. 2017, doi: 10.1016/J.ACTBIO.2016.10.036.

[5] X. Jin, F. Zhu, H. Mao, M. Shen, and K. H. Yang, "A comprehensive experimental study on material properties of human brain tissue," *Journal of Biomechanics*, vol. 46, no. 16, pp. 2795–2801, Nov. 2013, doi: 10.1016/J.JBIOMECH.2013.09.001.

[6] K. Miller and K. Chinzei, "Constitutive modelling of brain tissue: Experiment and theory," *Journal of Biomechanics*, vol. 30, no. 11–12, pp. 1115–1121, Nov. 1997, doi: 10.1016/S0021-9290(97)00092-4.

[7] T. P. Prevost, A. Balakrishnan, S. Suresh, and S. Socrate, "Biomechanics of brain tissue," *Acta Biomaterialia*, vol. 7, no. 1, pp. 83–95, Jan. 2011, doi: 10.1016/J.ACTBIO.2010.06.035.

[8] K. Miller and K. Chinzei, "Mechanical properties of brain tissue in tension," *Journal of Biomechanics*, vol. 35, no. 4, pp. 483–490, Apr. 2002, doi: 10.1016/S0021-9290(01)00234-2.

[9] F. Velardi, F. Fraternali, and M. Angelillo, "Anisotropic constitutive equations and experimental tensile behavior of brain tissue," *Biomechanics and Modeling in Mechanobiology*, vol. 5, no. 1, Mar. 2006, doi: 10.1007/s10237-005-0007-9.

[10] B. Rashid, M. Destrade, and M. D. Gilchrist, "Mechanical characterization of brain tissue in tension at dynamic strain rates," *Journal of the Mechanical Behavior of Biomedical Materials*, vol. 33, no. 1, pp. 43–54, May 2014, doi: 10.1016/J.JMBBM.2012.07.015.

[11] K. M. Labus and C. M. Puttlitz, "Viscoelasticity of brain corpus callosum in biaxial tension," *Journal of the Mechanics and Physics of Solids*, vol. 96, pp. 591–604, Nov. 2016, doi: 10.1016/J.JMPS.2016.08.010.

[12] J. E. Galford and J. H. McElhaney, “A viscoelastic study of scalp, brain, and dura,” *Journal of Biomechanics*, vol. 3, no. 2, pp. 211–221, Mar. 1970, doi: 10.1016/0021-9290(70)90007-2.

[13] H. Saraf, K. T. Ramesh, A. M. Lennon, A. C. Merkle, and J. C. Roberts, “Mechanical properties of soft human tissues under dynamic loading,” *Journal of Biomechanics*, vol. 40, no. 9, pp. 1960–1967, Jan. 2007, doi: 10.1016/J.JBIOMECH.2006.09.021.

[14] S. Cheng and L. E. Bilston, “Unconfined compression of white matter,” *Journal of Biomechanics*, vol. 40, no. 1, pp. 117–124, Jan. 2007, doi: 10.1016/J.JBIOMECH.2005.11.004.

[15] F. Pervin and W. W. Chen, “Dynamic mechanical response of bovine gray matter and white matter brain tissues under compression,” *Journal of Biomechanics*, vol. 42, no. 6, pp. 731–735, Apr. 2009, doi: 10.1016/J.JBIOMECH.2009.01.023.

[16] L. Z. Shuck and S. H. Advani, “Rheological Response of Human Brain Tissue in Shear,” *Journal of Basic Engineering*, vol. 94, no. 4, pp. 905–911, Dec. 1972, doi: 10.1115/1.3425588.

[17] B. R. Donnelly and J. Medige, “Shear Properties of Human Brain Tissue,” *Journal of Biomechanical Engineering*, vol. 119, no. 4, pp. 423–432, Nov. 1997, doi: 10.1115/1.2798289.

[18] S. Chatelin, J. Vappou, S. Roth, J. S. Raul, and R. Willinger, “Towards child versus adult brain mechanical properties,” *Journal of the Mechanical Behavior of Biomedical Materials*, vol. 6, pp. 166–173, Feb. 2012, doi: 10.1016/J.JMBBM.2011.09.013.

[19] B. Rashid, M. Destrade, and M. D. Gilchrist, “Mechanical characterization of brain tissue in simple shear at dynamic strain rates,” *Journal of the Mechanical Behavior of Biomedical Materials*, vol. 28, pp. 71–85, Dec. 2013, doi: 10.1016/J.JMBBM.2013.07.017.

[20] M. T. Prange and S. S. Margulies, “Regional, Directional, and Age-Dependent Properties of the Brain Undergoing Large Deformation,” *Journal of Biomechanical Engineering*, vol. 124, no. 2, pp. 244–252, Apr. 2002, doi: 10.1115/1.1449907.

[21] A. E. Forte, S. M. Gentleman, and D. Dini, “On the characterization of the heterogeneous mechanical response of human brain tissue,” *Biomechanics and modeling in mechanobiology*, vol. 16, no. 3, pp. 907–920, 2017.

[22] A. Menichetti, D. B. MacManus, M. D. Gilchrist, B. Depreitere, J. vander Sloten, and N. Famaey, “Regional characterization of the dynamic mechanical properties of human brain tissue by microindentation,” *International Journal of Engineering Science*, vol. 155, p. 103355, Oct. 2020, doi: 10.1016/J.IJENGSCI.2020.103355.

[23] S. Budday, T. C. Ovaert, G. A. Holzapfel, P. Steinmann, and E. Kuhl, “Fifty Shades of Brain: A Review on the Mechanical Testing and Modeling of Brain Tissue,” *Archives of computational methods in engineering*, vol. 27, no. 4, pp. 1187–1230, 2020.

[24] T. el Sayed, A. Mota, F. Fraternali, and M. Ortiz, “Biomechanics of traumatic brain injury,” *Computer Methods in Applied Mechanics and Engineering*, vol. 197, no. 51–52, pp. 4692–4701, Oct. 2008, doi: 10.1016/J.CMA.2008.06.006.

[25] A. Post and T. Blaine Hoshizaki, “Rotational Acceleration, Brain Tissue Strain, and the Relationship to Concussion,” *Journal of Biomechanical Engineering*, vol. 137, no. 3, Mar. 2015, doi: 10.1115/1.4028983.

[26] A. Post and T. B. Hoshizaki, “Mechanisms of brain impact injuries and their prediction: A review,” *Trauma*, vol. 14, no. 4, Oct. 2012, doi: 10.1177/1460408612446573.

[27] E. S. Gurdjian, “Re-evaluation of the biomechanics of blunt impact injury of the head,” *Surgery, gynecology & obstetrics*, vol. 140, no. 6, p. 845—850, Jun. 1975, [Online]. Available: http://europepmc.org/abstract/MED/1093271

[28] GURDJIAN and E. S., “Intercranial pressure and acceleration accompanying head impacts in human cadavers,” *Surgery Gynecol.Obstetr.*, vol. 113, pp. 185–190, 1961, Accessed: Oct. 23, 2021. [Online]. Available: http://ci.nii.ac.jp/naid/10004624181/en/

[29] L. M. Thomas, V. L. Roberts, and E. S. Gurdjian, “Experimental intracranial pressure gradients in the human skull.,” *Journal of Neurology, Neurosurgery & Psychiatry*, vol. 29, no. 5, Oct. 1966, doi: 10.1136/jnnp.29.5.404.

[30] B. F. Haddad, H. R. Lissner, J. E. Webster, and E. S. Gurdjian, “Experimental Concussion,” *Neurology*, vol. 5, no. 11, p. 798, 1955, doi: 10.1212/WNL.5.11.798.

[31] A. M. Nahum, R. Smith, and C. C. Ward, “Intracranial Pressure Dynamics During Head Impact.” 1977.

[32] E. A. C. Johnson and P. G. Young, “The Analysis of Pressure Response in Head Injury,” Jul. 2006. doi: 10.4271/2006-01-2368.

[33] E. S. Gurdjian, V. R. Hodgson, L. M. Thomas, and L. M. Patrick, “Significance of Relative Movements of Scalp, Skull, and Intracranial Contents During Impact Injury of the Head,” *Journal of Neurosurgery*, vol. 29, no. 1, Jul. 1968, doi: 10.3171/jns.1968.29.1.0070.

[34] L. M. Thomas, V. L. Roberts, and E. S. Gurdjian, “Impact-Induced Pressure Gradients Along Three Orthogonal Axes in the Human Skull,” *Journal of Neurosurgery*, vol. 26, no. 3, Mar. 1967, doi: 10.3171/jns.1967.26.3.0316.

[35] D. R. S. Bradshaw, J. Ivarsson, C. L. Morfey, and D. C. Viano, “Simulation of acute subdural hematoma and diffuse axonal injury in coronal head impact,” *Journal of Biomechanics*, vol. 34, no. 1, Jan. 2001, doi: 10.1016/S0021-9290(00)00135-4.

[36] W. N. Hardy, T. B. Khalil, and A. I. King, “Literature review of head injury biomechanics,” *International Journal of Impact Engineering*, vol. 15, no. 4, Aug. 1994, doi: 10.1016/0734-743X(94)80034-7.

[37] A. K. Ommaya and T. A. Gennarelli, “Cerebral Concussion and Traumatic Unconsciousnes: Correlation of Experimental and Clinical Observations on Blunt Head Injuries,” *Brain*, vol. 97, no. 4, pp. 633–654, Dec. 1974, doi: 10.1093/brain/97.4.633.

[38] N. Yoganandan, J. Li, J. Zhang, F. A. Pintar, and T. A. Gennarelli, “Influence of angular acceleration–deceleration pulse shapes on regional brain strains,” *Journal of Biomechanics*, vol. 41, no. 10, Jul. 2008, doi: 10.1016/j.jbiomech.2008.04.019.

[39] J. H. Adams, D. I. Graham, T. A. Gennarelli, and W. L. Maxwell, “Diffuse axonal injury in non-missile head injury.,” *Journal of Neurology, Neurosurgery & Psychiatry*, vol. 54, no. 6, Jun. 1991, doi: 10.1136/jnnp.54.6.481.

[40] F. Unterharnscheidt and L. S. Higgins, “Neuropathologic effects of translational and rotational acceleration of the head in animal experiments,” *The Late Effects of Head Injury. Illinois: Springfield*, pp. 158–167, 1969.

[41] T. A. Gennarelli, J. M. Abel, H. Adams, and D. Graham, “Differential Tolerance of Frontal and Temporal Lobes to Contusion Induced by Angular Acceleration,” Feb. 1979. doi: 10.4271/791022.

[42] Kathy Mileski, “Diffuse Axonal Brain Injury: Causes, Symptoms, Treatment,” *Propel Physiotherapy*, 2020.

[43] T. Gennarelli and A. Ommaya, “Comparison of translational and rotational accelerations in experimental cerebral concussion,” 1971.

[44] T. A. Gennarelli, L. E. Thibault, and A. K. Ommaya, “Pathophysiologic Responses to Rotational and Translational Accelerations of the Head,” Feb. 1972. doi: 10.4271/720970.

[45] T. B. Hoshizaki, A. Post, R. A. Oeur, and S. E. Brien, “Current and Future Concepts in Helmet and Sports Injury Prevention,” *Neurosurgery*, vol. 75, Oct. 2014, doi: 10.1227/NEU.0000000000000496.

[46] S. Rowson and S. M. Duma, “Brain Injury Prediction: Assessing the Combined Probability of Concussion Using Linear and Rotational Head Acceleration,” *Annals of Biomedical Engineering*, vol. 41, no. 5, May 2013, doi: 10.1007/s10439-012-0731-0.

[47] T. B. Hoshizaki *et al.*, “The development of a threshold curve for the understanding of concussion in sport,” *Trauma*, vol. 19, no. 3, Jul. 2017, doi: 10.1177/1460408616676503.

[48] D. I. and G. T. A. Adams J. H. and Graham, “Head Injury in Man and Experimental Animals: Neuropathology,” in *Trauma and Regeneration*, 1983, pp. 15–30.

[49] T. A. Gennarelli, L. E. Thibault, J. H. Adams, D. I. Graham, C. J. Thompson, and R. P. Marcincin, “Diffuse axonal injury and traumatic coma in the primate,” *Annals of Neurology*, vol. 12, no. 6, Dec. 1982, doi: 10.1002/ana.410120611.

[50] C. Deck and R. Willinger, “The current state of the human head finite element modelling,” *International Journal of Vehicle Safety*, vol. 4, no. 2, pp. 85–112, 2009, doi: 10.1504/IJVS.2009.028921.

[51] S. Kleiven, “Predictors for Traumatic Brain Injuries Evaluated through Accident Reconstructions,” *Stapp Car Crash Journal*, vol. 51, pp. 81–114, Oct. 2007, [Online]. Available: https://www.proquest.com/scholarly-journals/predictors-traumatic-brain-injuries-evaluated/docview/223249836/se-2?accountid=14578

[52] E. G. Takhounts, M. J. Craig, K. Moorhouse, J. McFadden, and V. Hasija, “Development of brain injury criteria (BrIC),” *Stapp car crash journal*, vol. 57, pp. 243–266, 2013.

[53] L. F. Gabler, J. R. Crandall, and M. B. Panzer, “Development of a Metric for Predicting Brain Strain Responses Using Head Kinematics,” *Annals of Biomedical Engineering*, vol. 46, no. 7, Jul. 2018, doi: 10.1007/s10439-018-2015-9.

[54] S. S. Margulies and L. E. Thibault, “A proposed tolerance criterion for diffuse axonal injury in man,” *Journal of Biomechanics*, vol. 25, no. 8, Aug. 1992, doi: 10.1016/0021-9290(92)90231-O.

[55] W. N. Hardy, C. D. Foster, M. J. Mason, K. H. Yang, A. I. King, and S. Tashman, “Investigation of Head Injury Mechanisms Using Neutral Density Technology and High-Speed Biplanar X-ray,” Nov. 2001. doi: 10.4271/2001-22-0016.

[56] L. F. Gabler, J. R. Crandall, and M. B. Panzer, “Investigating Brain Injury Tolerance in the Sagittal Plane Using a Finite Element Model of the Human Head,” *International Journal of Automotive Engineering*, vol. 7, no. 1, 2016, doi: 10.20485/jsaeijae.7.1_37.

[57] S. H. Backaitis and H. J. Mertz, “Hybrid III: The first human-like crash test dummy,” *Warrendale, PA: Society of Automotive Engineers*, p. 830, 1993.

[58] R. Jadischke, D. C. Viano, N. Dau, A. I. King, and J. McCarthy, “On the accuracy of the Head Impact Telemetry (HIT) System used in football helmets,” *Journal of Biomechanics*, vol. 46, no. 13, pp. 2310–2315, Sep. 2013, doi: 10.1016/J.JBIOMECH.2013.05.030.

[59] D. A. Bruneau and D. S. Cronin, “Head and Neck Response of an Active Human Body Model and Finite Element Anthropometric Test Device During a Linear Impactor Helmet Test,” *Journal of Biomechanical Engineering*, vol. 142, no. 2, Feb. 2020, doi: 10.1115/1.4043667.

[60] L. Zhang, K. H. Yang, and A. I. King, “A Proposed Injury Threshold for Mild Traumatic Brain Injury,” *Journal of Biomechanical Engineering*, vol. 126, no. 2, Apr. 2004, doi: 10.1115/1.1691446.

[61] C. Withnall, N. Shewchenko, R. Gittens, and J. Dvorak, “Biomechanical investigation of head impacts in football,” *British Journal of Sports Medicine*, vol. 39, no. suppl 1, pp. i49–i57, Aug. 2005, doi: 10.1136/BJSM.2005.019182.

[62] E. J. Pellman, D. C. Viano, A. M. Tucker, I. R. Casson, and J. F. Waeckerle, "Concussion in Professional Football: Reconstruction of Game Impacts and Injuries," *Neurosurgery*, vol. 53, no. 4, Oct. 2003, doi: 10.1093/neurosurgery/53.3.799.

[63] P. Rousseau, A. Post, T. B. Hoshizaki, R. Greenwald, A. Ashare, and S. W. Dean, "A Comparison of Peak Linear and Angular Headform Accelerations Using Ice Hockey Helmets," *Journal of ASTM International*, vol. 6, no. 1, pp. 1–11, 2009, doi: 10.1520/JAI101877.

[64] N. R. Coulson, S. G. Foreman, T. B. Hoshizaki, R. Greenwald, A. Ashare, and S. W. Dean, "Translational and Rotational Accelerations Generated During Reconstructed Ice Hockey Impacts on a Hybrid III Head Form," *Journal of ASTM International*, vol. 6, no. 2, 2009, doi: 10.1520/JAI101890.

[65] P. Rousseau and T. B. Hoshizaki, "Defining the effective impact mass of elbow and shoulder strikes in ice hockey," *Sports Biomechanics*, vol. 14, no. 1, Jan. 2015, doi: 10.1080/14763141.2015.1025236.

[66] K. G. McIver *et al.*, "Impact attenuation of male and female lacrosse helmets using a modal impulse hammer," *Journal of Biomechanics*, vol. 95, Oct. 2019, doi: 10.1016/j.jbiomech.2019.08.007.

[67] T. G. Bowman, K. M. Breedlove, M. R. Lininger, and S. v. Caswell, "Impact Mitigation Properties of Women's Lacrosse Headgear," *Annals of Biomedical Engineering*, vol. 48, no. 5, May 2020, doi: 10.1007/s10439-020-02467-3.

[68] J. M. Clark and T. B. Hoshizaki, "The Ability of Men's Lacrosse Helmets to Reduce the Dynamic Impact Response for Different Striking Techniques in Women's Field Lacrosse," *The American Journal of Sports Medicine*, vol. 44, no. 4, Apr. 2016, doi: 10.1177/0363546515623272.

[69] K. A. Rodowicz, J. E. Olberding, and A. C. Rau, "Head Injury Potential and the Effectiveness of Headgear in Women's Lacrosse," *Annals of Biomedical Engineering*, vol. 43, no. 4, Apr. 2015, doi: 10.1007/s10439-014-1154-x.

[70] J. M. Buice, A. O. Esquivel, and C. J. Andrecovich, "Laboratory Validation of a Wearable Sensor for the Measurement of Head Acceleration in Men's and Women's Lacrosse," *Journal of Biomechanical Engineering*, vol. 140, no. 10, Oct. 2018, doi: 10.1115/1.4040311.

[71] J. Funk, J. Cormier, C. Bain, H. Guzman, and E. Bonugli, "Validation and application of a methodology to calculate head accelerations and neck loading in soccer ball impacts (No. 2009-01-0251)," 2009.

[72] E. Hanlon and C. Bir, "Validation of a Wireless Head Acceleration Measurement System for Use in Soccer Play," *Journal of Applied Biomechanics*, vol. 26, no. 4, Nov. 2010, doi: 10.1123/jab.26.4.424.

[73] A. Bartsch, E. Benzel, V. Miele, D. Morr, and V. Prakash, “Hybrid III anthropomorphic test device (ATD) response to head impacts and potential implications for athletic headgear testing,” *Accident Analysis & Prevention*, vol. 48, Sep. 2012, doi: 10.1016/j.aap.2012.01.032.

[74] R. Jadischke, D. C. Viano, N. Dau, A. I. King, and J. McCarthy, “On the accuracy of the Head Impact Telemetry (HIT) System used in football helmets,” *Journal of Biomechanics*, vol. 46, no. 13, Sep. 2013, doi: 10.1016/j.jbiomech.2013.05.030.

[75] J. G. Beckwith, R. M. Greenwald, and J. J. Chu, “Measuring Head Kinematics in Football: Correlation Between the Head Impact Telemetry System and Hybrid III Headform,” *Annals of Biomedical Engineering*, vol. 40, no. 1, Jan. 2012, doi: 10.1007/s10439-011-0422-2.

[76] S. M. Duma *et al.*, “Analysis of Real-time Head Accelerations in Collegiate Football Players,” *Clinical Journal of Sport Medicine*, vol. 15, no. 1, 2005, [Online]. Available: https://journals.lww.com/cjsportsmed/Fulltext/2005/01000/Analysis_of_Real_time_Head_Accelerations_in.2.aspx

[77] K. M. Guskiewicz *et al.*, “MEASUREMENT OF HEAD IMPACTS IN COLLEGIATE FOOTBALL PLAYERS,” *Neurosurgery*, vol. 61, no. 6, Dec. 2007, doi: 10.1227/01.neu.0000306103.68635.1a.

[78] M. A. McCaffrey, J. P. Mihalik, D. H. Crowell, E. W. Shields, and K. M. Guskiewicz, “MEASUREMENT OF HEAD IMPACTS IN COLLEGIATE FOOTBALL PLAYERS,” *Neurosurgery*, vol. 61, no. 6, Dec. 2007, doi: 10.1227/01.neu.0000306102.91506.8b.

[79] S. Rowson, G. Brolinson, M. Goforth, D. Dietter, and S. Duma, “Linear and Angular Head Acceleration Measurements in Collegiate Football,” *Journal of Biomechanical Engineering*, vol. 131, no. 6, Jun. 2009, doi: 10.1115/1.3130454.

[80] B. Schnebel, J. T. Gwin, S. Anderson, and R. Gatlin, “IN VIVO STUDY OF HEAD IMPACTS IN FOOTBALL,” *Neurosurgery*, vol. 60, no. 3, Mar. 2007, doi: 10.1227/01.NEU.0000249286.92255.7F.

[81] S. Rowson and S. M. Duma, “Development of the STAR Evaluation System for Football Helmets: Integrating Player Head Impact Exposure and Risk of Concussion,” *Annals of Biomedical Engineering*, vol. 39, no. 8, Aug. 2011, doi: 10.1007/s10439-011-0322-5.

[82] J. P. Mihalik, K. M. Guskiewicz, S. W. Marshall, J. T. Blackburn, R. C. Cantu, and R. M. Greenwald, “Head Impact Biomechanics in Youth Hockey: Comparisons Across Playing Position, Event Types, and Impact Locations,” *Annals of Biomedical Engineering*, vol. 40, no. 1, Jan. 2012, doi: 10.1007/s10439-011-0405-3.

[83] K. L. O’Connor, M. M. Baker, S. L. Dalton, T. P. Dompier, S. P. Broglio, and Z. Y. Kerr, “Epidemiology of Sport-Related Concussions in High School Athletes: National Athletic Treatment, Injury and Outcomes Network (NATION), 2011–2012 Through 2013–2014,” *Journal of Athletic Training*, vol. 52, no. 3, Mar. 2017, doi: 10.4085/1062-6050-52.1.15.

[84] K. L. O'Connor, S. Rowson, S. M. Duma, and S. P. Broglio, "Head-Impact–Measurement Devices: A Systematic Review," *Journal of Athletic Training*, vol. 52, no. 3, Mar. 2017, doi: 10.4085/1062-6050.52.2.05.

[85] K. R. Campbell *et al.*, "Laboratory Evaluation of the gForce Tracker™, a Head Impact Kinematic Measuring Device for Use in Football Helmets," *Annals of Biomedical Engineering*, vol. 44, no. 4, Apr. 2016, doi: 10.1007/s10439-015-1391-7.

[86] M. A. Allison, Y. S. Kang, M. R. Maltese, J. H. Bolte, and K. B. Arbogast, "Measurement of Hybrid III Head Impact Kinematics Using an Accelerometer and Gyroscope System in Ice Hockey Helmets," *Annals of Biomedical Engineering*, vol. 43, no. 8, Aug. 2015, doi: 10.1007/s10439-014-1197-z.

[87] A. Harriss, A. M. Johnson, D. M. Walton, and J. P. Dickey, "Head impact magnitudes that occur from purposeful soccer heading depend on the game scenario and head impact location," *Musculoskeletal Science and Practice*, vol. 40, Apr. 2019, doi: 10.1016/j.msksp.2019.01.009.

[88] A. S. McIntosh *et al.*, "An assessment of the utility and functionality of wearable head impact sensors in Australian Football," *Journal of Science and Medicine in Sport*, vol. 22, no. 7, Jul. 2019, doi: 10.1016/j.jsams.2019.02.004.

[89] J. Reyes *et al.*, "The potential of head acceleration measurement to augment current best practice in concussion screening in professional Australian football players," *Physical Therapy in Sport*, vol. 43, May 2020, doi: 10.1016/j.ptsp.2020.03.007.

[90] J. V. K. Nguyen, J. H. Brennan, B. Mitra, and C. Willmott, "Frequency and Magnitude of Game-Related Head Impacts in Male Contact Sports Athletes: A Systematic Review and Meta-Analysis," *Sports Medicine*, vol. 49, no. 10, Oct. 2019, doi: 10.1007/s40279-019-01135-4.

[91] R. K. Le, T. D. Saunders, K. M. Breedlove, D. A. Bradney, J. M. Lucas, and T. G. Bowman, "Differences in the Mechanism of Head Impacts Measured Between Men's and Women's Intercollegiate Lacrosse Athletes," *Orthopaedic Journal of Sports Medicine*, vol. 6, no. 11, Nov. 2018, doi: 10.1177/2325967118807678.

[92] R. C. LYNALL *et al.*, "Head Impact Biomechanics in Women's College Soccer," *Medicine & Science in Sports & Exercise*, vol. 48, no. 9, Sep. 2016, doi: 10.1249/MSS.0000000000000951.

[93] D. King, P. A. Hume, M. Brughelli, and C. Gissane, "Instrumented Mouthguard Acceleration Analyses for Head Impacts in Amateur Rugby Union Players Over a Season of Matches," *The American Journal of Sports Medicine*, vol. 43, no. 3, Mar. 2015, doi: 10.1177/0363546514560876.

[94] J. R. Funk, S. Rowson, R. W. Daniel, and S. M. Duma, "Validation of Concussion Risk Curves for Collegiate Football Players Derived from HITS Data," *Annals of Biomedical Engineering*, vol. 40, no. 1, Jan. 2012, doi: 10.1007/s10439-011-0400-8.

[95] J. N. Press and S. Rowson, “Quantifying Head Impact Exposure in Collegiate Women’s Soccer,” *Clinical Journal of Sport Medicine*, vol. 27, no. 2, Mar. 2017, doi: 10.1097/JSM.0000000000000313.

[96] E. McCuen *et al.*, “Collegiate women’s soccer players suffer greater cumulative head impacts than their high school counterparts,” *Journal of Biomechanics*, vol. 48, no. 13, Oct. 2015, doi: 10.1016/j.jbiomech.2015.08.003.

[97] J. D. Morse, J. A. Franck, B. J. Wilcox, J. J. Crisco, and C. Franck, “An Experimental and Numerical Investigation of Head Dynamics Due to Stick Impacts in Girls’ Lacrosse,” *Annals of Biomedical Engineering*, vol. 42, no. 12, Dec. 2014, doi: 10.1007/s10439-014-1091-8.

[98] J. M. Clark, T. B. Hoshizaki, and M. D. Gilchrist, “Assessing women’s lacrosse head impacts using finite element modelling,” *Journal of the Mechanical Behavior of Biomedical Materials*, vol. 80, Apr. 2018, doi: 10.1016/j.jmbbm.2018.01.020.

[99] L. F. Gabler, J. R. Crandall, and M. B. Panzer, “Assessment of Kinematic Brain Injury Metrics for Predicting Strain Responses in Diverse Automotive Impact Conditions,” *Annals of Biomedical Engineering*, vol. 44, no. 12, Dec. 2016, doi: 10.1007/s10439-016-1697-0.

[100] E. S. Gurdjian, V. L. Roberts, and L. M. Thomas, “TOLERANCE CURVES OF ACCELERATION AND INTRACRANIAL PRESSURE AND PROTECTIVE INDEX IN EXPERIMENTAL HEAD INJURY,” *Journal of Trauma*, vol. 6, no. 5, pp. 600–604, 1966.

[101] C. W. Gadd, “Use of a Weighted-Impulse Criterion for Estimating Injury Hazard,” Feb. 1966. doi: 10.4271/660793.

[102] R. M. Greenwald, J. T. Gwin, J. J. Chu, and J. J. Crisco, “HEAD IMPACT SEVERITY MEASURES FOR EVALUATING MILD TRAUMATIC BRAIN INJURY RISK EXPOSURE,” *Neurosurgery*, vol. 62, no. 4, Apr. 2008, doi: 10.1227/01.neu.0000318162.67472.ad.

[103] “ND001: Standard test method and equipment used in evaluating the performance characteristics of protective headgear/equipment,” Overland Park, KS, 2020.

[104] J. Versace, “A Review of the Severity Index,” Feb. 1971. doi: 10.4271/710881.

[105] J. Newman, “A generalized acceleration model for brain injury threshold (GAMBIT),” 1986.

[106] J. A. Newman and N. Shewchenko, “A Proposed New Biomechanical Head Injury Assessment Function - the Maximum Power Index,” Nov. 2000. doi: 10.4271/2000-01-SC16.

[107] S. Kleiven, “Predictors for traumatic brain injuries evaluated through accident reconstructions,” *Stapp car crash journal*, vol. 51, pp. 81–114, 2007.

[108] H. Kimpara and M. Iwamoto, “Mild Traumatic Brain Injury Predictors Based on Angular Accelerations During Impacts,” *Annals of Biomedical Engineering*, vol. 40, no. 1, Jan. 2012, doi: 10.1007/s10439-011-0414-2.

[109] T. Yanaoka, Y. Dokko, and Y. Takahashi, “Investigation on an Injury Criterion Related to Traumatic Brain Injury Primarily Induced by Head Rotation,” Apr. 2015. doi: 10.4271/2015-01-1439.

[110] L. F. Gabler, J. R. Crandall, and M. B. Panzer, “Development of a Metric for Predicting Brain Strain Responses Using Head Kinematics,” *Annals of Biomedical Engineering*, vol. 46, no. 7, Jul. 2018, doi: 10.1007/s10439-018-2015-9.

[111] L. F. Gabler, J. R. Crandall, and M. B. Panzer, “Development of a Second-Order System for Rapid Estimation of Maximum Brain Strain,” *Annals of Biomedical Engineering*, vol. 47, no. 9, Sep. 2019, doi: 10.1007/s10439-018-02179-9.

[112] F. A. Fernandes and R. J. A. de Sousa, “Head injury predictors in sports trauma – A state-of-the-art review,” *Proceedings of the Institution of Mechanical Engineers, Part H: Journal of Engineering in Medicine*, vol. 229, no. 8, Aug. 2015, doi: 10.1177/0954411915592906.

[113] S. Rowson *et al.*, “Rotational Head Kinematics in Football Impacts: An Injury Risk Function for Concussion,” *Annals of Biomedical Engineering*, vol. 40, no. 1, Jan. 2012, doi: 10.1007/s10439-011-0392-4.

[114] M. Marar, N. M. McIlvain, S. K. Fields, and R. D. Comstock, “Epidemiology of Concussions Among United States High School Athletes in 20 Sports,” *The American Journal of Sports Medicine*, vol. 40, no. 4, Apr. 2012, doi: 10.1177/0363546511435626.

[115] L. M. Gessel, S. K. Fields, C. L. Collins, R. W. Dick, and R. D. Comstock, “Concussions among United States high school and collegiate athletes,” *Journal of athletic training*, vol. 42, no. 4, pp. 495–803, 2007.

[116] E. B. Wasserman, Z. Y. Kerr, S. L. Zuckerman, and T. Covassin, “Epidemiology of Sports-Related Concussions in National Collegiate Athletic Association Athletes From 2009-2010 to 2013-2014,” *The American Journal of Sports Medicine*, vol. 44, no. 1, Jan. 2016, doi: 10.1177/0363546515610537.

[117] J. A. Rosenthal, R. E. Foraker, C. L. Collins, and R. D. Comstock, “National High School Athlete Concussion Rates From 2005-2006 to 2011-2012,” *The American Journal of Sports Medicine*, vol. 42, no. 7, Jul. 2014, doi: 10.1177/0363546514530091.

[118] Z. Y. Kerr *et al.*, “Concussion Rates in U.S. Middle School Athletes, 2015–2016 School Year,” *American Journal of Preventive Medicine*, vol. 53, no. 6, Dec. 2017, doi: 10.1016/j.amepre.2017.05.017.

[119] S. v. Caswell *et al.*, “Characterizing Verified Head Impacts in High School Girls’ Lacrosse,” *The American Journal of Sports Medicine*, vol. 45, no. 14, Dec. 2017, doi: 10.1177/0363546517724754.

[120] A. E. Lincoln, R. Y. Hinton, J. L. Almquist, S. L. Lager, and R. W. Dick, "Head, Face, and Eye Injuries in Scholastic and Collegiate Lacrosse," *The American Journal of Sports Medicine*, vol. 35, no. 2, Feb. 2007, doi: 10.1177/0363546506293900.

[121] J. McGill, "Double Protection or Double Standard?: Male and Female Athletes - The Delta Statement." https://deltastatement.com/5344/archives/fall-2018/double-protection-or-double-standard-male-and-female-athletes/ (accessed Nov. 23, 2021).

[122] S. D. G. Paul T. Diamond, "Head injuries in men's and women's lacrosse: a 10 year analysis of the NEISS database," *Brain Injury*, vol. 15, no. 6, Jan. 2001, doi: 10.1080/02699050120402.

[123] S. v. Caswell, A. E. Lincoln, J. L. Almquist, R. E. Dunn, and R. Y. Hinton, "Video Incident Analysis of Head Injuries in High School Girls' Lacrosse," *The American Journal of Sports Medicine*, vol. 40, no. 4, Apr. 2012, doi: 10.1177/0363546512436647.

[124] R. Y. Hinton, A. E. Lincoln, J. L. Almquist, W. A. Douoguih, and K. M. Sharma, "Epidemiology of Lacrosse Injuries in High School-Aged Girls and Boys," *The American Journal of Sports Medicine*, vol. 33, no. 9, Sep. 2005, doi: 10.1177/0363546504274148.

[125] J. J. Crisco, L. Costa, R. Rich, J. B. Schwartz, and B. Wilcox, "Surrogate Headform Accelerations Associated with Stick Checks in Girls' Lacrosse," *Journal of Applied Biomechanics*, vol. 31, no. 2, Apr. 2015, doi: 10.1123/JAB.2014-0102.

[126] A. Schwarz, "A Case Against Helmets in Lacrosse," *The New York Times*.

[127] "ASTM F3137-15: Standard Specification for Headgear Used in Women's Lacrosse (excluding Goalkeepers)," 2015.

[128] A. Post, A. Oeur, B. Hoshizaki, and M. D. Gilchrist, "An examination of American football helmets using brain deformation metrics associated with concussion," *Materials & Design*, vol. 45, Mar. 2013, doi: 10.1016/j.matdes.2012.09.017.

[129] L. Zhang, X. Yao, S. Zang, and Y. Gu, "Temperature- and strain rate-dependent constitutive modeling of the large deformation behavior of a transparent polyurethane interlayer," *Polymer Engineering & Science*, vol. 55, no. 8, Aug. 2015, doi: 10.1002/pen.24026.

[130] D. T. Morton, A. Reyes, A. H. Clausen, and O. S. Hopperstad, "Mechanical response of low density expanded polypropylene foams in compression and tension at different loading rates and temperatures," *Materials Today Communications*, vol. 23, Jun. 2020, doi: 10.1016/j.mtcomm.2020.100917.

[131] J. Johnsen, F. Grytten, O. S. Hopperstad, and A. H. Clausen, "Experimental set-up for determination of the large-strain tensile behaviour of polymers at low temperatures," *Polymer Testing*, vol. 53, Aug. 2016, doi: 10.1016/j.polymertesting.2016.06.011.

[132] M. R. Shariatmadari, R. English, and G. Rothwell, "Effects of temperature on the material characteristics of midsole and insole footwear foams subject to quasi-static compressive

and shear force loading," *Materials & Design*, vol. 37, May 2012, doi: 10.1016/j.matdes.2011.10.045.

[133] National Operating Committee on Standards for Athletic Equipment, "NOCSAE DOC (ND) 081-18am19a: STANDARD PNEUMATIC RAM TEST METHOD AND EQUIPMENT USED IN EVALUATING THE PERFORMANCE CHARACTERISTICS OF PROTECTIVE HEADGEAR AND FACE GUARDS," 2019.

[134] American Society for Testing and Materials, "ASTM F3137-15: Standard Specification for Headgear Used in Women's Lacrossse (excluding Goalkeepers)," 2015.

[135] M. Mohr, P. Krustrup, H. Andersson, D. Kirkendal, and J. Bangsbo, "Match Activities of Elite Women Soccer Players at Different Performance Levels," *Journal of Strength and Conditioning Research*, vol. 22, no. 2, Mar. 2008, doi: 10.1519/JSC.0b013e318165fef6.

[136] P. KRUSTRUP, M. MOHR, H. ELLINGSGAARD, and J. BANGSBO, "Physical Demands during an Elite Female Soccer Game: Importance of Training Status," *Medicine & Science in Sports & Exercise*, vol. 37, no. 7, Jul. 2005, doi: 10.1249/01.mss.0000170062.73981.94.

[137] L. A. Livingston, "Recent crosse designs increase ball velocity: Implications for injury in women's lacrosse," *Journal of Science and Medicine in Sport*, vol. 9, no. 4, Aug. 2006, doi: 10.1016/j.jsams.2006.05.022.

[138] Society of Automotive Engineers, "SAE J211-1: Instrumentation for Impact Test - Part 1 - Electronic Instrumentation," 2014.

[139] N. Cortes *et al.*, "Video Analysis Verification of Head Impact Events Measured by Wearable Sensors," *The American Journal of Sports Medicine*, vol. 45, no. 10, Aug. 2017, doi: 10.1177/0363546517706703.

[140] R. K. Le, T. D. Saunders, K. M. Breedlove, D. A. Bradney, J. M. Lucas, and T. G. Bowman, "Differences in the Mechanism of Head Impacts Measured Between Men's and Women's Intercollegiate Lacrosse Athletes," *Orthopaedic Journal of Sports Medicine*, vol. 6, no. 11, Nov. 2018, doi: 10.1177/2325967118807678.

[141] K. vanden Bosche, Y. Mosleh, B. Depreitere, J. vander Sloten, I. Verpoest, and J. Ivens, "Anisotropic polyethersulfone foam for bicycle helmet liners to reduce rotational acceleration during oblique impact," *Proceedings of the Institution of Mechanical Engineers, Part H: Journal of Engineering in Medicine*, vol. 231, no. 9, Sep. 2017, doi: 10.1177/0954411917711201.

[142] Y. Mosleh, M. Cajka, B. Depreitere, J. vander Sloten, and J. Ivens, "Designing safer composite helmets to reduce rotational accelerations during oblique impacts," *Proceedings of the Institution of Mechanical Engineers, Part H: Journal of Engineering in Medicine*, vol. 232, no. 5, May 2018, doi: 10.1177/0954411918762622.

[143] K. Hansen *et al.*, "Angular Impact Mitigation system for bicycle helmets to reduce head acceleration and risk of traumatic brain injury," *Accident Analysis & Prevention*, vol. 59, Oct. 2013, doi: 10.1016/j.aap.2013.05.019.

[144] N. Mills, "Polymer foams for personal protection: cushions, shoes and helmets," *Composites Science and Technology*, vol. 63, no. 16, Dec. 2003, doi: 10.1016/S0266-3538(03)00272-0.

[145] D. H. Daneshvar, C. M. Baugh, C. J. Nowinski, A. C. McKee, R. A. Stern, and R. C. Cantu, "Helmets and Mouth Guards: The Role of Personal Equipment in Preventing Sport-Related Concussions," *Clinics in Sports Medicine*, vol. 30, no. 1, Jan. 2011, doi: 10.1016/j.csm.2010.09.006.

[146] K. C. Rusch, "Energy-absorbing characteristics of foamed polymers," *Journal of Applied Polymer Science*, vol. 14, no. 6, Jun. 1970, doi: 10.1002/app.1970.070140603.

[147] S. S. Sarva, S. Deschanel, M. C. Boyce, and W. Chen, "Stress–strain behavior of a polyurea and a polyurethane from low to high strain rates," *Polymer*, vol. 48, no. 8, Apr. 2007, doi: 10.1016/j.polymer.2007.02.058.

[148] J. Yi, M. C. Boyce, G. F. Lee, and E. Balizer, "Large deformation rate-dependent stress–strain behavior of polyurea and polyurethanes," *Polymer*, vol. 47, no. 1, Jan. 2006, doi: 10.1016/j.polymer.2005.10.107.

[149] L. Zhang, X. Yao, S. Zang, and Y. Gu, "Temperature- and strain rate-dependent constitutive modeling of the large deformation behavior of a transparent polyurethane interlayer," *Polymer Engineering & Science*, vol. 55, no. 8, Aug. 2015, doi: 10.1002/pen.24026.

[150] H. J. Qi and M. C. Boyce, "Stress–strain behavior of thermoplastic polyurethanes," *Mechanics of Materials*, vol. 37, no. 8, Aug. 2005, doi: 10.1016/j.mechmat.2004.08.001.

[151] S. Ouellet, D. Cronin, and M. Worswick, "Compressive response of polymeric foams under quasi-static, medium and high strain rate conditions," *Polymer Testing*, vol. 25, no. 6, Sep. 2006, doi: 10.1016/j.polymertesting.2006.05.005.

[152] B. J. Ramirez and V. Gupta, "Evaluation of novel temperature-stable viscoelastic polyurea foams as helmet liner materials," *Materials & Design*, vol. 137, Jan. 2018, doi: 10.1016/j.matdes.2017.10.037.

[153] Peter Dunn, "Why do plastics get brittle when they get cold?," *MIT School of Engineering*, Jun. 02, 2009.